ELECTROCHEMICAL POLISHING OF SELECTIVE LASER MELTED INCONEL 718

A Thesis

by

SRISHTI JAIN

Submitted to the Office of Graduate and Professional Studies of
Texas A&M University
in partial fulfillment of the requirements for the degree of

MASTER OF SCIENCE

Chair of Committee, Wayne Hung
Co-Chair of Committee, Bruce Tai
Committee Member, Hong Liang

Head of Department, Andreas Polycarpou

December 2018

Major Subject: Mechanical Engineering

ABSTRACT

Additive manufacturing (AM) has gained prominence in the field of manufacturing and is becoming a strong competition to conventional manufacturing technologies such as casting, forming etc. It is used for manufacturing of critical metallic parts for aerospace and automotive industries. Inconel 718, a Ni-Cr-Fe based superalloy, has been extensively used in extreme environments such as nuclear, oil/gas, aircraft applications. Inconel powder can be consolidated by using selective laser melting (SLM) process, which helps in preserving material properties and allows more design freedom. However, one of the drawbacks of additive manufacturing is the rough surface of the produced parts. This study aims to improve the surface finish of Inconel parts manufactured by SLM using electrochemical polishing (ECP) process. This study also compares the SLM parts with the extruded parts of the same metal polished by ECP. The parts are first hand-ground and then polished by ECP process. Inconel 718 is used as workpiece material, titanium rod is used as a tool, and a commercial acid-based electrolyte is used for running experiments. SEM studies are performed on the parts for analysis of results.

Pulsed direct currents with varying duty cycles are used to study the effect of off-time during polishing process. Results show that the higher current values are desirable for extruded Inconel parts resulting in shinier surfaces, whereas for SLM manufactured Inconel parts, a very high current can lead to deterioration in surface properties due to presence of non-conductive particles. Successful polishing reduces surface roughness to a sub-micron value (<1 μm).

DEDICATION

Dedicated to:

My parents, *Vandana and Sanjay Jain* for being my pillars of strength and motivation. You believed in me when no one did. I owe every bit of what I am today, to you.

Kunal Agrawal, Shaurabh Kumar Singh and Umema Bohari, for helping me keep my sanity and for always believing in me. This would not have been possible, had you not got my back.

Samyak Jain for being the invisible force that has inspired me in more ways than I can express.

ACKNOWLEDGEMENTS

The most important thing, research has taught me is: patience. No problem can be solved overnight and there is no problem that can't be solved. It is about being persistent in your efforts and working hard towards your goal. This would not have been possible without the constant support, tremendous knowledge, and guidance of my advisor and mentor, Dr. Wayne Hung. I would like to express my sincere gratitude towards him for being so understanding and showing the right path all along.

I would like to thank Dr. Bruce Tai and Dr. Hong Liang, for agreeing to be on my committee and for their valuable feedback, and guidance.

I owe a thank you to Adam Farmer, the former laboratory instructor for constant help during the course of this thesis work.

I would also like to thank the former graduate researchers, Jigar Patel and Dr. Zhujian Feng in micro-nano manufacturing lab for their help throughout the course of this research study. It would not have been possible without your insightful thoughts.

I owe a big thank you to the staff and faculty at mechanical engineering department and all my friends and colleagues at Texas A&M University, who made my experience here worthwhile.

CONTRIBUTORS AND FUNDING SOURCES

This work was supervised by a thesis committee consisting of Dr. Wayne Hung, Dr. Bruce Tai and Dr. Hong Liang of the department of Mechanical engineering.

All work for the thesis was completed by the student, under the advisement of Dr. Wayne Hung of the department of Mechanical engineering.

This work was made possible in part by the contribution of KGSBO, ESMA Inc. and Electropolishing Systems in the form of material/resources needed. Data contribution from teachers in the NSF-RET program at Texas A&M University was appreciated.

Its contents are solely the responsibility of the authors and do not necessarily represent the official views of any outside agency.

TABLE OF CONTENTS

Page

LIST OF FIGURES

Page

LIST OF TABLES

Page

1. INTRODUCTION

This research aims to improve the surface finish of 3D printed metal parts. A 3D printed part is typically produced with a rough surface finish. For some industrial applications it becomes vital to improve their surface finish to increase part performance, reduce friction and provide better tolerances.

There are a variety of polishing methods used for the purpose of finishing metals. Buffing is a polishing method for metals, woods or composites using a cloth wheel impregnated with polishing compounds or rouges. The cloth buff carries the compound, while the compound does the polishing. Buffing is known for fine removal of pits, coarse abrasive lines, and even deep scratches. Another process used for polishing is lapping, in which two surfaces are rubbed together with a layer of abrasive slurry between them. Lapping involves a softer material like ceramic for the lap, which is charged with the abrasive. The lap is then used to polish a harder material which is workpiece. The abrasive embeds within the softer material, which holds it and permits the polishing of harder material. Finer abrasives produce a smoother polished surface. Polishing by magnetic abrasive is another method used to achieve fine polished surfaces. This process uses abrasive particles induced by a magnetic field and are filled in the working gap between workpiece and magnet. The magnetic abrasive particles form a flexible magnetic brush and act like a multipoint cutting tool for the polishing operation. The use of such polishing mechanisms has limitations as a majority of them remove the material by physical contact. Thus, mechanical polishing of highly accurate and delicate parts can be challenged. The physical contact between the tool and the workpiece may be detrimental, causing contamination, rounded corners, and significant subsurface damage. These methods also face certain disadvantages as

some of the abrasives and compounds remain embedded in the metal surface. For high purity applications in the semiconductor, pharmaceutical and medical industries, mechanically polished parts could be harmful.

The ECP , or electropolishing (EP), is a promising method for polishing of conductive materials without involving mechanical actions. ECP is one of the main applications of electrochemical machining (ECM) and is based on the same principles as ECM.

Electropolishing effectively removes high peaks on a surface by means of an electrochemical action. ECP removes the top layer of metal along with contaminants in the base metal. This not only removes impurities and surface material but creates an oxygen rich environment that allows for the formation of an excellent chrome oxide layer and renders the material passive (Technologies, 2014). Thus, ECP has many applications in the metal finishing industry because of its simplicity and its ability to be used on irregularly-shaped objects. In ECP, the positive workpiece is immersed in an electrolyte and serves as an anode, and the tool is connected to the negative terminal of the power supply acting as a cathode. When the set-up is immersed in electrolyte and the current is passed through the circuit, the metal ions are removed from the anode. The advantages of ECP include negligible tool wear, burr-free surfaces, and independence of material hardness.

Inconel is a hard-to-machine alloy made of nickel and chromium. Inconel 718 accounts for about 50% of the weight of aircraft turbojet engines and is the main component for discs, blades, and casings of high-pressure section of the compressor (Group, 2018). It is a high strength alloy well suited for extreme environments. Owing to such high hardness, it becomes difficult to machine or polish Inconel with common mechanical processes. A variety of AM techniques such as electron beam melting (EBM), selective laser sintering (SLS) and SLM can

be used for manufacturing of Inconel parts. This research uses the Inconel 718 produced by the cost effective SLM method. SLM uses a high-power density laser to melt and fuse metallic powders together in a layer by layer technique. The entire process takes place inside a chamber with a tightly controlled argon gas atmosphere. Inconel 718 manufactured by AM techniques even exceeded the mechanical properties of cast and wrought components (Trosch et al., 2016).

However, parts manufactured using SLM are known to have a rough surface finish due to shrinkage, layer-wise building sequence and spreading of melting powder prior to melting (Figure 1). To minimize or eliminate such surface defects, post-processing of SLM-manufactured part becomes highly necessary.

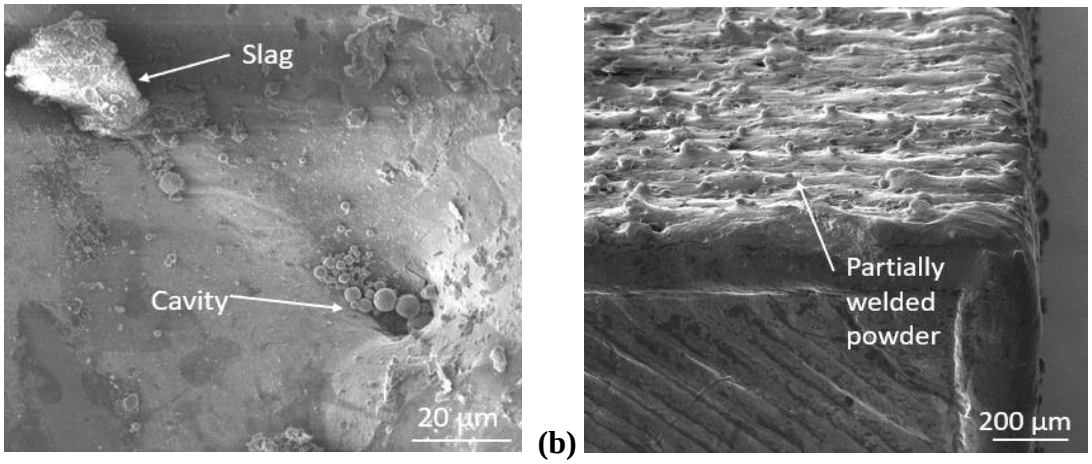

Figure 1: SEM image using secondary electron mode for surface defects on SLM produced parts (a) slag, cavity (b) partially welded particles

This research aims to improve the surface finish of SLM manufactured Inconel 718 using ECP method. It also compares the ECP results of SLM parts with those of extruded parts of the same metal. Experiments are conducted on a full factorial design to achieve sub-micron level surface finish. Microscopic study using scanning electron microscope (SEM) and optical microscopy are used to compare the polished surface of SLM and extruded samples.

1.1 Motivation

Additive manufacturing is becoming a strong competitor to conventional manufacturing technologies, such as casting, forming, and machining, for the manufacture of function-critical metallic parts for industrial sectors such as aerospace, medical and automotive. Such critical applications demand the parts to be highly accurate with good surface and material properties. Surface finish is considered one of the standard quality properties for mechanical products. However, the poor surface quality of AM parts is one of the biggest challenges to overcome.

Over the past years, many researchers have made efforts to improve the surface quality of SLM manufactured parts. However, majority of these studies are limited to evaluation and optimization of laser parameters. It has been showed that changing of hatch distance and laser density caused modification in geometric characteristics of tracks and consequently, changing surface morphology. A significant surface improvement using laser re-melting was reported with the improvement in roughness R_a from 12 to 1.5 μm.

There has been some work in improving the surface finish of AM parts by post-processing methods such as chemical etching and polishing, but the material used has been majorly stainless steel.

Thus, there is an uninvestigated area for reducing surface roughness of Inconel, which served as a motivation for this research. Hence, this research is aimed to perform ECP on Inconel 718 (IN718) for reducing surface roughness further to a submicron level.

1.2 Objectives and Scope

The objectives of this study are to:

1. Design and develop an experimental set-up for carrying out local polishing using electrochemical reactions.
2. Study the influence of ECP parameters.
3. Compare the surface finish of Inconel parts produced by SLM method with those manufactured by extrusion method

The scope of this study is limited to ECP of Inconel 718 produced by SLM and extrusion methods. Current density, polishing time and duty cycle are treated as variable parameters to achieve the desired polishing results. Fixed parameters included the electrolyte used, temperature of the cell, frequency, and the inter-electrode gap.

2. LITERATURE REVIEW

2.1 Principle of ECP

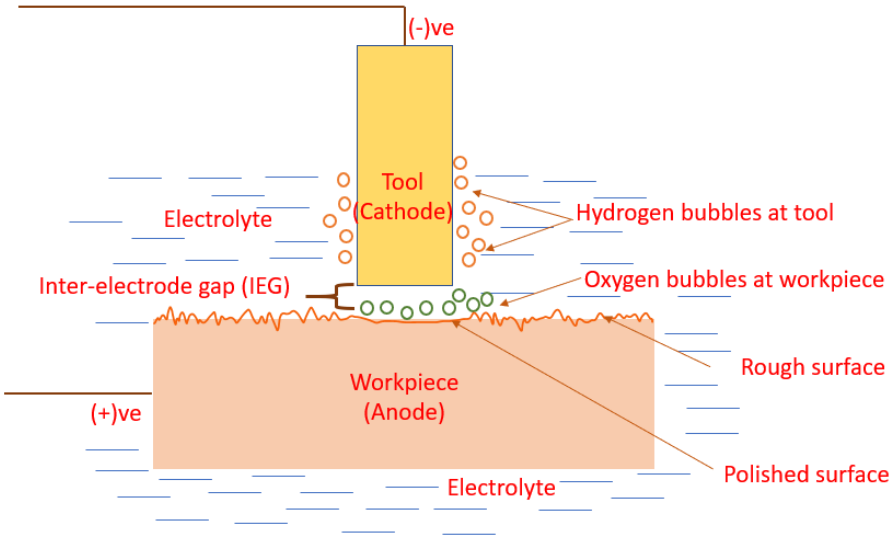

Figure 2: Schematic of ECP Process

The ECP is an important application of ECM. It comes from the concept of electroplating, where the anode material is removed and deposited on the cathode by ion transporting in the electrode gap. With proper ion flushing in ECP, the anode material is removed but not deposited on the cathode. ECP is suitable for polishing of complex shaped and hard materials, as the workpiece and electrode are not in contact with each other.

The ECP effect occurs because of differential dissolution on application of current. The lower peaks (troughs) on the rough metal surface are dissolved slowly because of the covering of the oxidation film, which has a high specific gravity, viscosity, and insulation, while the higher peaks (crests) are dissolved more quickly as they are not covered with the oxidization film and receive greater current from the cathode (Figure 2). By applying current between the anode and

cathode in an electrolyte solution, oxygen is given off at the anode with workpiece dissolution and hydrogen is given off at the cathode without any dissolution (Lee, 2000).

2.1.1 Theory

Material removal rate (MRR) in ECP and ECM is derived from Faraday's law of electrolysis.

$$MRR = \frac{V}{t} = \left(\frac{M}{zFd}\right)\left(\frac{EA}{gr}\right) = C\left(\frac{EA}{gr}\right) = CI \quad (1)$$

Where,

MRR : material removal rate (mm^3/min)
V : removal volume at anode (mm^3/min)
t : processing time (min)
M : Atomic mass of anode (g/mol)
F : Faraday's constant = 96500 (Coulomb/mole)
z : valency of anode material
d : density of anode material (g/mm^3)
I : working current (A)
E : voltage across electrodes (V)
A : effective area between electrodes (mm^2)
g : inter-electrode gap (mm)
r : resistivity of system (Ω cm)
C : specific removal rate (mm^3/min/A)
ρ : density of material (g/mm^3)

2.1.2 Advantages and Issues

The advantages of ECP are realized by the ability of the process to machine materials that are usually hard to machine with mechanical polishing processes. One of the major advantages is the flexibility in the tool selection, as a relatively soft tool can be used to polish hard materials. The tool wear in an ideal ECP process is zero. But even in practical applications, the tool wear is negligible, saving a lot of set up and tool changing costs. The electrolyte used to complete the electrical circuit can be filtered and reused thus, saving cost for the entire polishing process. The polished parts have no burrs and can be automated for repeatable results.

The biggest limitation of ECP is that only electrically conductive material can be polished and the process is very slow compared to any mechanical process. Another key issue is the corrosive property of commonly used electrolytes, having the potential to damage the experimental equipment. Excessive heating of the electrolyte is also observed in cases of increased electrolyte resistance. Another challenge associated with ECP is the proper formulation of the electrolyte, suitable for the workpiece material. Improper electrolytes can result in highly undesirable results leading to corrosion and pitting of the workpiece. Hence, a proper electrolyte and safe working environment is vital for proper results.

2.1.3 Applications

Polishing works on the same principle as machining except the material removed in machining is much higher compared to that in polishing. ECP is an excellent and economical tool for deburring and provides preferential removal of unwanted material. It does so without altering the part’s dimensions.

Polishing can be performed using any conductive metal tube or pin of appropriate diameter. A highly corrosion resistant metal, titanium, was chosen for the electrode as it does not wear out or corrode during execution.

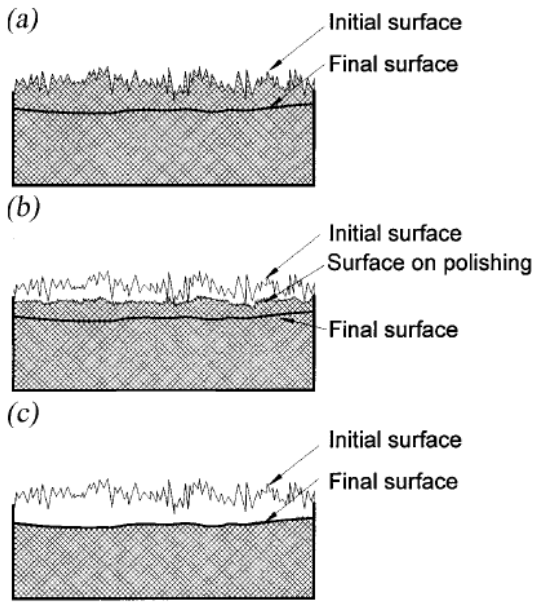

Figure 3: Electropolishing mechanism for levelling the surface, reprinted from (Lee, 2000)

Figure 3 explains the sequential levelling process of the surface: (a) represents the initial rough surface before electropolishing takes place, (b) the higher peaks are dissolved faster than the lower peaks after polishing, and (c) after the electropolishing process is completed, the workpiece surface becomes smooth, shiny, and leveled.

Process parameters of ECP are given by equation (1). Varying the parameters can modify the entire process to give desirable results and are discussed below.

2.1.4 Electrolyte

The primary function of the electrolyte is to provide optimal conditions for machining to take place. The electrolyte acts as the conducting medium between the two electrodes creating a favorable environment for dissolution of workpiece material. The ideal electrolyte used during polishing must have high conductivity, low viscosity, should be non-corrosive, and should not vaporize. The electrolyte should be able to maintain its properties over a long period of time and be used repeatedly after filtration.

In polishing, because of the small gap between the tool and the electrode, the density of current is very high, leading to heating and vaporization of electrolyte. Thus, the chosen electrolyte should not vaporize and should carry the debris away from the workpiece. The toxicity of electrolytes is a major cause of concern towards widespread implementation of ECP. However, use of citric acid as electrolyte to achieve environment-friendly ECP is one of the attempts to overcome this limitation (Ryu, 2015).

The concentration of electrolyte affects the process as the higher conductivity of electrolyte facilitates higher current flow, thus increasing the amount of material removed. When polishing Ni-based alloys, the commonly used solutions are composed of one or more concentrated acids, such as perchloric, sulfuric, phosphoric, and acetic acids (Huang et al., 2009). Phosphoric acid ensures a slow and uniform dissolution at the appropriate working conditions without corrosion or erosion, whereas sulfuric acid increases current density by causing the initial dissolution of the surface of workpiece. Yang et al. (2017) used a non-aqueous alcoholic

solution comprising of ethyl and isopropyl alcohol for the electropolishing of Inconel 718 fabricated via laser melting. The surface roughness (R_a) of the samples was reduced from 7.9 to 3 µm.

According to Huang et al. (2009) addition of water content to a mixture of perchloric acetic acid, enhanced the brightening effect along with leveling on the as-rolled Inconel 718 sheet to achieve R_a of 0.03 µm. Figure 4 shows the leveling and brightening of the workpiece when shifting to 40 vol % from 20 vol %. perchloric acid.

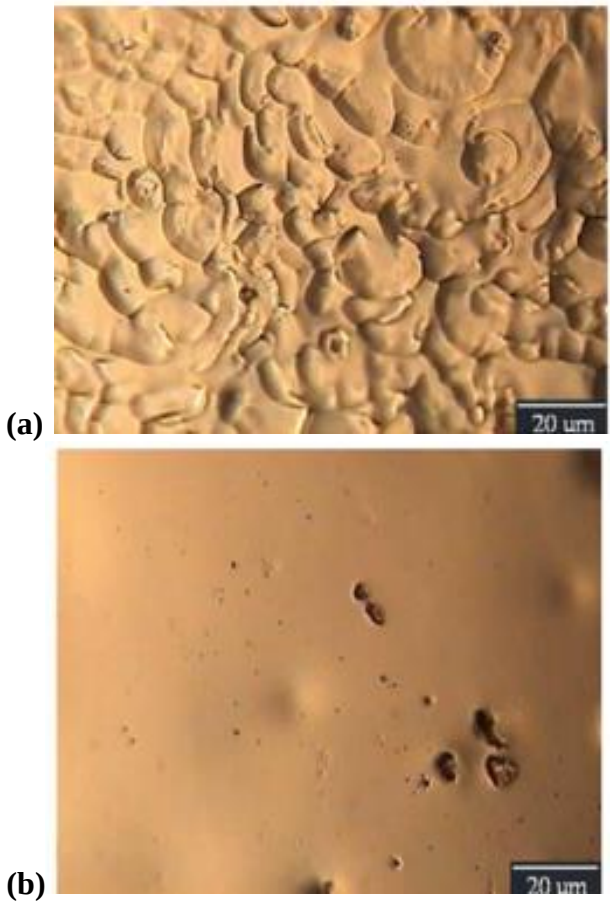

Figure 4: Surface morphologies of IN718 polished in acid mixtures (a) 20% (b) 40% vol $HClO_4$, reprinted from (Huang et al., 2009)

2.1.5 Voltage and Current

An electrical double layer was defined by the structure of charged ions, was formed at the interface of the tool and the workpiece electrode when they are immersed in the electrolyte. Due to the profile of this double layer, when the voltage is applied the electrolytic cell can be considered equivalent to a circuit consisting of capacitors and resistors (Kim et al., 2004). Current density, which is the ratio of current and effective electrode surface area, is determined by the rate at which ions arrive at the electrode, which further depends on the applied voltage, concentration of electrolyte, and IEG.

Researchers have used pulsed current over continuous current to enhance the electrochemical polishing process. On-time and off-time must be defined in pulsed current. The off-time is crucial and aids in the flushing away of any by-products formed during the on-time, which allows the beginning of the next phase with fresh electrolyte in the IEG every time and minimal deposition of the debris on the tool. However, the off-time leads to a decrease in the current efficiency as shown in Figure 5.

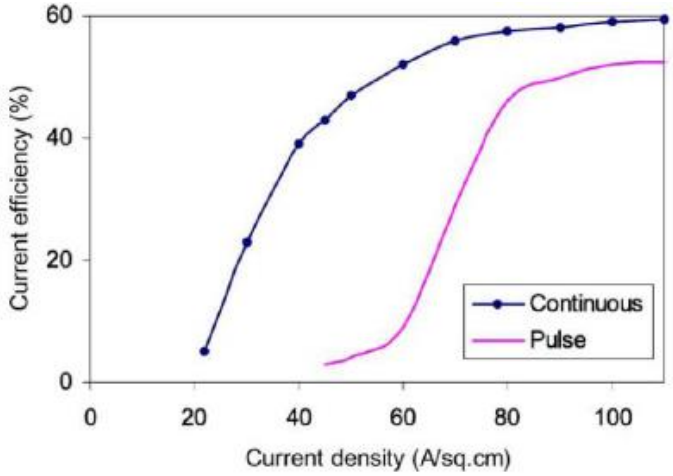

Figure 5: Comparing current density vs efficiency for pulsed and continuous current, reprinted from (Bhattacharyya et al., 2007)

Polarization effect refers to the mechanical side effects in an electrochemical process by which isolating barriers develop at the interface between electrode and electrolyte. According to Rajurkar et al. (1999), a shorter pulse on-time decreased the concentration polarization effect, which increased the peak current and reduced the selective dissolution, resulting in better surface roughness. Thus, even though shorter on-times are desired, on-time should still be long enough for the anodic surfaces to get charged and polarized and to start the dissolution process.

There exists a plateau region in the plot of current density versus voltage curve for a given tool, workpiece, and electrolyte combination. The optimal current density for electropolishing was expected to be at the end of the plateau region (Lee, 2000). According to Lee et al. (2003) a viscous film was formed in the plateau region (c-d) in the current versus voltage (I-V) curve (Figure 6) and the levelling and brightening of the workpiece took place within this viscous film.

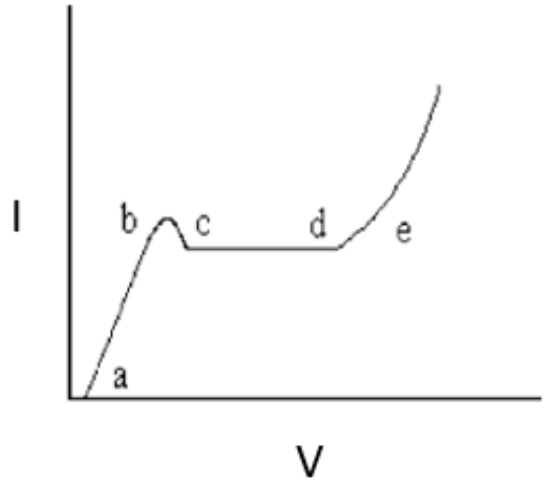

Figure 6: I-V curve, reprinted from (Lee et al., 2003)

Wang et al. (2015) showed the plot of current efficiency (ce) vs. current density (j) for Inconel 718 electropolished with $NaNO_3$ solution. It compared the curves with SS304 and showed how it differed strongly (Figure 7). Up to 20 A/cm^2 there is a downward trend for current efficiency. It is also found that at current density of 3 A/cm^2 current efficiency is as high as 85%. It suggested that dissolution of Inconel 718 persists even at very low current densities contrasting to the case for SS304.

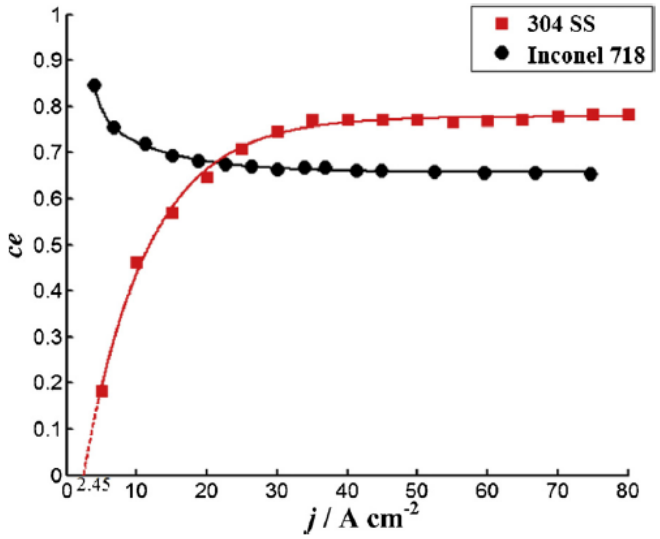

Figure 7: Current efficiency (ce) vs. current density (j/ A) curves in 10% $NaNO_3$ solution, reprinted from (Wang et al., 2015)

2.1.6 Interelectrode Gap

Interelectrode gap is the distance between the tool (cathode) and the workpiece (anode). The electrolyte acts as the bridge between the two electrodes, allowing the ions to move while polishing. Larger IEG gives wider zones of polished profiles due to larger activation area by strayed current while the smaller IEG gives narrower zones. The role of IEG is crucial to the outcome of the ECP process, and hence, maintaining and controlling the IEG is vital to suit the application.

Lee (2000) also demonstrated that while electropolishing stainless steel, the wider gap of more than 1.5 mm worsened the surface roughness of the workpiece more than the untreated one. This is caused by wide electrode gap. It has also been shown that as the gap becomes narrow, pits can be formed at a certain small spot due to high current density. Thus, an appropriate IEG must be selected for electropolishing the workpiece.

2.2 Inconel 718

Inconel is a family of austenitic-nickel-chromium bases superalloys. Their corrosion resistance properties make them well suited for extreme environments subjected to pressure and heat. Inconel is known to retain strength over a wide temperature range and during high temperature up to 980°C, applications where metals like aluminum and steel would succumb to creep.

Inconel are superalloys composed of nickel, chromium, and iron. Different Inconels have widely different composition, but all of them are predominantly nickel, with chromium as a second element. For this research the alloy 718 was chosen due to its widespread applications and excellent properties.

2.2.1 Properties

Inconel 718 is a precipitation hardenable, high strength corrosion resistant, nickel-chromium material used at -252°C to 704°C (Corporation, 2007). The alloy associates good creep and rupture strength with a high resistance to fatigue. It possesses long term strength and toughness at higher temperatures while still maintaining corrosion resistance along with better welding characteristics.

Inconel 718 is considered one of the predominant superalloys in the world. Introduced in 1965 at industrial scale, Inconel 718 is used extensively nowadays. Its Young's modulus is almost twice that of Ti6Al4V and similar to that of an CK45 hardenable carbon steel.

Owing to such superior properties, Inconel 718 accounts for up to 50% of the weight of aircraft turbojet engines, being the main component of discs, blades, and casings of the high-pressure section of the compressor as well as a primary material in discs and blades of the

turbine section (Group, 2018). Alloy 718 also finds several applications in rocket engines and cryogenic environments due to its toughness at low temperatures, preserving parts from a brittle fracture. Table 1 below shows the different compositions of various elements in the Inconel 718 alloy.

Table 1: Chemical composition of Inconel 718, reprinted from (Metals, 2015)

Element	Min	Max
Carbon	--	0.08
Manganese	--	0.35
Silicon	--	0.35
Phosphorus	--	0.015
Sulfur	--	0.015
Nickel + Cobalt	50.0	55.0
Chromium	17.0	21.0
Cobalt	--	1.00
Iron	Balance	
Aluminum	0.35	0.80
Molybdenum	2.80	3.30
Titanium	0.65	1.15
Boron	0.001	0.006
Copper	--	0.15
Cb + Ta	4.75	5.50

Inconel 718 contains a significant amount of Iron (17%), which lowers its price per kilogram while endowing it with precipitation hardening effect (Group, 2018). Specific alloying elements give Inconel 718 a strong resistance to corrosion up to 1000°C. Inconel 718 has excellent corrosion resistance to most of the media, which is a function of its composition.

Nickel contributes to corrosion resistance and also becomes useful in combating chloride-ion stress-corrosion cracking. Chromium imparts the ability to withstand attack by oxidizing media and sulfur compounds, and molybdenum has been known to contribute to resistance to pitting.

The high strength, toughness and work hardening makes polishing Inconel 718 a big challenge. Shaping of Inconel using traditional techniques is difficult due to rapid work hardening and built-up edges. Owing to such issues, machining, and polishing of Inconel is preferred using unconventional methods, majorly in a solutionized form.

2.2.2 Heat Treatment

Heat treatment is a controlled process intended to alter the microstructure of metals and alloys to impart the properties, which benefit the working life of a component. Heat treatment generally involves heating or chilling to extreme temperatures, aiming to achieve results such as hardening or softening the material. Common heat treatment techniques include annealing, case hardening, precipitation strengthening, tempering, normalizing, and quenching.

Inconel 718 is an age hardenable austenitic material in which strength is largely dependent on the precipitation of the gamma prime (γ') phase during heat treatment. For a majority of applications, Inconel 718 is specified as solution annealed and precipitation hardened. Alloy 718 is hardened by the precipitation of secondary phases, e.g. (γ') and gamma double prime (γ'') into the metal matrix. The precipitation of these phases is induced by heat treating in the temperature range of 593 to 815°C.

Two heat treatments are commonly utilized for Inconel 718 (Special Metals Corporation, 2007):

i. Solution anneal at 925-1010°C (1700-1850°F) followed by rapid cooling, usually in water and precipitation hardening at 720°C (1325°F) for 8 hours, furnace cool to 620°C (1150°F), hold at 620°C (1150°F) for a total aging time of 18 hours, followed by air cooling.
ii. Solution anneal at 1038-1065°C (1900-1950°F) followed by rapid cooling, usually in water, and precipitation hardening at 760°C (1400°F) for 10 hours, furnace cool to 650°C (1200°F), hold at 650°C (1200°F) for a total aging time of 20 hours, followed by air cooling.

The two heat treatments has their own properties. The first heat treatment at 925-1010°C (1700-1850°F) is the optimum heat treatment where a combination of rupture life, notch rupture life, and rupture ductility is of greatest concern. This heat treatment is also associated with the highest room-temperature tensile and yield strengths (Table 2). Additionally, due to the fineness of the grain developed, this heat treatment produces the highest fatigue strength.

Table 2: Material properties of alloy 718 after first heat treatment at 925-1010°C, reprinted from (Corporation, 2007)

Property	Room Temperature	1200°F
Tensile Strength, ksi	180	140[a]
		145[b]
Yield Strength (0.2% Offset), ksi	150	115[a]
		120[b]
Elongation in 2 In.,%	12	5
Hardness	Rc 36 or equivalent	-
Stress Rupture		
Stress, ksi	-	95[a]
	-	100[b]
Life, hr	-	23
Elongation, %	-	4

[a]Up to 0.025-in. thickness, inclusive.
[b]Over 0.025-in. thickness.

The second heat treatment at 1038-1065°C (1900-1950°F) is the preferred treatment for tensile limited applications since it produces the best transverse ductility in heavy sections, impact strength, and low temperature notch tensile strength. The material meets the requirements as shown in Table 3 after heat treatment.

Table 3: Material properties of alloy 718 after second heat treatment at 1038-1065°C, reprinted from (Corporation, 2007)

Property[a]	AMS 5664 Bars, Forgings, & Rings	AMS 5597 Sheet, Strip, & Plate	AMS 5590 Seamless Tubing[d]
Tensile Strength, ksi	180	180	170
Yield Strength (0.2% Offset), ksi	150	150	145
Elongation, %	10[b]	15	15
	12[c]		
Reduction of Area, %	12[b]	-	-
	15[c]		
Hardness	341 BHN or equivalent	Rc 38 or equivalent	

[a]Transverse direction.
[b]Bars.
[c]Forgings and flash-welded rings.
[d]Properties apply only to O.D. of 0.125-in. and over with wall thickness of 0.015-in. and over.

Figure 8 depicts the matrix of sample treated for 1 hour contains more tiny precipitates while the precipitates of the sample treated for 7 hours appear bigger along the grain boundaries. These particles are identified as carbides (Tucho et al., 2017).

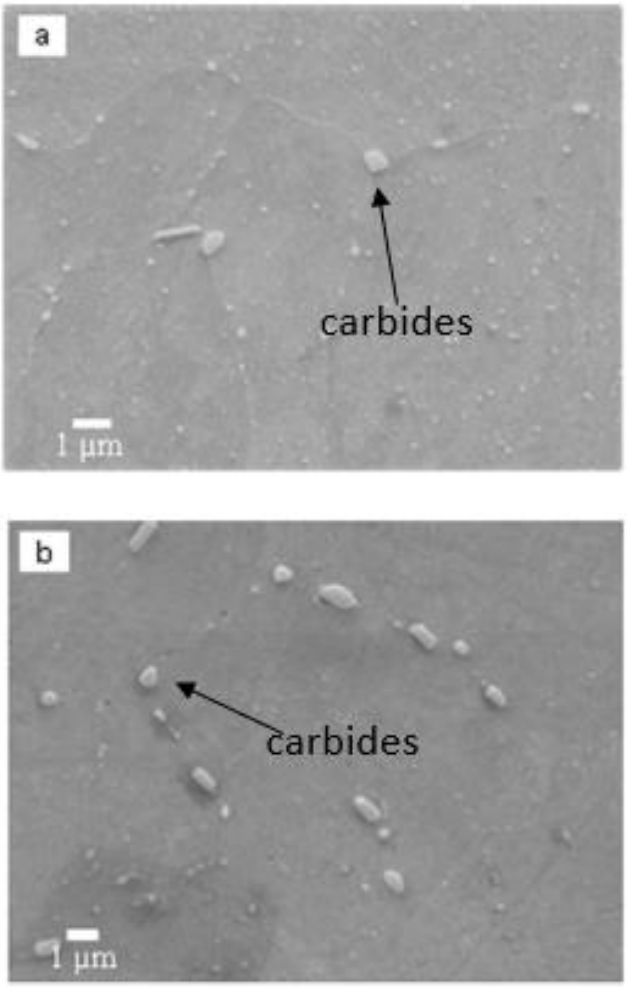

Figure 8: SEM image of heat-treated samples (a) 1100°C/ 1 hr (b) 1100°C/ 7hr, reprinted from (Tucho et al., 2017)

There are other heat treatment methods used for oil field applications. Material for such applications is heat treated at 1010-1038°C (1850-1900°F), aged at 790°C (1450°F) for 6-8 hours, then and air cooled. Table 4 shows the mechanical properties of such heat-treated Inconel 718.

Table 4: Mechanical properties of IN718 for oil tool applications, reprinted from (Corporation, 2007)

Condition	Diameter, in.(mm)	Tensile Strength, ksi (Kg/cm²) min.	Yield Strength (0.2% Offset), ksi (Kg/cm²)		Elongation in 2 in. (50.8 mm) or 4D% minimum	Reduction of Area, % minimum	Impact Strength, ft•lb (Kg•m) min. aver.	Hardness, Rockwell C	
			minimum	maximum				minimum	maximum
Cold worked, solution annealed & aged	0.5 (12.7) to 3 (76.2), inclusive	150 (10,545)	120 (8436)	140 (9842)	20	25	40 (5.55)	30	40
Hot worked, solution annealed & aged	0.5 (12.7) to 8 (203.2), inclusive	150 (10,545)	120 (8436)	140 (9842)	20	25	40 (5.55)	30	40
Hot worked, solution annealed & aged	8 (203.2) to 10 (254), inclusive	150 (10,545)	120 (8436)	140 (9842)	20	25	40 (5.55)	30	40

Every material has its limitations, and for Inconel 718 it is 650°C (1200°F). This implies that when stress and creep resistance is expected, applications are restricted below because the γ'' phase rapidly overages under prolonged exposure at or above this temperature. Figure 9 shows the loss of strength and especially creep life above 650°C (Group, 2018).

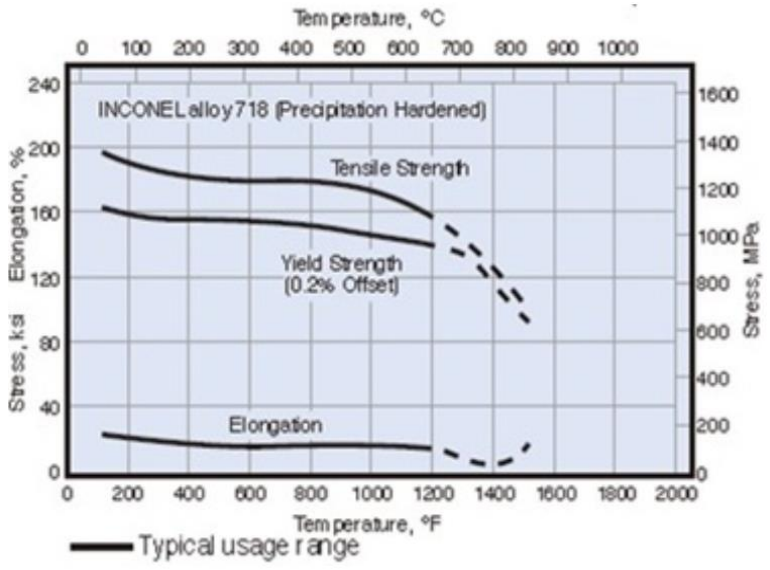

Figure 9: Temperature dependence of mechanical properties for the aged Inconel 718, reprinted from (Group, 2018)

2.2.3 Manufacturing

2.2.3.1 Traditional Manufacturing

Investment casting can produce Inconel 718 parts as it allows final complex net shape compared to other subtractive metal processing methods. However, investment casting can be disadvantageous because of Inconel 718 susceptibility to metallurgical defects such as porosity, segregation, and very coarse grain sizes. Investment casting also reduces functionality and requires further processing, adding to the cost of finished components. For non-structural applications, Inconel 718 is used in the cast and heat-treated condition but for structural applications, investment casted Inconel 718 is hot isostatically pressed (HIP) to minimize shrinkage, porosity, and casting segregation.

Rao et al. (2004) showed that the microstructure of HIPed Inconel 718 after solution treatment at 995^{o}C for 1 hour followed by water quenching and ageing treatment at 720^{o}C for 8 hours of furnace cooling to 620^{o}C and holding at 620^{o}C for 8 hours of air cooling to room temperature. Figure 10 shows (a) broken prior particle boundaries and formation of irregular shaped boundaries (b) uniform precipitation of γ'' and γ' and randomly distributed MC carbides and globular delta (δ) phase in the γ matrix.

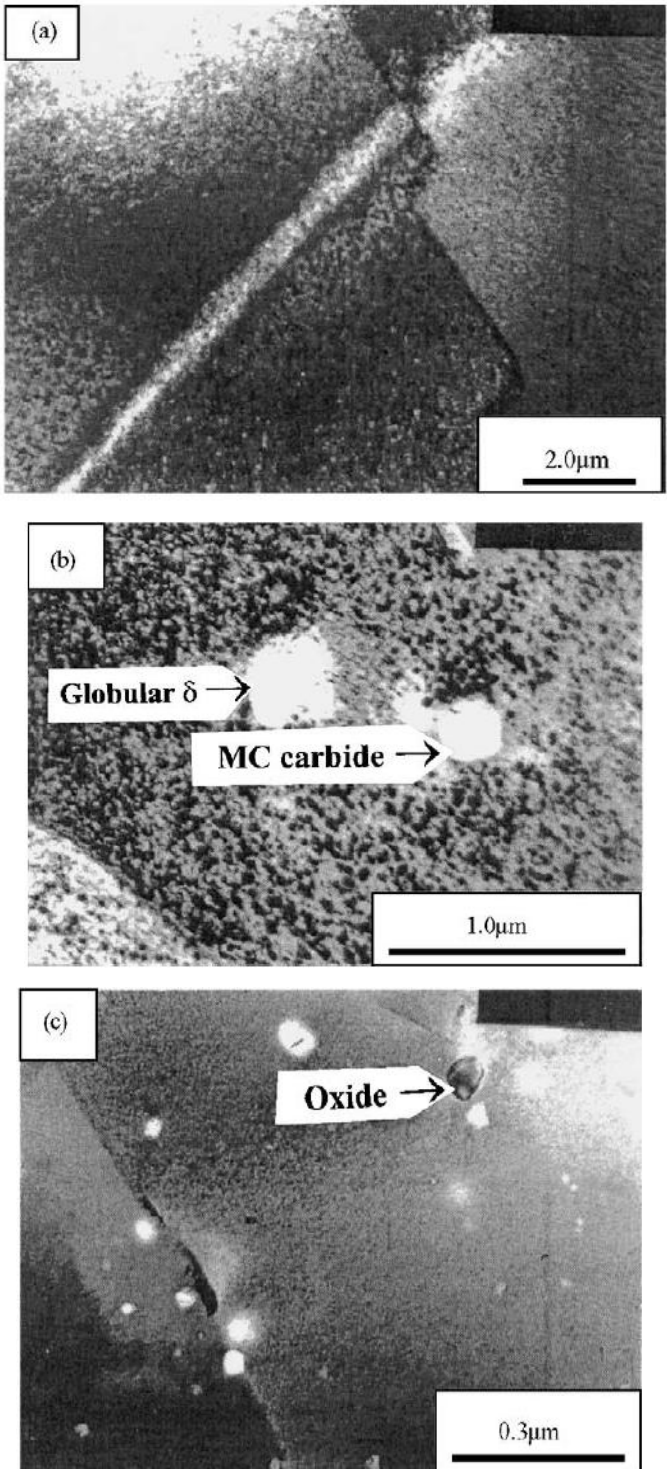

Figure 10: TEM brightfield micrographs of HIPed superalloy 718 at 1150°C, reprinted from (Rao et al., 2004)

Another disadvantage of investment casting is that the zones of local segregation produce regions of high local hardness during heat treatment. These regions induce an increased tool wear and occasional catastrophic tool failure.

Other manufacturing methods like machining, forging, and welding are challenging when applied to Inconel 718. This leads to inferior material properties and lower high temperature corrosion and creep resistance.

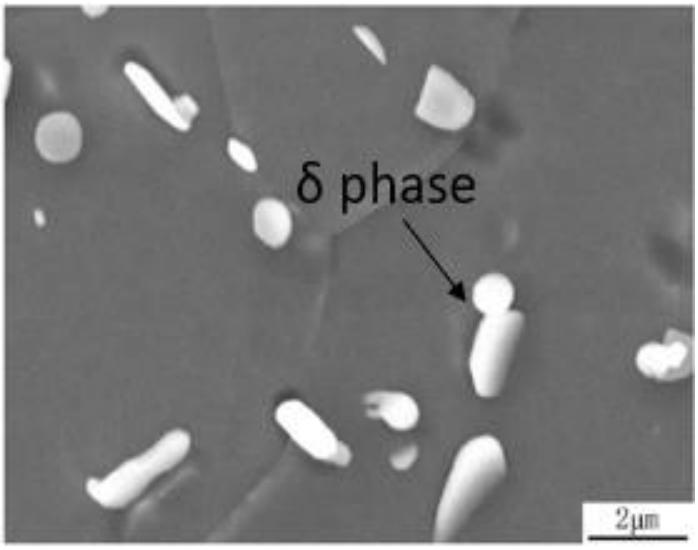

Figure 11: SEM image of delta phase microstructure of forged sample, reprinted from (Wang et al., 2010)

After hot forging or welding microstructure of Inconel 718 included coarse grain sizes and heavy dendritic segregation, caused by the low cooling rate during solidification (Miao et al., 2012). With the rapid development of modern industry, there is a high demand of Inconel 718 parts with complex structures, high dimensional precision and further elevated mechanical properties. Thus, it generates the need of application of novel processing technology to the net-shaped production of Inconel 718 parts with high performing complex configurations. Additive manufacturing has been applied to produce complex Inconel 718 engineering parts.

2.2.3.2 Additive Manufacturing

Additive manufacturing is a term assigned to technologies that build the 3D objects or parts by adding layer upon layer of material in the desired shape or geometry. It can be used with many materials like plastic, metal, ceramic, or paper.

Some of the basic advantages associated with AM of Inconel are:

1. There a variety of AM techniques including direct energy deposition (DED), electron beam melting (EBM), SLM, or selective laser sintering (SLS) used for Inconel manufacturing to preserve the material properties.
2. Additive manufacturing stimulates creativity as engineers get more design freedom to deal with complexity and push for light weighing parts by lattice-structuring design.
3. There is almost no material wastage of expensive superalloys. With layer wise building of components with near-final contours, the process produces only about 5% waste (Group, 2018).

Table 5: AM processes used for each material group, reprinted from (Townsend et al., 2016)

Material	EBM	SLM/ SLS	DED
Nickel alloys	0	100%	0
Aluminum alloys	0	100%	0
Stainless steel	0	87%	13%
Other steels	0	83%	17%
Titanium alloys	35%	50%	15%
Others	0	100%	0

2.2.3.3 Selective Laser Melting (SLM) of Inconel

The SLM is an additive manufacturing method designed to use a high power-density laser to melt and fuse metallic powders together. This category falls under the umbrella of direct metal laser sintering (DMLS) which uses laser to melt or sinter the particles to build 3D objects. It creates the 3D parts, directly from the user defined computer aided design (CAD) data, using a controlled scanning laser beam.

Inconel 718 was well known for its good weldability due to its slow precipitation kinetics (Qi et al., 2009). Precipitation kinetics refers to the slow age-overage precipitation hardening behavior of the γ - γ'' strengthening system. As precipitation kinetics was slow, constraint at the weld interface is minimized, and the stress never rose enough to initiate cracking (Schafrik et al., 2001). This property offers minimal post weld cracking possibilities, which is a conducive property to allow the material to be produced using SLM process.

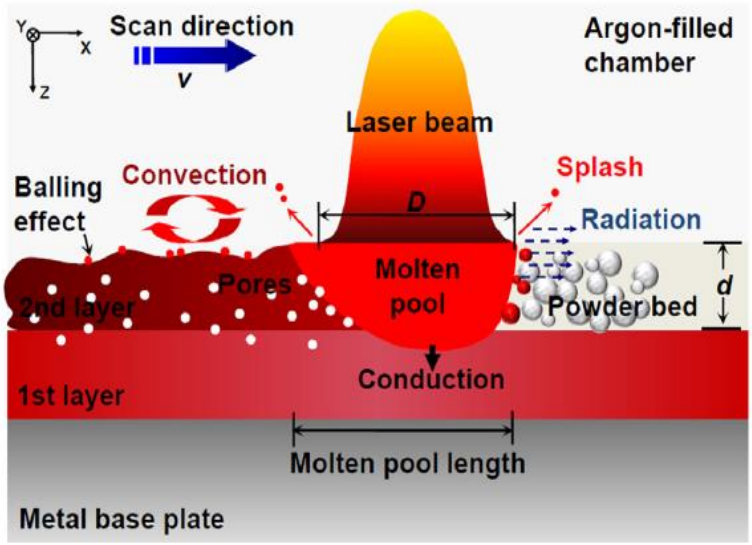

Figure 12: Schematic overview of the interaction zone between laser radiation and powder bed in SLM process, reprinted from (Shi et al., 2016)

As can be seen in Figure 12, as the top surface of the powder bed is irradiated by the incident laser beam, a fraction of the energy is dissipated by radiation and convection. The remaining percentage of the energy is absorbed by the powder particles leading to rapid heating and localized melting. A molten pool is created as the Gaussian laser heat source moves from the melt region and a rapid consolidation of the melt takes place. Finally, the metallurgical bonding is formed between the adjacent tracks and the neighbor layers.

Choi et al. (2017) investigated the microstructure of Inconel 718 part fabricated by SLM method. SLM'ed samples fabricated at scanning speed of 800 mm/s and consisted of uniform microstructure with sound metallurgical bonding. Figure 13 (a-b) depicts that the microstructure of the SLM samples can be characterized by the presence of fine and complex cellular sub-structures confined inside each individual large grain. It was also found that the sub-structures consisted of two different kinds of cellular structures, equiaxed and elongated grains, and that the average size of both cells was between 0.5 and 1 μm.

The microstructure study revealed that the δ particles were deposited at the grain boundaries in forged and cast samples after heat treatment. However, in the SLM samples the δ particles were not only distributed at grain boundaries but also inside the grains (Figure 13a). This is caused by micro segregations of Niobium (Nb) due to the rapid cooling of the melted material (Trosch et al., 2016).

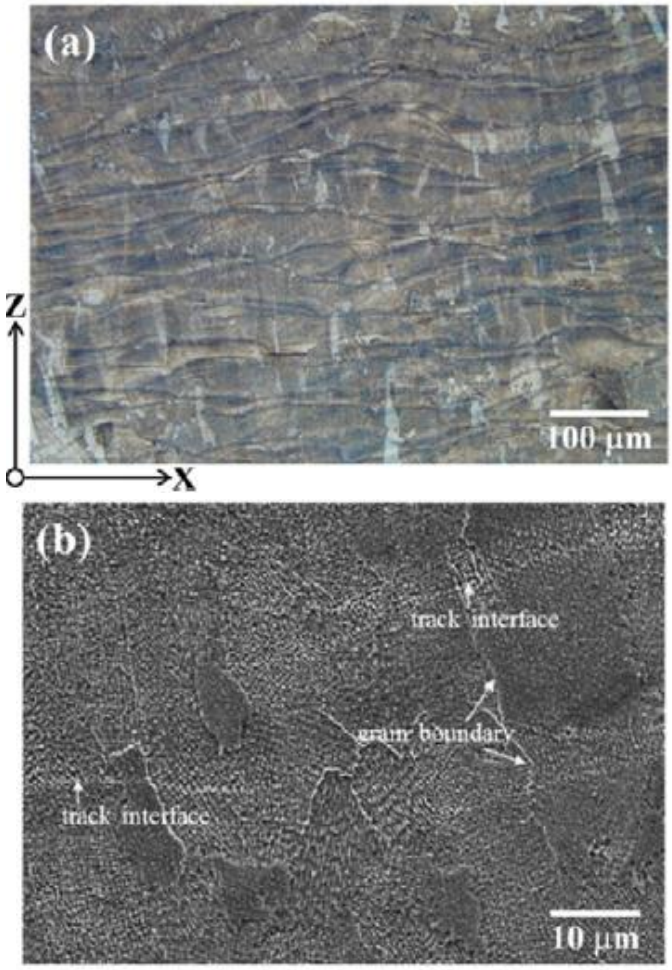

Figure 13: (a) Optical microscope image (b) SEM image of SLM'ed Inconel 718 samples, reprinted from (Choi et al., 2017)

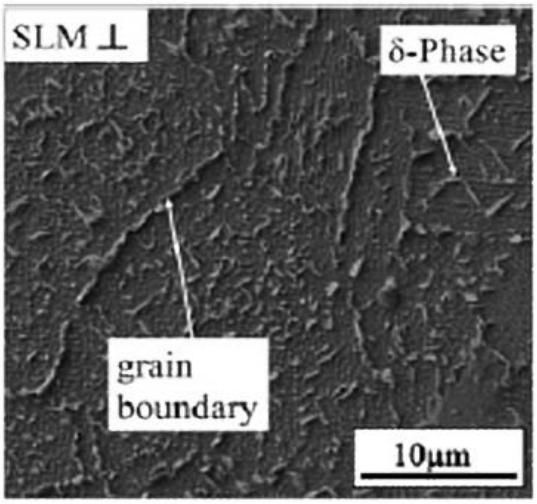

(a)

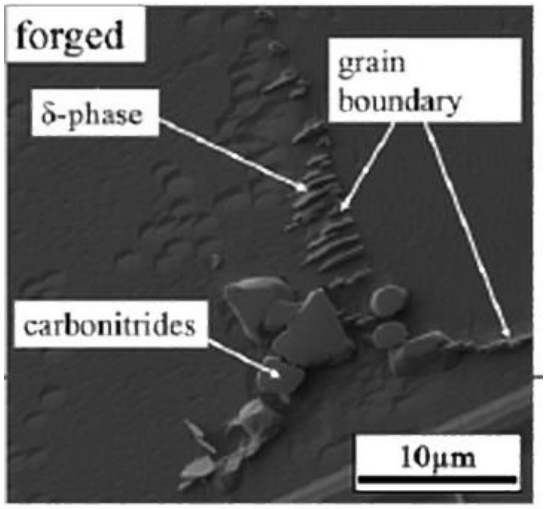

(b)

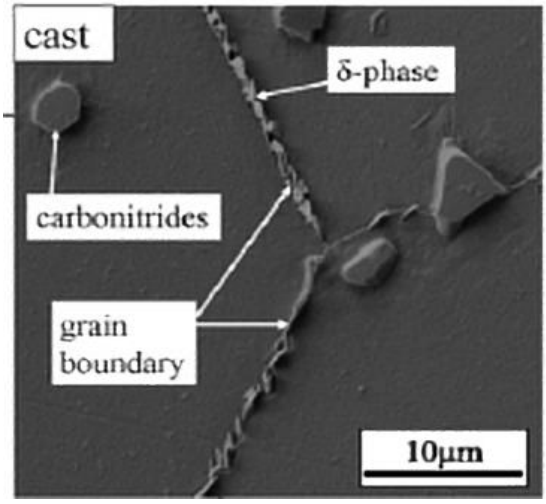

(c)

Figure 14: SEM images of microstructure of (a) SLM perpendicular (b) forged (c) Cast Inconel 718, reprinted from (Trosch et al., 2016)

However, even after achieving the complex geometry, the desired microstructures are inevitably affected due to the complicated physical and chemical behaviors within the molten pool.

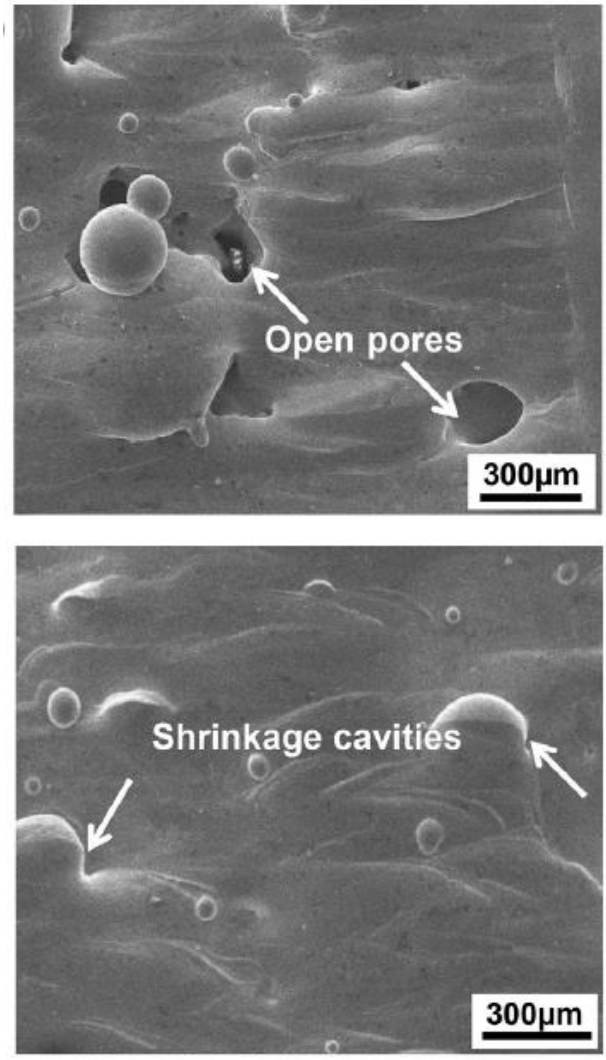

Figure 15: SEM images of surface morphology of SLM manufactured Inconel 718, reprinted from (Jia et al., 2014)

Jia et al. (2014) studied the effect of processing parameters of SLM process on surface morphologies, microstructures, and material properties on Inconel 718. The surface integrity varied significantly for different laser intensities. At a lower laser density, the scanning tracks

were discontinuous having large balls surrounded by open pores (Figure 15a). As the laser density was increased and the scanning speed was lowered, and the scanning tracks became continuous but rudimentary balls with residual shrinkage cavities were still present (Figure 15b).

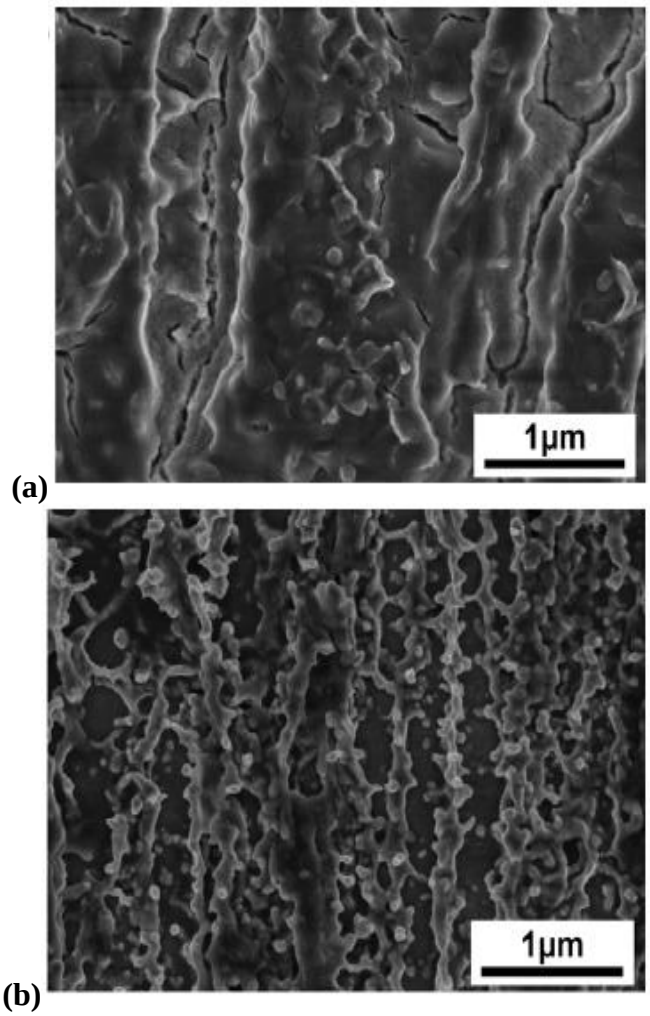

Figure 16: SEM images of microstructure of SLM manufactured Inconel 718, reprinted from (Jia et al., 2014)

The effects of different laser energy density on microstructure was also studied. At lower laser density and high scan speed, columnar dendrites were found long-cracked in the center of the whole trunk (Figure 16a). As the scan speed was decreased, the dendritic arrays got refined

but it was difficult to distinguish due to its severe clustering during the solidification process in the molten pool (Figure 16b).

Multiple studies have shown that even though laser-based AM of Inconel 718 offers advantages compared to subtractive methods, it has a lot of disadvantages such as pores, unmelted powder, and bonding effects as seen in casting. Zhang et al. (2013) found pores with a spherical shape present in the deposits. The pores were likely to be entrapped gas bubbles in the molten metal bead that could not rise and escape to the top surface before solidification. Balling phenomenon and instability of scan tracks were also reported by Niu et al. (1999). These defects were a factor of scan speeds and linear laser density. The inert gas like argon with which the SLM process chamber was filled to avoid contamination, may be got encapsulated inside the pores. Eventually, these pores acted as strong stress raisers and finally lead to failure under fatigue conditions (Wang et al., 2017). Wang et al. (2017) published that the second common defect was the unmelted particles that may appear on the top surface or at the boundary of the deposited layers. Depending on the melting conditions, these particles may have good metallurgical bonding or lack of bonding with the base metal. In some cases, these may also result from spattering.

2.2.4 Applications

As discussed above, Inconel 718 is a superalloy that possesses exceptional mechanical properties and chemical resistance at high temperature. The alloy typically finds its high demanding applications in aerospace, oil/gas, nuclear or turbomachinery industries. Around 50% of produced Inconel 718 is only used in manufacturing aircraft engines in their essential parts including blades, sheets, and discs. It is also widely used in rocket engines and cryogenic

applications (Co.Ltd., 2015). IN718 is a common metal for jet engine structural parts that are operated at high temperatures. It is widely used in General Electric (GE) aircraft engines.

Slow precipitation kinetics makes alloy 718 relatively easy to weld and cast. This enables the use of large, complex structural castings since fabrication and rework is readily accomplished. The same weldability advantage provides cost competition due to alternate processing methods.

Additional tensile and fatigue capability for wrought applications was realized with introduction of clean melt technologies for Inconel 718. A significant portion of fasteners, locking lugs, blade retainers and inserts were manufactured from alloy 718 due to the ease of material processing (Schafrik et al., 2001).

2.3 Summary of Literature Review

Inconel 718 is a popular material used with high temperature applications and in extreme working environments. Manufacturing of Inconel by subtractive methods is challenging due to loss of material properties. Hence, AM of Inconel is promising to meet the requirements of the industry. The SLM method is used for producing near net shaped Inconel 718 products. However, manufacturing on optimized SLM parameters is taking place to improve the quality of parts.

It has also been concluded that scan speed and laser energy density have a dominant effect on the density of the parts and, stair stepping effect can be minimized significantly upon using less thick powder in the SLM process. There has been a lot of research on improving the mechanical properties of SLM printed parts by a variety of processes like heat treatment, HIPing to get better tensile and yield properties compared to traditional manufactured parts. Several statistical approaches have been studied to evaluate the effect of the process parameters on the surface roughness of SLM parts and hence optimize them.

However, there has been little research in the field of using post-processing techniques to improve the surface finish of SLM produced parts. The as-built SLM part's surface is very rough with partially welded particles at the surface. The loosely welded particles and other defects such as solidification shrinkage and surface crack are a major concern for the reliability of the component.

Thus, in this study, ECP is used to polish the Inconel 718 parts produced by SLM. Since ECP is a non-mechanical method and does not involve tool and workpiece contact, it is an ideal method for polishing a hard material as Inconel.

3. LABORATORY SYSTEM

This section describes the design and set-up of the laboratory system. It also covers the preparation of the workpiece by SLM.

3.1 Lab Set-Up

The laboratory set-up for ECP experiments is shown in Figures 17 and 18.

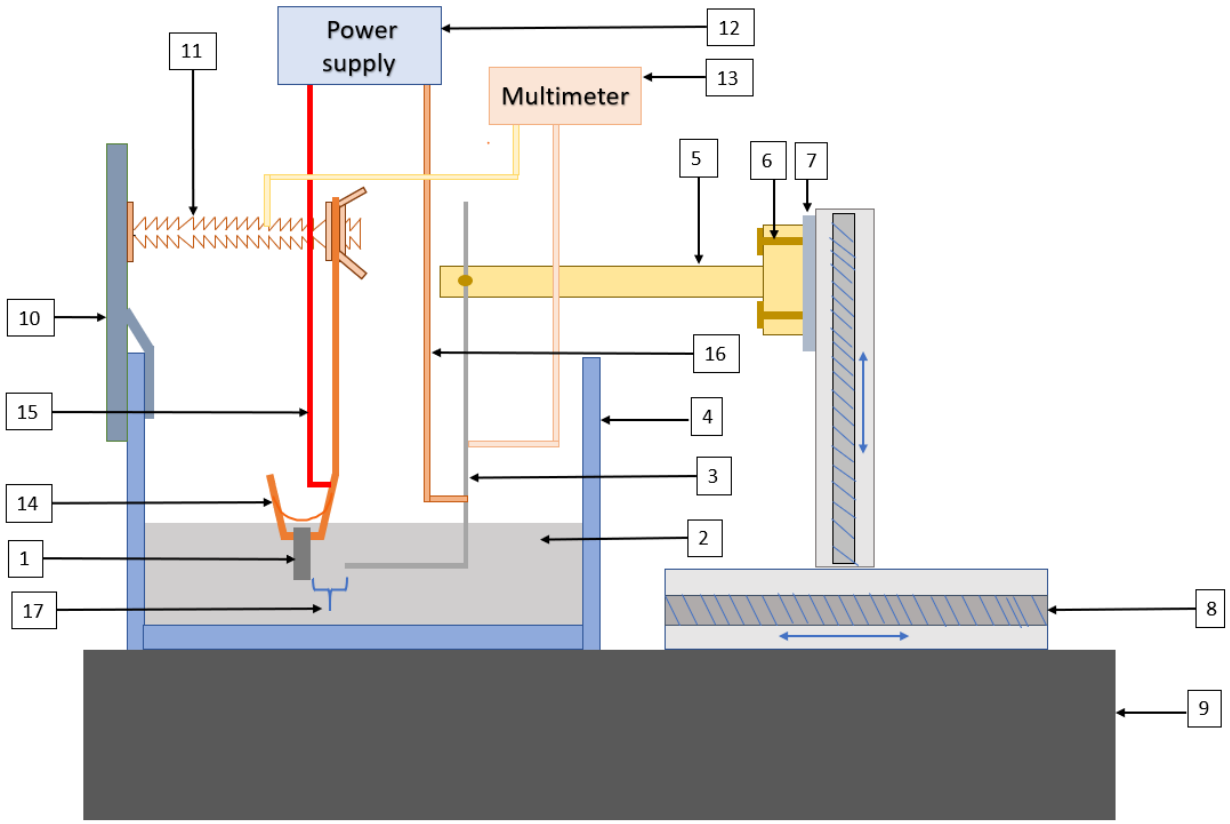

Figure 17: Schematic of Electropolishing system (Front-view)

(a) 

(b) 

Figure 18: (a) Actual ECP set-up (b) Details of ECP cell

The components of the laboratory system are as follows:

1. Inconel workpiece

2. Acid based electrolyte, EP-2000

3. Titanium electrode

4. ECP cell, ESMA model E1085-1S

5. Polyjet printed tool holder and insulator

6. M5 Bolts

7. Metal plate

8. Two-axis Velmex bi-slide system

9. Granite block

10. Support for workpiece attachment

11. Titanium screw

12. Dynatronix (CRS-LFP(R)) power supply

13. Tenma 72-6202 multimeter

14. Titanium clips

15. Anode terminal

16. Cathode terminal

17. Inter-electrode gap (IEG)

The entire set-up rests on a granite block, as depicted by (Figure 17-9) to minimize vibration and maintain rigidity during experiments. The existing laboratory system was designed to make the tool move horizontally. The 2 mm diameter tool electrode was made from a titanium rod to avoid rusting due to contact with the electrolyte. The tool had spherical end to avoid and eliminate workpiece or tool mounting errors (Figure 19). Figure 19a shows that if the tip of the tool was flat and there was an error in mounting of the workpiece (as depicted by dashed lines in Figure 19a), the IEG would not be held constant throughout the entire polishing zone and similarly if the tool is not mounted perpendicularly (as depicted by dashed lines in Figure 19b) to the workpiece, there will be an inconsistent IEG. Both these scenarios would lead to inaccurate results and varied polishing effect. Thus, the tip of the tool was rounded to a hemispherical shape for avoiding such errors (Figure 19c).

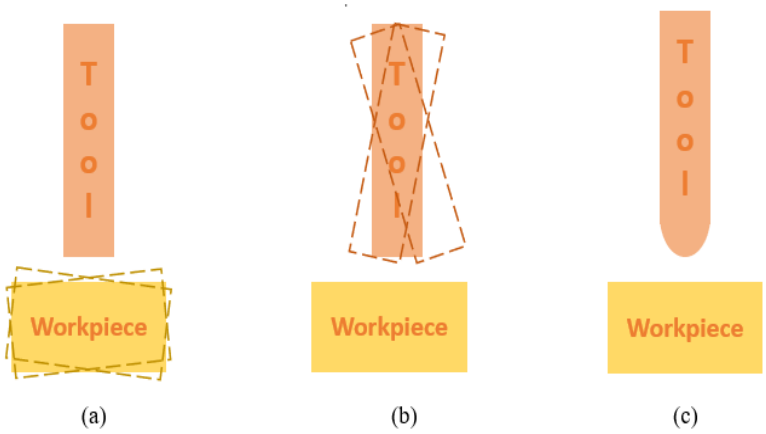

Figure 19: Effect of electrode tool tip geometry on interelectrode gap

The titanium electrode tool tip was rounded by grinding its end in a 10 mm thick, 60 x60 mm steel plate. A round tip drill bit of diameter 2.5 mm was used to drill a 4 mm deep hole in the center of the steel plate as shown in Figure 20. To allow smooth finishing of the tool tip a water-based diamond polishing paste with diamond size of 7/5 µm was fed in to the drilled hole. The flat end titanium rod tool was then rotated using a drilling machine at 30 rpm to round the end, keeping it inside the previously drilled hole with diamond paste. The tip was then viewed under a magnifying glass to ensure proper roundness.

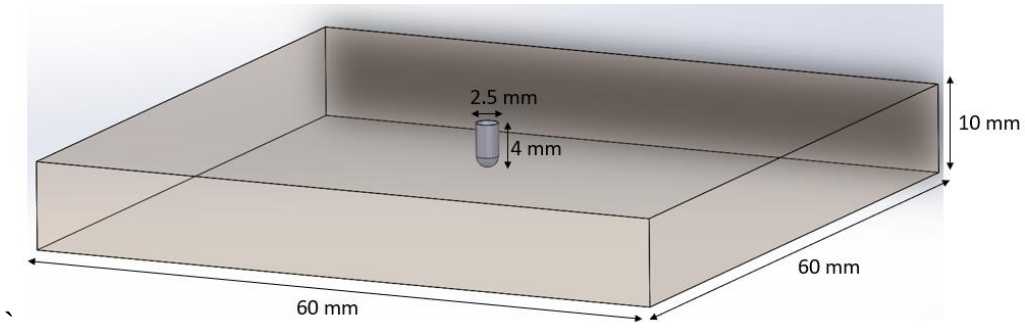

Figure 20: Fixture for rounding titanium tool tip

The workpiece holder has a titanium clip at its end for securing (Figure 17-14) the Inconel workpiece. The gap between the workpiece (Figure 17-1) and the tool (Figure 17-3) is called as IEG (Figure 17-17). It can be adjusted by moving the electrode using a COSMOS program on the Velmex bi-slide system, in two directions, vertically and horizontally at 2.5 µm resolution. (Appendix A).

The tool holder (Figure 17-5) was additively manufactured using the polyjet printing process or vat photopolymerization. The non-conductive material of the tool holder ensured that it acted as the insulator and did not carry the current applied for experiments to the Velmex bi-slide system. This is important as the current from the power supply might damage the stepper

motors used in the bi-slide system. The detailed drawing of the tool holder is attached in Appendix B.

The EP 2000 electrolyte (Figure 17-2) was poured into the ECP cell, till it completely submerged the workpiece and the tool. The electrolyte should be handled carefully with the use of gloves and safety goggles. The anodic terminal (Figure 17-15) and cathodic terminal (Figure 17-16) were clipped on to the workpiece (Figure 17-1) for connecting the workpiece to the power supply (Figure 17-12).

Detailed description of all components can be found in the Appendix B.

3.2 Workpiece Preparation

The Inconel 718 blocks were SLM printed to 15 x 20 x 5 mm on the Renishaw AM250 system. The 15 x 20 mm base surface was on the scanning x-y plane while the 5mm was on the building z-direction (Figure 21). The average diameter of IN718 powder was 50 µm. Powder was fused together using a YAG laser at 160 W power with a hatching distance of 110 µm in argon gas.

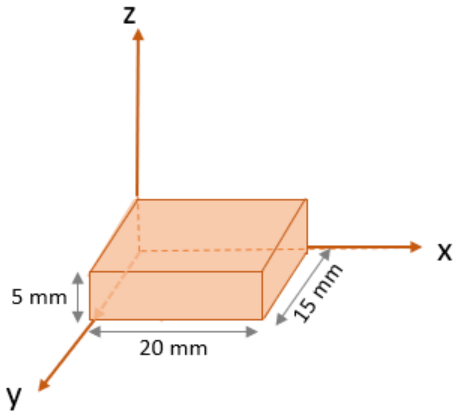

Figure 21: Orientation of SLM'ed IN718 block

The stripe scanning strategy was adopted for the manufacturing of blocks. In the stripe configuration the deposition direction is not changed in the same layer, but angle is shifted by 67° from layer to layer (Figure 22). After every 7 layers, the pattern repeats itself. All specimen columns were cut off, perpendicular to the z-axis to separate them from the machine platform using wire type electrical discharge machining (wire EDM).

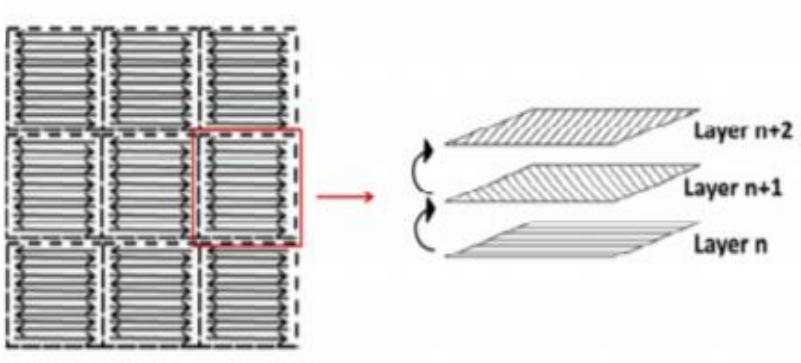

Figure 22: Stripe Strategy for SLM of IN718, reprinted from (Mancisidor et al., 2016)

4. EXPERIMENTS

4.1 Design of Experiments

A full factorial experiment was conducted based on three ECP input parameters. The variables selected were based on the literature review and previous research in similar fields (Baicheng et al., 2017; Feng, 2018; Wang et al., 2015). Three levels of every parameter were designed to study the detailed effect.

It should be noted that current density varies as the peak current changes. The current density for every current value is given in Table 6. The current density is calculated by:

$$Current\ density\ (\ A/mm^2) = \frac{Peak\ Current\ (A)}{Cross\ sectional\ area\ of\ the\ electrode\ (mm^2)} \quad (2)$$

Table 6: Current density for corresponding values of current

Current (A)	Electrode diameter (mm)	Current density (A/mm^2)
1.0	2.5	0.2
3.5		0.7
6.0		1.2

Table 7 shows different experimental factors and their levels.

Table 7: Experimental input parameters

Independent variables	**Levels**
Peak current (A)	1.0, 3.5, 6.0
Polishing time (sec)	90, 180, 270
Duty cycle (%)	25, 50, 75
Dependent variables	**Levels**
On-time (ms)	10, 20, 30
Current density (A/mm^2)	0.2, 0.7, 1.2
Constant Parameters	
Current frequency (Hz)	25
Interelectrode gap (mm)	0.5
Temperature (°C)	25 - 28
Electrolyte	Commercial acid-based, EP 2000
Workpiece material	Inconel 718
Tool material	Titanium

- Electrolyte

A commercial and proprietary mixture of phosphoric and sulphuric acids was used. It consisted of a high percentage of phosphoric acid about 40-80% and sulphuric acid with 5-35% by weight. Although, this electrolyte can be used up to 65°C (150°F) but was used at room temperature in this study, since a high temperature leads to aggressive chemical reactions suitable for machining but not polishing. A fresh electrolyte was used for every set of 27 experiments.

- Inter-electrode Gap

The IEG of 0.5 mm was kept constant for this experimental study. A variety of experiments were performed at different levels of IEG to decide the optimal gap. Gap was varied from 0.5 to 2 mm

for preparatory experiments. A gap too large combined with low level of current lead to lower current density and resulted in almost no change in surface finish. A gap too small might cause short-circuit of the electrical system.

- Frequency

A low frequency of 25Hz was applied to all experiments while varying the duty cycle at three levels.

Thus, a full factorial resulted in 27 experiments (Table 8) which were performed on Inconel SLM as well as extruded Inconel parts.

Table 8: Factorial design

Number	Current (A)	Current density (A/mm^2)	Time (sec)	Duty Cycle (%)
1	1	0.2	90	25
2	3.5	0.7		
3	6	1.2		
4	1	0.2	180	
5	3.5	0.7		
6	6	1.2		
7	1	0.2	270	
8	3.5	0.7		
9	6	1.2		
10	1	0.2	90	50
11	3.5	0.7		
12	6	1.2		
13	1	0.2	180	
14	3.5	0.7		
15	6	1.2		
16	1	0.2	270	
17	3.5	0.7		
18	6	1.2		
19	1	0.2	90	75
20	3.5	0.7		
21	6	1.2		
22	1	0.2	180	
23	3.5	0.7		
24	6	1.2		
25	1	0.2	270	
26	3.5	0.7		
27	6	1.2		

4.2 Experimental Procedure

Before running every experiment, the IEG was set using a digital multimeter and the Velmex positioning system as follows:

i. The workpiece was secured in the clip holder and the tip of the tool was always cleaned to ensure proper conductivity.

ii. The terminals of the digital multimeter were connected to the workpiece (anode) and the tool (cathode).

iii. The tool was slowly brought close to the workpiece using the Velmex system (Figure 23a).

iv. As the tool touched the workpiece, beeping sound on the multimeter indicated the contact (Figure 23b) and the movement of the tool was stopped immediately.

v. This stage indicated zero interelectrode gap between workpiece and tool.

vi. Using COSMOS program, the tool was moved 0.5 mm away from the workpiece, and thus, the initial IEG was set (Figure 23c).

vii. These steps were repeated 3-5 times to ensure the repeatability of the IEG.

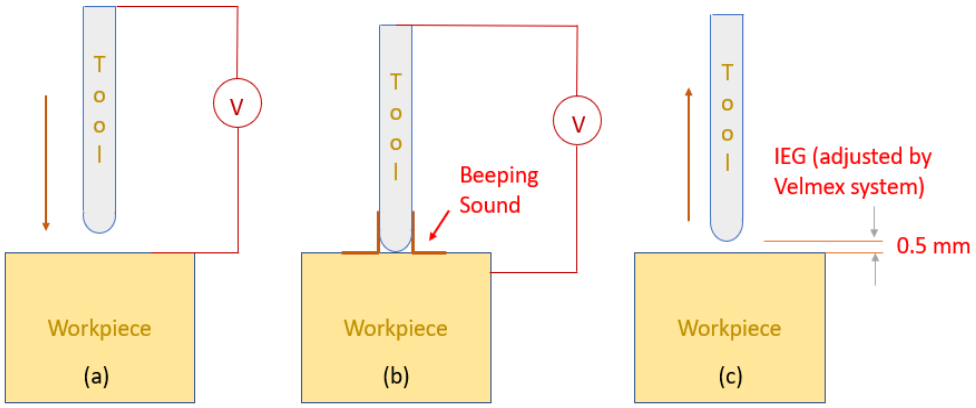

Figure 23: Schematic representation for setting IEG

4.2.1 Step by Step Procedure for Running the Experiments

1. Every workpiece (extruded or SLM) was ground on a 180-grit paper. The direction of grinding was kept constant for all the workpieces.

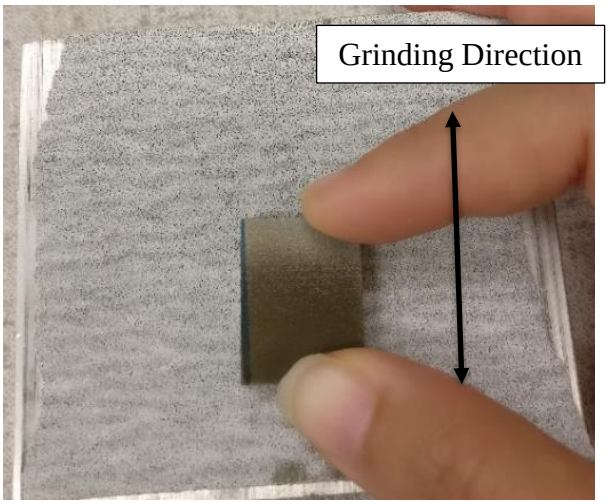

Figure 24: Grinding direction on a 180-grit paper

2. It was then cleaned ultrasonically for 7-8 minutes by completely immersing in rubbing alcohol to remove any contaminants.

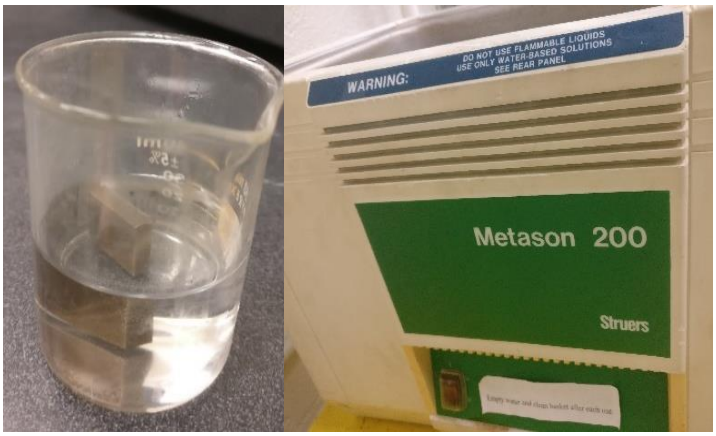

Figure 25: Ground block immersed in rubbing alcohol (left), ultrasonic cleaner (right)

3. After ultrasonic cleaning, the workpiece was dried with compressed air, holding it through the edges using a tweezer.
4. Before running experiments, half of every block was taped with plating tape as every block was used for running 2 experiments. This ensured that the taped half is not affected by the electrolyte while the other half is getting polished. The taping is done along the width of the block.

Figure 26: Half-taped workpiece

5. Other input parameters like current, time and duty cycle are then set on the Dynatronix power supply by using the software Microstar pulse interface.
6. All the connections are ensured, and the power supply is turned on to 'operate' mode for running an experiment.
7. The power supply automatically turns off, after the set polishing duration.
8. After the experiment is performed, the workpiece is removed along with the holder and cleaned with running tap water.
9. The workpiece is finally dried using compressed air and stored in dry box.
10. Surface analysis is carried out later.

4.3 Measurement of Output Parameters

The quantities measured as output parameters are: Surface roughness (S_a, S_q) and, Line roughness (R_a, R_q). S_a and R_a are the most commonly used parameters because they provide a simple value for accept/reject decisions. They are the arithmetic average heights of the roughness-component irregularities (peak heights and valleys) from the mean line. S_q and R_q are also called as root mean square or RMS. They are more sensitive to occasional highs and lows and is a valuable complement to S_a and R_a . S_q and R_q are the geometric average heights of roughness component irregularities from the mean line. The main difference between two scales is that S_q and R_q amplifies occasional high or low readings, while S_a and R_a simply averages them.

The Alicona IF 3D profiler was used to measure the surface roughness (S_a) and line roughness (R_a) of the electrochemical polished Inconel 718 surface. The profiler generates 3D models of the polished features based on the principle of focus variation.

4.3.1 Surface Finish Measurement

A surface finish was measured in two directions, parallel and perpendicular to the grinding marks. The profiles were scanned in the two orientations using Alicona IF 3D profiler as shown schematically in Figure 27. A polished zone of the polished spot was the junction of tool electrode axis and workpiece.

Surface waviness of a polished surface was expected due to spherical end of the electrode; however, the waviness profile was removed using the Alicona form removal tool before the surface roughness measurements were performed.

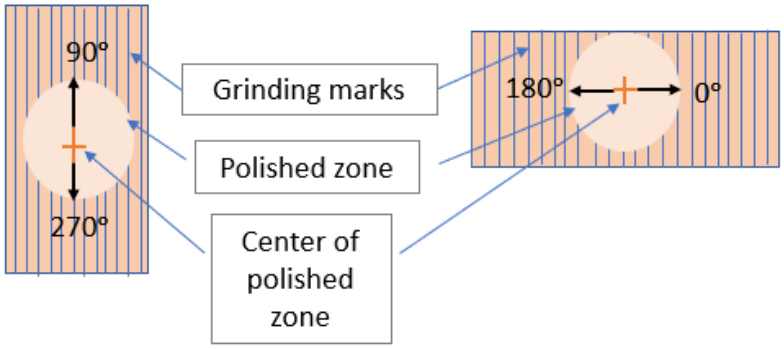

(a) (b)

Figure 27: (a) Parallel to grinding marks, (b) Perpendicular to grinding marks

The surface finish readings were recorded at four points for every single experiment, by moving away from the polished spot. As seen in Figure 28, the locations 0, 1, 2, and 3 represent the points where area surface roughness S_a was measured in the area of 1mm x 1mm square area and line roughness R_a was measure along a 1mm line. For each measurement, a new line and new area were established for repeatability assessment. The origin O represents the electrode center line, location #1 represents the spot right next to it moving away 1mm in either direction (0° or 90°). Similar procedure was followed for locations #2 and #3 located 2mm and 3mm away from the central zone.

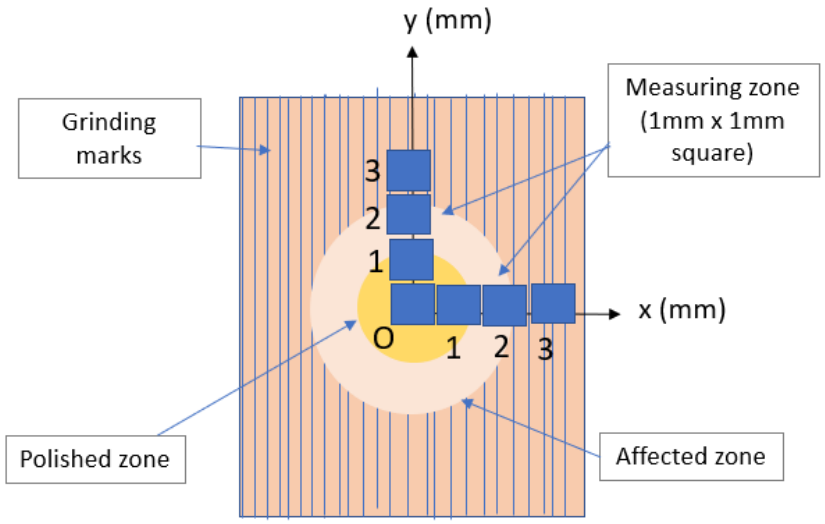

Figure 28: ECP sample and measuring locations

Microstructure study was performed using Olympus optical microscope and VEGA3 TESCAN SEM. Regression models were built from surface finish data of the samples using Minitab software.

4.3.2 Measuring Surface Roughness (S_a and R_a)

(a) Measuring parallel to grinding direction

After the spot was polished and scanned, the profile of the polished sample was evaluated using the profile form measurement on Alicona. Figure 29 shows the cross-section of a typical profile under evaluation. The central dip in the profile indicated the polished spot; it provided the exact coordinates for locating points #0-3. The line and area surface roughness measurement were then performed.

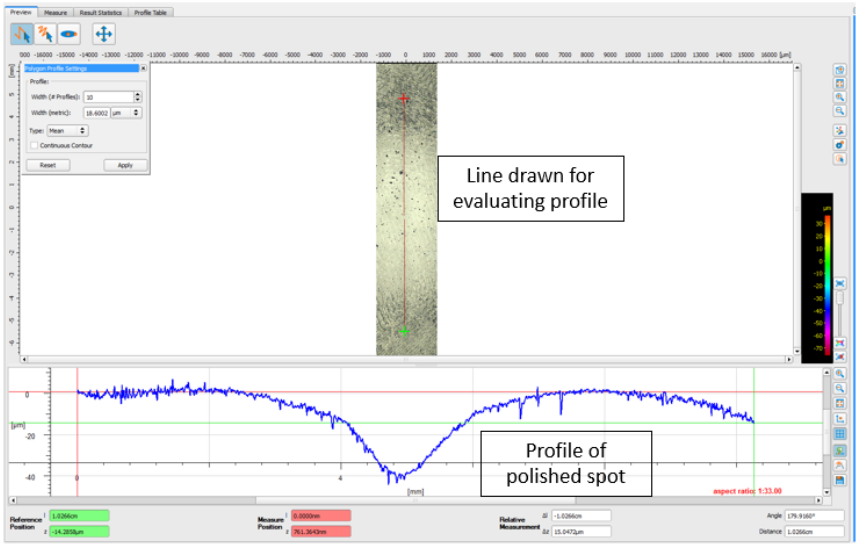

Figure 29: Cross-section of the profile for polished sample in parallel direction

After the extraction of coordinates, the form removal tool of Alicona was used to remove the waviness and then based on the coordinates of the polished spot from Figure 29, a 1mm x 1mm square area was drawn (Figure 30a), the magnified region of the square was depicted by Figure 30b, and finally the area roughness values were recorded (Figure 30c).

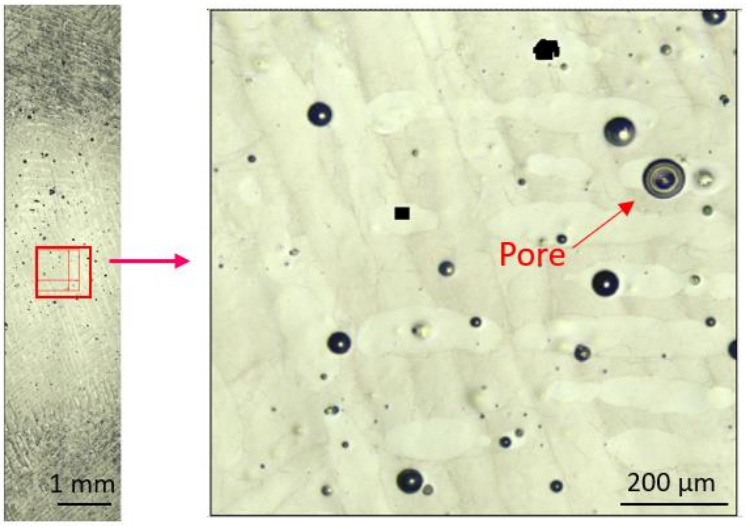

(a) (b)

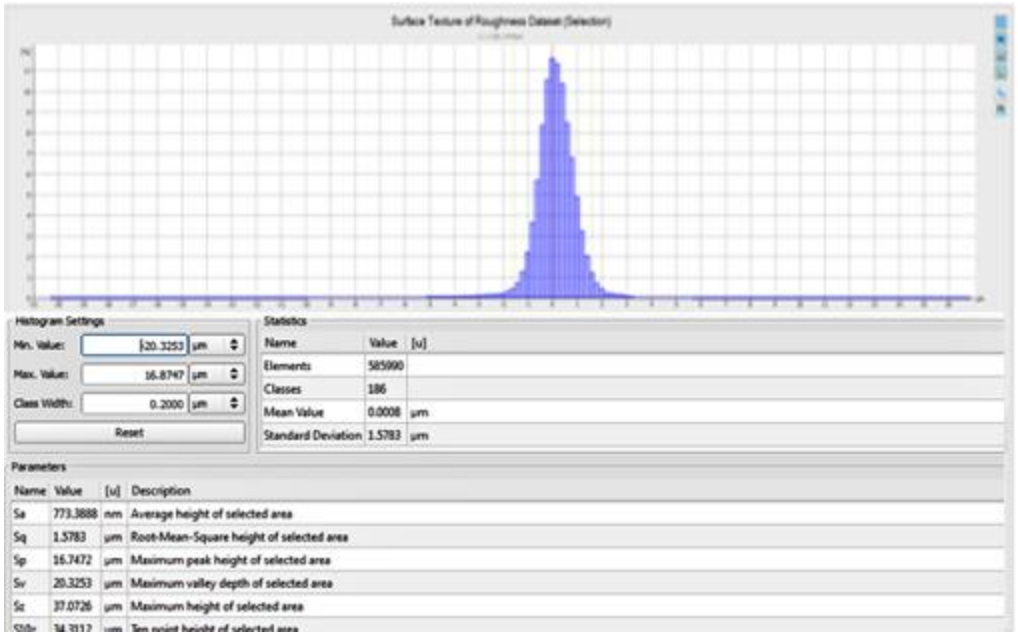

(c)

Figure 30: Sa measured for parallel grinded sample (a) 1mm x 1mm square for measuring S_a, (b) Magnified image of selected region (c) surface roughness value of the area selected

Line roughness (Ra) measurement along a line parallel to the grinding direction was carried out in the same way as S_a , over 1 mm line. New area and line were drawn in the neighborhood for repeatability assessment.

(b) Measuring perpendicular to grinding direction

The sectional view of a profile along a line perpendicular to grinding direction is shown in Figure 31. The central dip of the curve in Figure 31 represents the polished spot on the sample. Based on the coordinates provided by the profile, line and area surface roughness were recorded after removing the form.

Figure 32 shows the measurement of line roughness (R_a) over a 1 mm profile length.

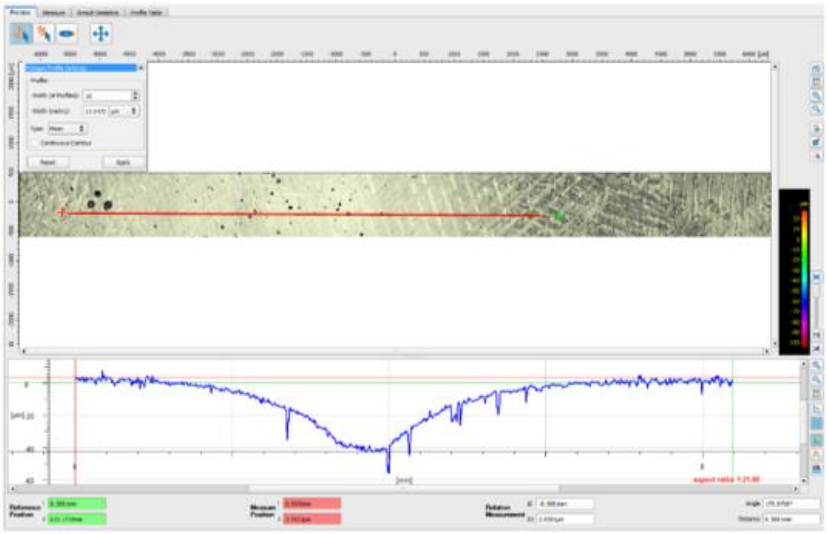

Figure 31: Cross-section of the profile for polished sample in perpendicular direction

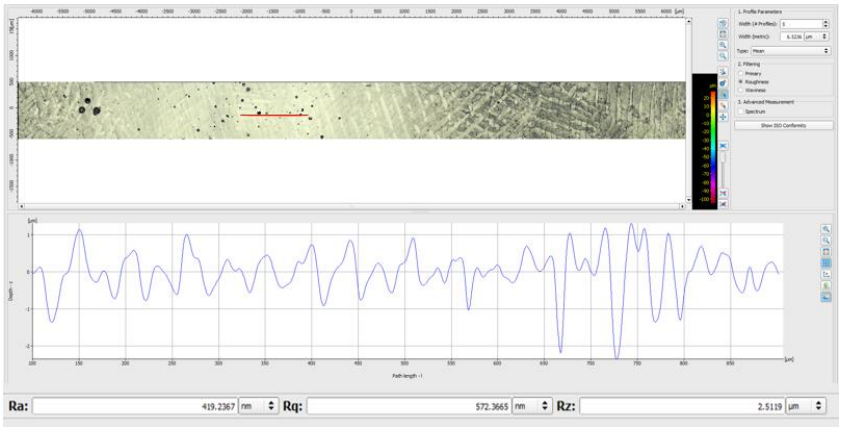

Figure 32: Line roughness over a profile length of 1 mm

Surface roughness (S_a) measurement for perpendicular grinding direction was carried out in the same way as Ra, over 1 mm x 1mm square area.

All 27 samples for each extruded and SLM samples were measured as mentioned above. Surface measurement at each location was repeated eight times for each polishing condition as mentioned in Table 10. They were then compared against the first four measurements to gage

any statistical significance. Assuming no significant difference on the results whether four or more measurement was made, only four data points were taken at every polished spot (two along the parallel direction, and two along the perpendicular direction). The raw data can be found in Appendix C.

After their surface finish measurements on Alicona, all samples were observed on the optical microscope. Two samples from both extruded and SLM groups were selected to be viewed for scanning electron study.

5. RESULTS AND DISCUSSION

This section discusses the repeatability of data, the effect of ECP process parameters on the surface finish of Inconel 718 parts. It also compares the different results on the extruded and SLM samples.

5.1 Surface Roughness

Figure 33 shows the surface roughness of the SLM parts at each stage. It shows the improvement in the surface finish of the samples from the as-built to after electropolished stage.

Table 9: Surface finish at different stages

Condition	Sa1 (µm)	Sa2 (µm)	Sa3 (µm)	Sa4 (µm)	Standard deviation
As-built	16	14.5	13	17.2	1.82
Sanded	4.5	3.2	5.6	4.1	0.99
ECP	0.7	0.73	0.77	0.52	0.11

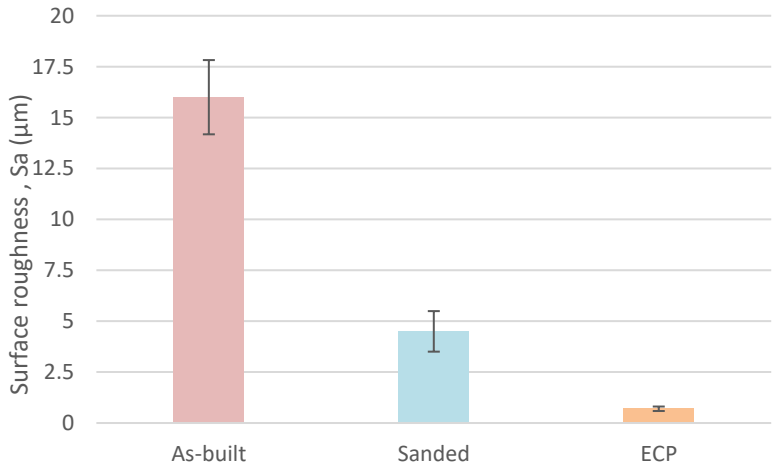

Figure 33: Improvement in surface finish of SLM sample.
ECP at 1.2 A/mm^2, 180 s, 50% duty cycle, average of 4 data points

The experiments were conducted based on the factorial design given in Table 8. As mentioned above, the surface roughness readings were measured in two directions, parallel and perpendicular. Figure 34 shows (i) comparable magnitudes and standard deviations of line surface roughness were achieved in both directions for a specific set of process variables, and (ii) sub-micron surface finish can be achieved. This shows that ECP is independent of direction and polishes the sample uniformly. Table 10 shows the data used for comparison.

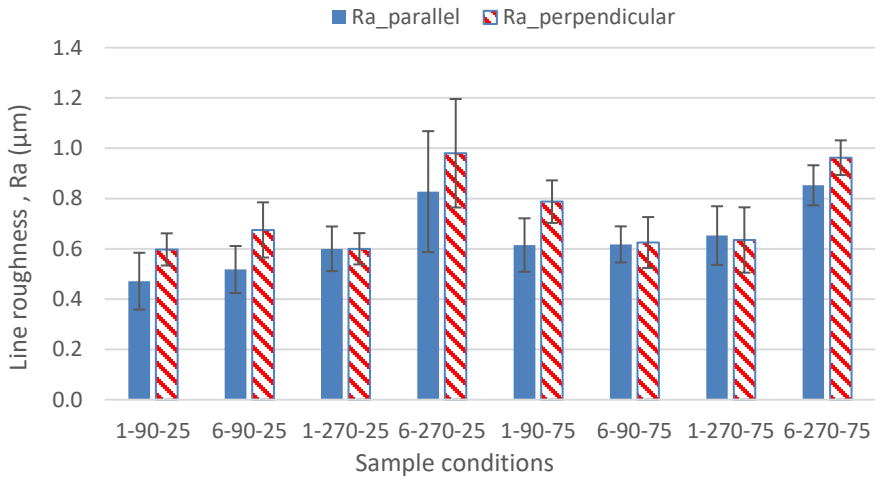

Figure 34: Graph depicting negligible deviation in parallel and perpendicular line roughness (Ra)

Table 10: Data for parallel and perpendicular roughness comparison

Polishing condition	Parallel				σ for Ra1-4	Perpendicular				σ for Ra5-8
	Ra1 (µm)	Ra2 (µm)	Ra3 (µm)	Ra4 (µm)		Ra5 (µm)	Ra6 (µm)	Ra7 (µm)	Ra8 (µm)	
1-90-25	0.425	0.64	0.4	0.42	0.11	0.57	0.53	0.61	0.55	0.06
6-90-25	0.61	0.58	0.48	0.47	0.09	0.62	0.58	0.63	0.59	0.11
1-270-25	0.57	0.65	0.69	0.49	0.09	0.67	0.63	0.57	0.53	0.06
6-270-25	1.18	0.66	0.78	0.99	0.24	0.97	0.93	1.05	0.61	0.22
1-90-75	0.73	0.67	0.49	0.57	0.11	0.74	0.7	0.82	0.71	0.08
6-90-75	0.59	0.53	0.66	0.69	0.07	0.65	0.59	0.51	0.75	0.10
1-270-75	0.77	0.5	0.71	0.63	0.12	0.69	0.65	0.45	0.75	0.13
6-270-75	0.94	0.84	0.78	0.81	0.08	0.93	0.89	0.94	0.85	0.07

It was shown above that ECP results are independent of measuring directions; therefore, the line surface roughness Ra for both the parallel or perpendicular measurements are considered equivalent. Table 11 shows and compares the standard deviations for four measurements (Dev.4) against eight measurements (Dev.8). Since the maximum percentage difference of those values is 11%, it was assume that four surface finish measurements at a single location would be sufficient to represent the surface finish at that location. All subsequent surface finish measurements were performed four times at each location.

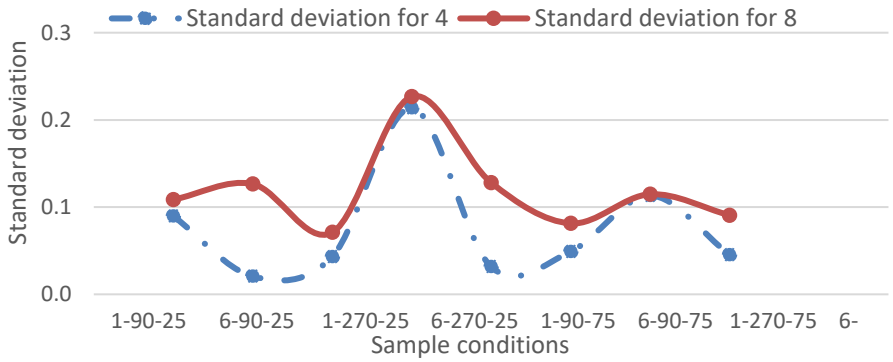

Figure 35: Standard deviation in points for 4 and 8 data points

Table 11: Comparison of standard deviation for 4 and 8 data points

Polishing Condition	Ra1 (µm)	Ra2 (µm)	Ra3 (µm)	Ra4 (µm)	Ra5 (µm)	Ra6 (µm)	Ra7 (µm)	Ra8 (µm)	Standard deviation		
									Dev.4 (Ra1-4)	Dev.8 (Ra1-8)	Difference (%)
1-90-25	0.425	0.64	0.57	0.53	0.4	0.42	0.61	0.68	0.09	0.11	2%
6-90-25	0.61	0.58	0.62	0.58	0.41	0.47	0.67	0.83	0.02	0.13	11%
1-270-25	0.57	0.65	0.67	0.63	0.69	0.49	0.57	0.53	0.04	0.07	3%
6-270-25	1.18	0.66	0.97	0.93	0.78	0.69	1.27	0.75	0.21	0.23	1%
1-90-75	0.73	0.67	0.74	0.7	0.49	0.57	0.82	0.89	0.03	0.13	10%
6-90-75	0.59	0.53	0.65	0.59	0.66	0.69	0.51	0.75	0.05	0.08	3%
1-270-75	0.77	0.5	0.69	0.65	0.71	0.63	0.45	0.75	0.11	0.11	0%
6-270-75	0.94	0.84	0.93	0.89	0.75	0.88	0.98	1.05	0.05	0.09	5%

5.1.1 Repeatability Study

A set of 15 extruded samples were electropolished in a random order to check the repeatability of the ECP system. Average error came to be within ± 7% as shown in Table 12 below.

Table 12: Repeatability of ECP results.

Sample number	Current density (A/mm^2)	Time (sec)	Duty cycle (%)	Original Ra (µm)	Repeated Ra (µm)	Percentage error (%)
1	0.20	180	25	0.77	0.75	-3%
2		180	75	0.58	0.55	-5%
3		270	25	0.73	0.69	-5%
4		270	75	0.55	0.53	-4%
5	0.70	90	75	0.54	0.58	7%
6		180	75	0.45	0.42	-7%
7		270	75	0.21	0.2	-5%
8		90	25	0.67	0.69	3%
9		180	25	0.63	0.65	3%
10		270	25	0.58	0.566	-2%
11	1.20	90	25	0.67	0.695	4%
12		90	75	0.43	0.46	7%
13		180	25	0.5	0.53	6%
14		180	75	0.45	0.465	3%
15		270	25	0.6	0.58	-3%

5.1.2 Comparison of SLM and Extruded Samples

Line roughness (R_a) at the polished spot (location O) was studied along with varying current density, time, and duty cycle to see the best conditions for polishing. The two graphs for SLM and extruded are shown to understand their behavior at the polishing conditions (Figure 36).

SLM **Extruded**

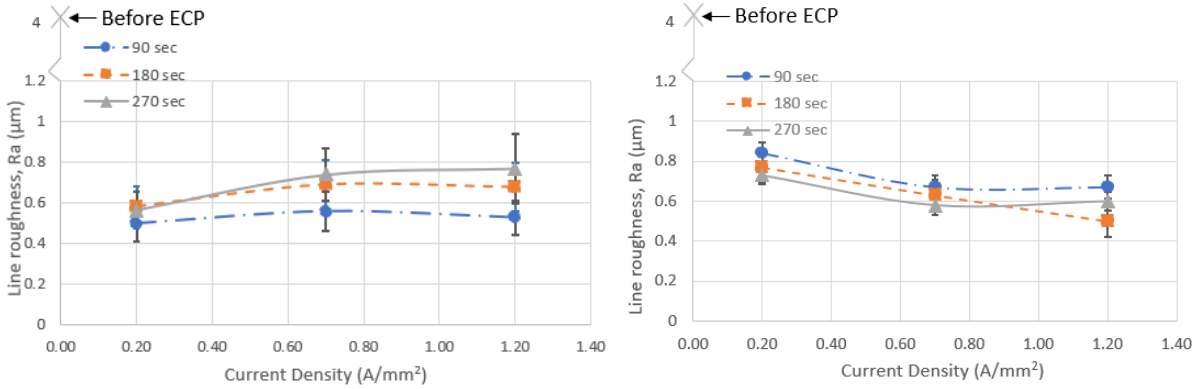

(a)

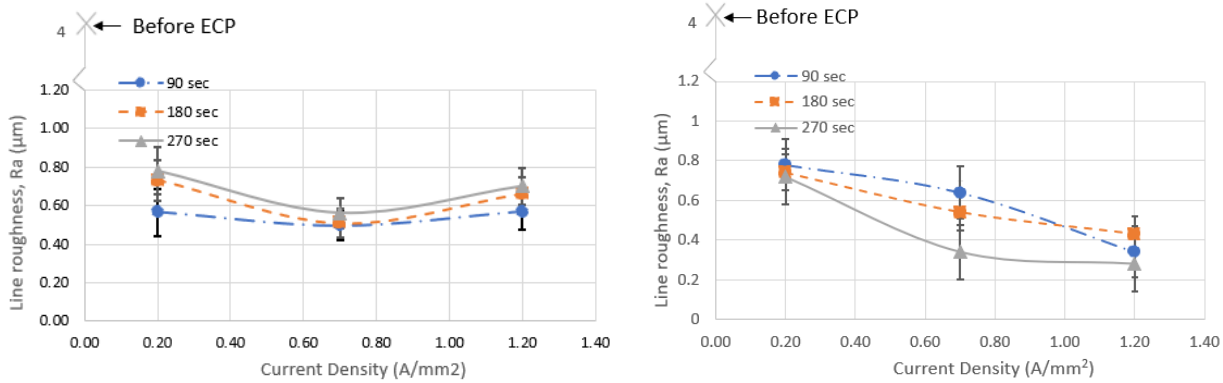

(b)

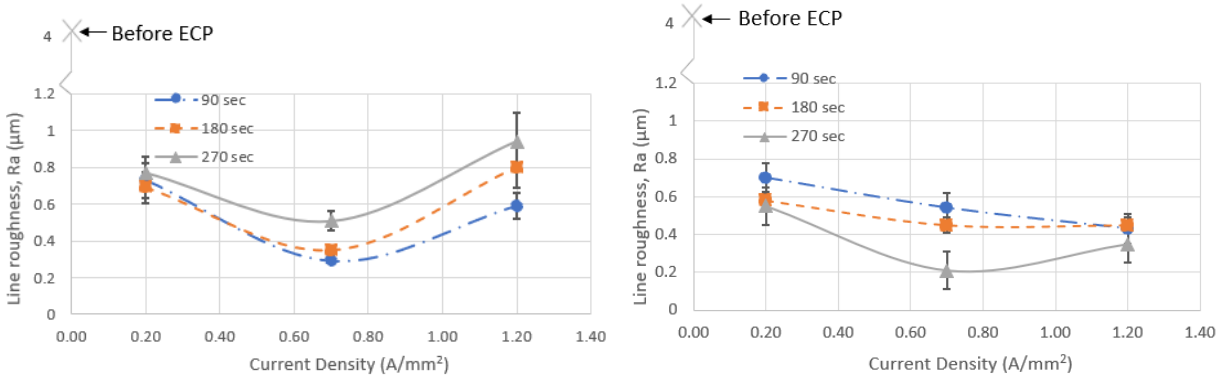

(c)

Figure 36: Line roughness (Ra) at polished spot versus current density at polished spot at (a) 25% (b) 50% (c)75% duty cycle at 25 Hz, average of 4 data point

It can be noted from Figure 36a-c that for SLM samples at every duty cycle, 90 seconds of polishing duration gives the best surface finish, but the roughness tends to increase as the polishing duration is increased to 270 seconds. This is due to the fact that as the polishing duration increases, more material is removed from the surface. It results in exposure of surface impurities in SLM parts, therefore, lowering the surface finish of the samples. This has been shown by the microstructure study by presence of cracks and pores at the polished spot. The best surface finish for SLM achieved is 0.28 μm, at 0.7 A/mm^2 of current density and 90 seconds of polishing time at 75% duty cycle. Contrastingly for extruded samples, the time duration of 270 seconds gives the best surface finish at every duty cycle. This has been further explained in the microstructure study in the next section.

Another set of plots are made to understand the variation of surface roughness by keeping the polishing duration constant (Figure 37).

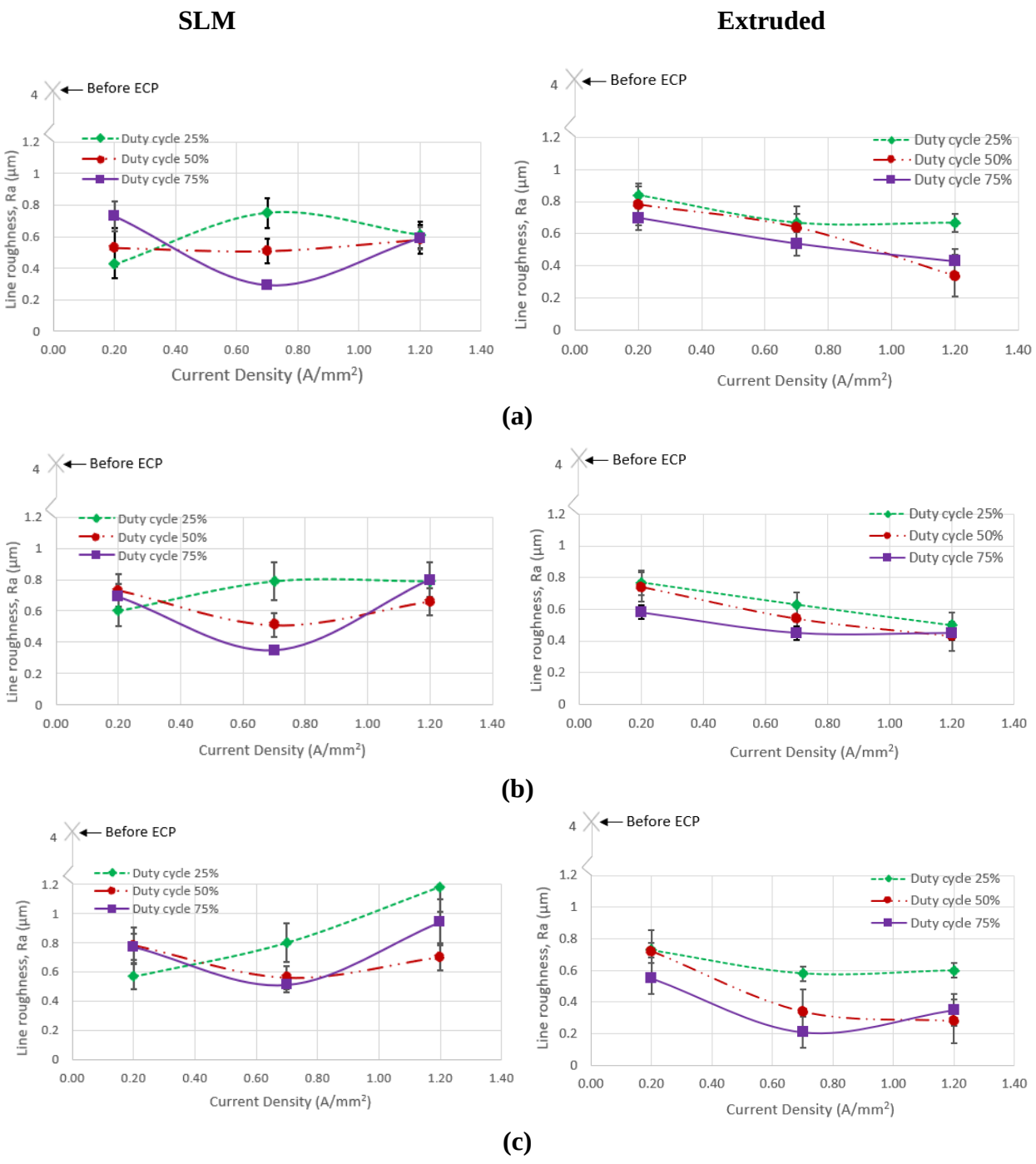

Figure 37: Plots showing line roughness (Ra) versus current density at polished spot at (a) 90 (b) 180 (c) 270 seconds at 25Hz, average of 4 data points

For SLM samples, 75% duty cycle gives the lowest roughness values and 75% duty cycle curve moves up as we go from Figure 37a to Figure 37c , indicating the increase in roughness values by increasing polishing time from 90 seconds to 270 seconds. It can also be seen that 25% duty cycle is not beneficial for improving the surface finish. This is because with a low duty cycle, polishing does not take place effectively as the electrical charge is insufficient to break the oxide layer. This has been shown in the microstructure study in the next section. Current density of 0.7 A/mm^2 seems to be optimum in every condition. Thus, the surface roughness for SLM parts deteriorates at high polishing duration, and low duty cycle. Extruded samples behave similar in this case, as 75% duty cycle gives good surface finish for all conditions.

Thus, the comparison studies show both SLM and extruded samples gives lower roughness values at 75% duty cycle, and rough surface at 25% duty cycle. But for extruded samples, surface roughness improves with high polishing duration in contrast to the SLM samples where low polishing duration is preferred.

5.2 Microstructure Study

This section depicts the microstructure of SLM and extruded samples to explains the surface finish results and trends as observed by the graphs.

5.2.1 SLM Parts

Samples were hand ground on a 180-grit sand paper prior to ECP process. Figure 38a shows the grinding marks on the sample before ECP and Figure 38b displays the laser hatching

lines on sample after ECP, showing the melt pools as observed with the optical microscope (OM).

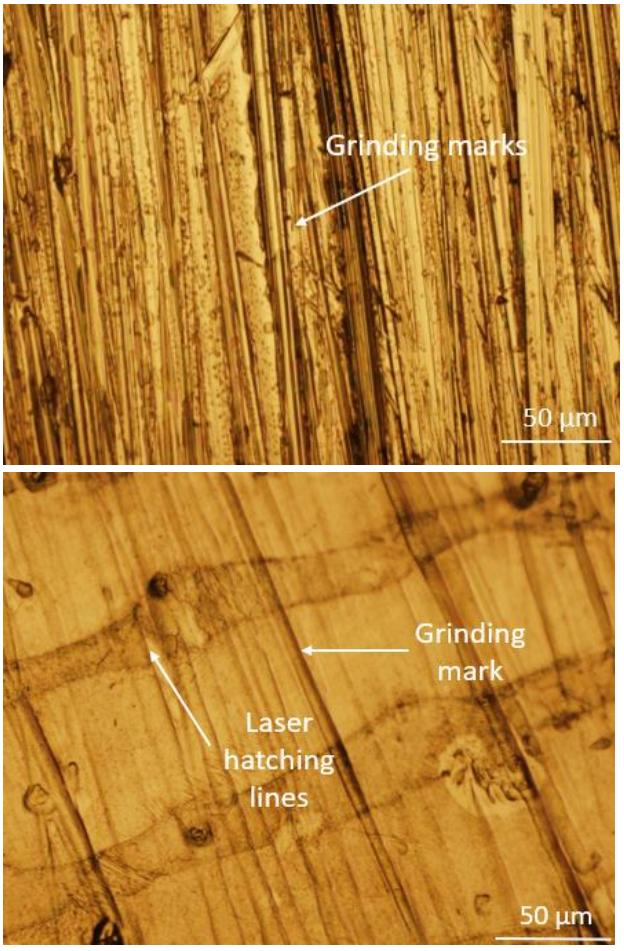

Figure 38: OM image of SLM sample showing (a) grinding marks (b) laser hatching marks along with grinding mark after ECP at 0.7 A/mm^2, 90 s, 50% duty cycle, 3 mm away from polished zone

Figure 39a shows the electropolished sample with the fading of grinding marks outside the polished region, Figure 39b shows surface defects on a sample electropolished at longer polishing duration of 270 seconds. This explained the increase in surface roughness at long duration as observed in Figure 36.

Line roughness (R_a) was measured avoiding the defects in both cases and hence gave lower values compared to area roughness (S_a).

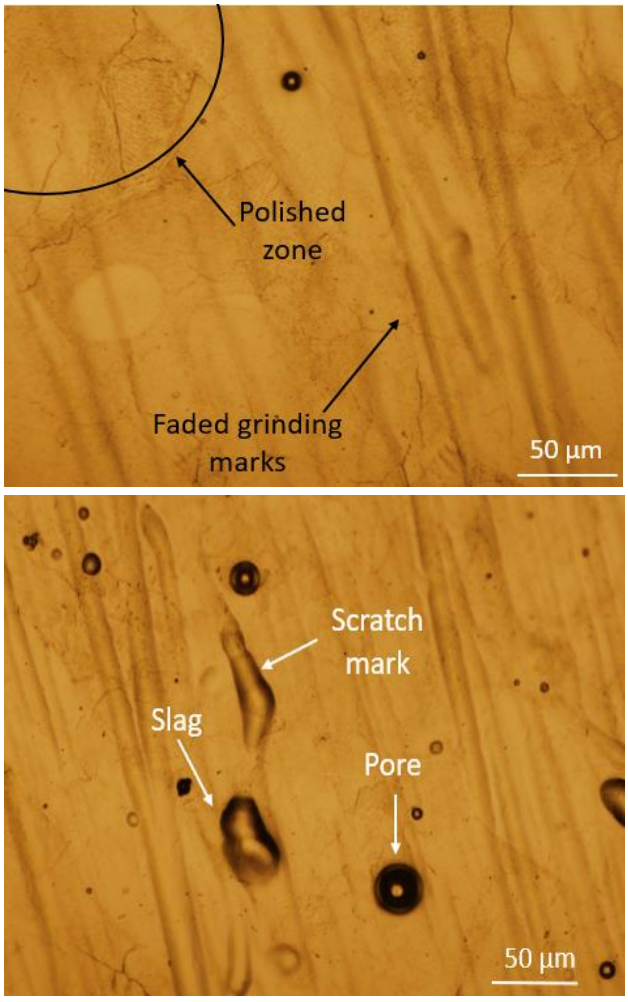

Figure 39: OM image of SLM sample after ECP (a) with fading grinding marks at 0.7 A/mm^2, 90 s and 50% duty cycle, (b) Surface impurities exposed at polished spot due to ECP at 0.7 A/mm^2, 270 s and 75% duty cycle

To visualize the effect of duty cycle on SLM sample's surface roughness, two samples at 25% and 75% duty cycles are shown in Figure 40. Figure 40a results in a smooth polished surface with removal of grinding marks whereas in Figure 40b, there is less effect of electropolishing due to low duty cycle.

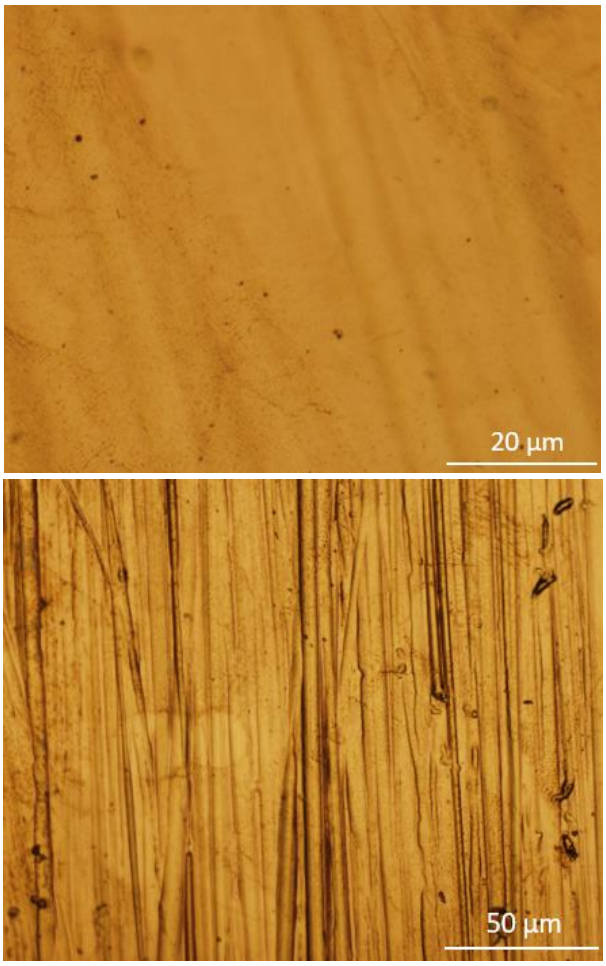

Figure 40: OM image of polished spot of SLM sample with ECP at (a) 0.7 A/mm^2, 90 s, 75% duty cycle (b) 0.7 A/mm^2, 90 s, 25% duty cycle

The sample in Figure 41a shows the electropolished sample with grain boundary, and Figure 41b demonstrates the polished zone in the center and removal of unmelted particles attached from the SLM surface. It also shows the laser hatching marks on the edges of the part which are not present in the polished zone, indicating a smooth surface.

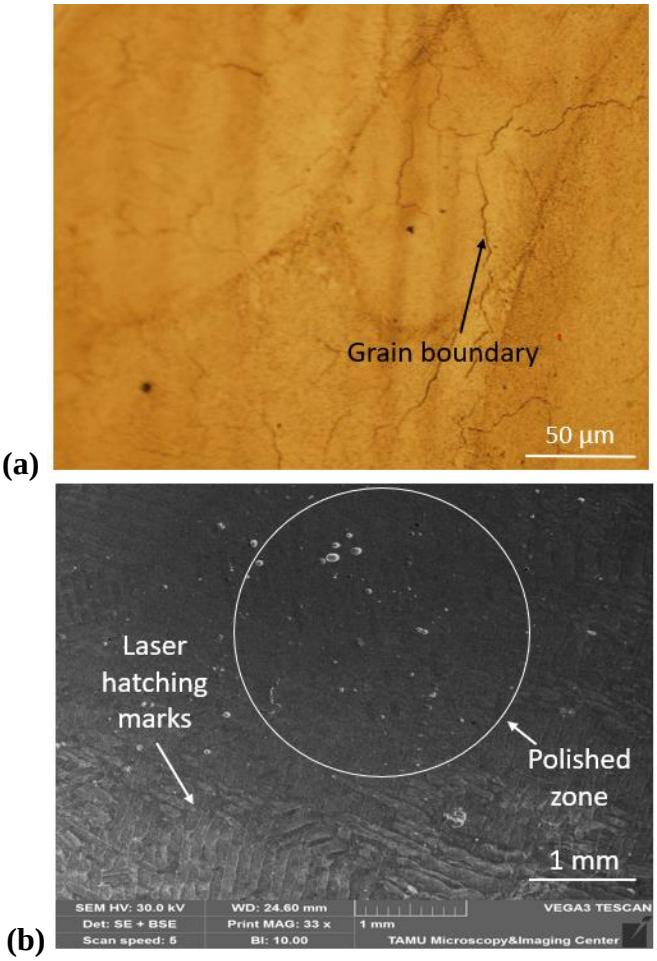

Figure 41: OM image of SLM samples after ECP (a) at 0.7 A/mm^2, 180 s, and 50% duty cycle (b) SEM image using secondary electron mode of same sample visualizing polished zone and hatching marks

SEM studies also exhibit defects like cracks, pores, and slag due to SLM process. The SLM process undergoes rapid melting and solidification which creates a high temperature gradient and correspondingly a large residual thermal stress, leading to crack initiation and propagation in the fabricated part. Pores represent the dissolved argon gas bubbles trapped in the molten pool before solidification, and slag occurs due to the presence of foreign particles in the

metal powder (Zhang et al., 2017). These defects are the reason behind prevention of further improvement in the surface roughness characteristics (Figure 42a-c).

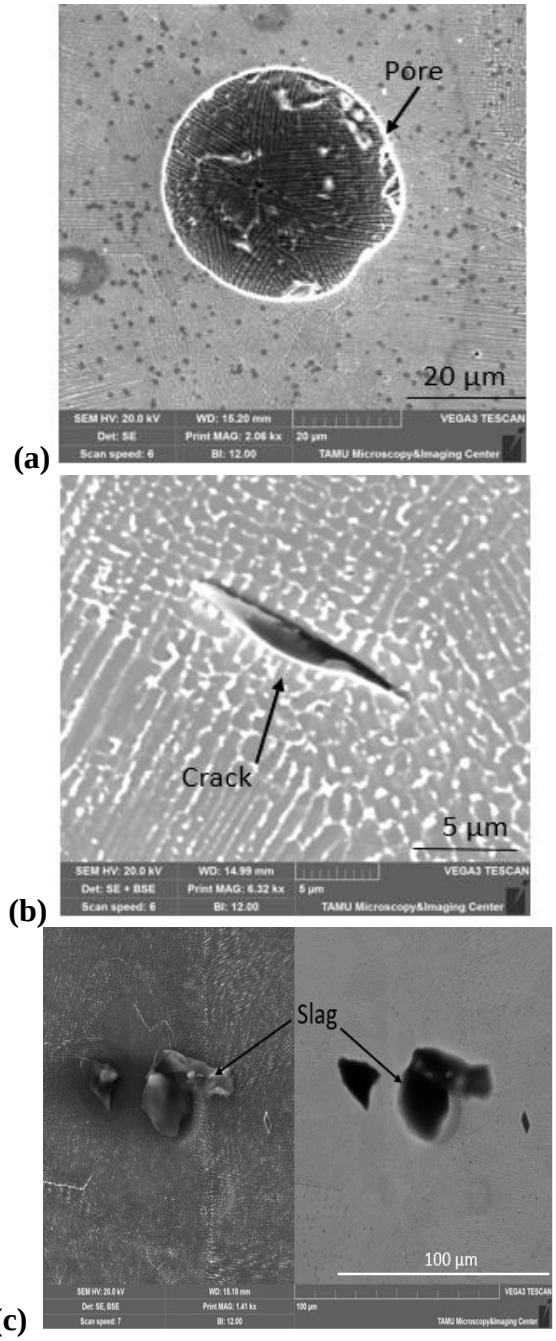

Figure 42: SEM image of defects in SLM samples after ECP at 1.2 A/mm^2, 270 s and 50% duty cycle (a) , (b) using secondary electron mode, (c) using secondary and back scattered electron modes

Figure 43a shows the polished zone and entrapped argon gas bubbles formed during the SLM process. Figure 43b shows the highlighted surface with a presence of crack in the middle.

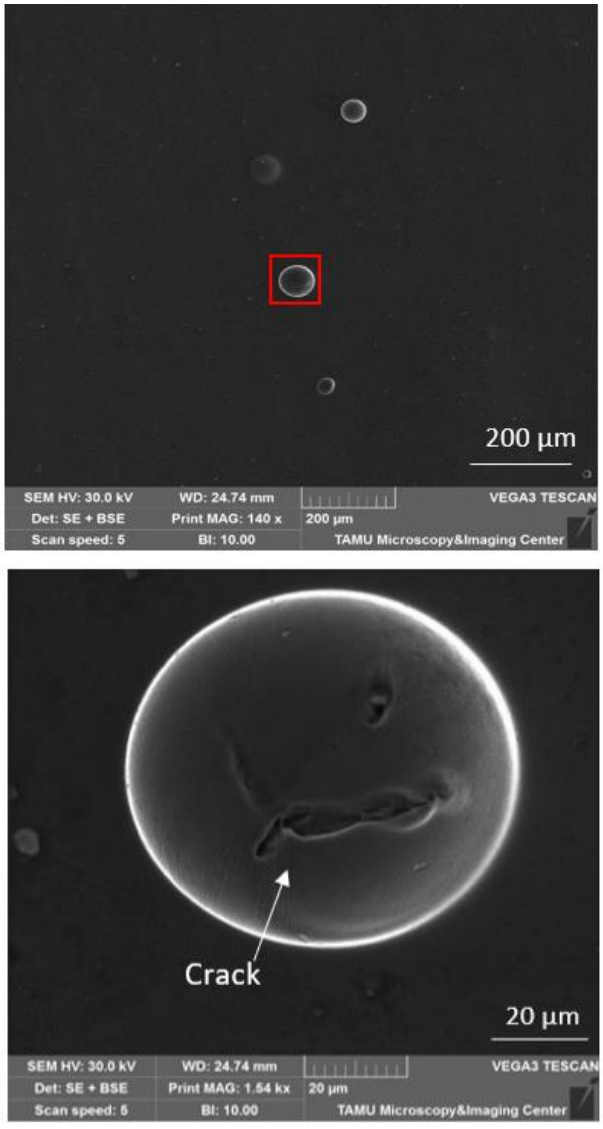

Figure 43: SEM image using secondary electron mode of the polished spot on SLM samples (a) ECP conditions of 0.7 A/mm^2 , 180 s, and 75% duty cycle (b) Magnified image of the crack in (a)

Inconel 718 is microstructurally complex containing intermetallic precipitates, nitrides, and carbides. The intermetallic phases are laves, σ, δ, γ', and metastable γ''. The major

strengthening phases are γ’ and γ’’ which produces coherency in the matrix. The Laves phase is a hexagonally close packed (hcp) phase and forms the interdendritic regions of 718 weld metals, basically due to micro segregation of alloying elements during weld solidification (Aghajani et al., 2016). The grain boundaries and sub-grain boundaries highly decorated with irregularly shaped Nb-rich precipitates. These precipitates as determined by energy dispersive X-ray spectroscopy (EDS) are mainly the Laves phase (Tucho et al., 2017).

The sample in Figure 44 shows the small particles towards the unpolished edges of the sample (location 3). These small samples are identified as carbides. Most of the carbon content in alloy 718 is bound in metallic carbides essentially NbC (Yadroitsev et al., 2011).

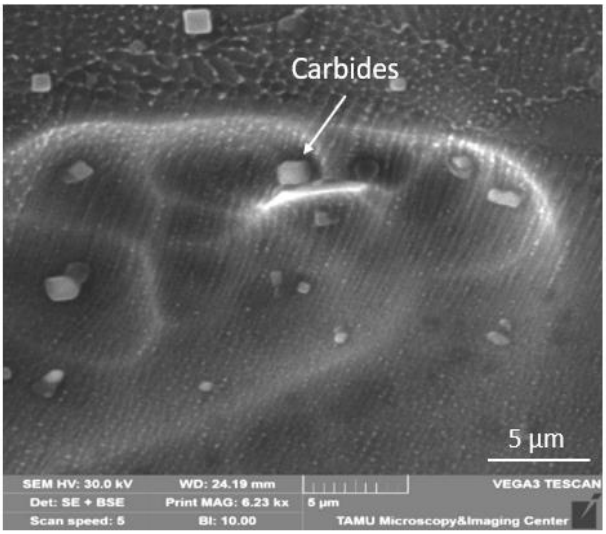

Figure 44: SEM image using secondary electron mode of SLM sample showing presence of carbides at the edge of polished zone after ECP at 1.2 A/mm^2, 180 s and 50% duty cycle

Thus, these studies show that at high current density and polishing time, SLM surface is deteriorated since exposure of impurities like cracks and pores.

5.2.2 Extruded Parts

Both OM and SEM analysis are carried out on electropolished extruded samples. Figure 45 shows OM image of a sample before and after ECP. Figure 45a shows the rough sample before grinding, while Figure 45b represents the electropolished zone.

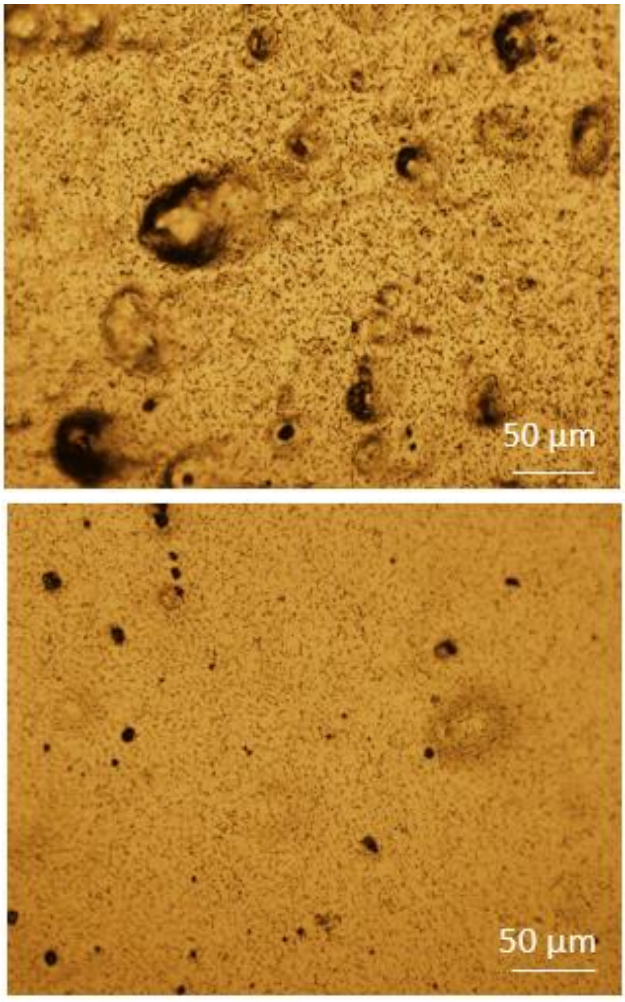

Figure 45: Extruded samples (a) Before ECP (b) ECP sample at 0.7 A/mm^2, 270 s and 50% duty cycle at 1mm away from polished spot

The SEM analysis were used to understand the microstructure of IN718. Aghajani et al. (2016) established that there are two types of carbides present in Nickel alloys: NbC and $M_{23}C_6$

(Figure 46), where M represented elements of Cr, Mo, and Nb. The dark zone around the NbC carbides (Figure 46a) indicates a niobium depleted zone which has insufficient Nb content for precipitation of γ'' phase. However, there is no depletion ring around $M_{23}C_6$ carbides (Figure 46b). EDS analysis by Aghajani et al. (2016) shows that in spite of similar morphology, chemistry of the two precipitates is different.

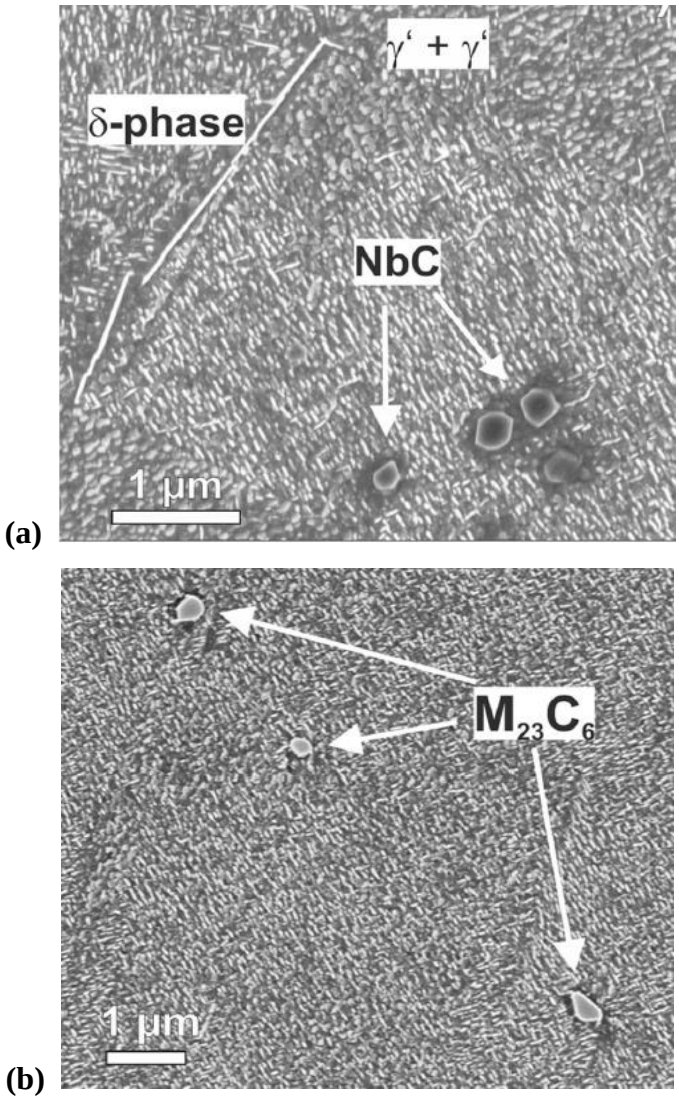

Figure 46: SEM micrographs identifying NbC and $M_{23}C_6$ carbides, reprinted from (Aghajani et al., 2016)

The electropolished sample when analyzed on SEM exhibited $M_{23}C_6$ carbides in the polished zone and the non-polished edges showed the precipitates of NbC having a dark zone around them.

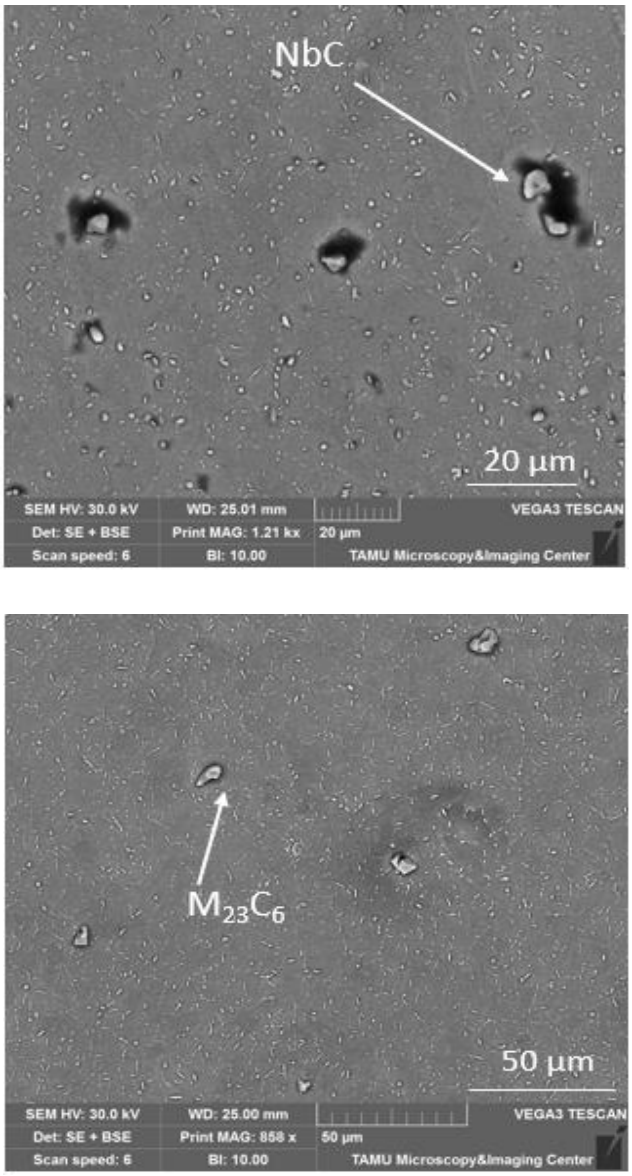

Figure 47: SEM image using secondary electron mode showing (a) NbC at the edge of the extruded sample (b) $M_{23}C_6$ in the center of the polished zone of the extruded sample

The SEM image of the polished zone showed presence of δ-phase distribution with the grains. The embedded particles are identified as δ-phase and the center particle as Laves.

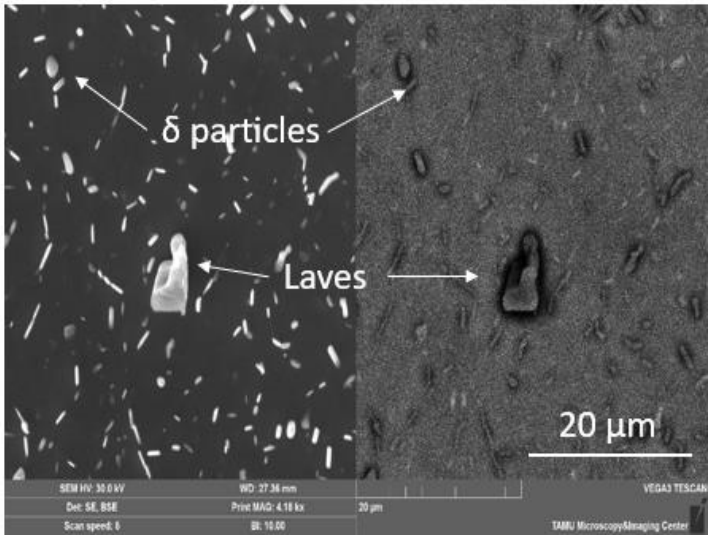

Figure 48: SEM image using secondary and back scattered electron mode of extruded sample after ECP at 0.7 A/mm^2, 270 seconds and 75% duty cycle

Thus, the microstructure study of extruded parts showed the presence of laves, δ particle in the metallic matrix. Any material defects as seen in SLM material like cavities and pores were absent. Owing to this, the surface finish of extruded parts is high (Figure 36) at higher polishing durations as more material is removed uniformly.

5.3 Regression Model

5.3.1 SLM Parts

Regression analysis of SLM parts was performed to model area roughness (S_a). This model was built based on the extreme values of the parameters, as shown in the Table 10, and then tested on intermediate values to predict the surface roughness (S_a).

The regression equation generated was as follows:

$$Sa = 0.49 + 0.37\,J + 0.00383\,t + 0.004\,dc - 0.0796\,d - 0.000051(t * dc) - 0.000329\,(t * d) + 0.00218(dc * d) \quad (3)$$

Where,

Table 13: Regression model parameters for SLM parts

J	Current density (A/mm^2)	0.2, 1.2
t	Time (sec)	90, 270
dc	Duty cycle (%)	25, 75
d	Distance (mm)	0, 3

The R^2 value for this model is 85.80%. As the regression equation involves interaction terms, suggesting the effect of one parameter depends on the value of another parameter. The coefficients of both current density and time are positive indicating that as they increase, the value of S_a increases, hence increasing roughness. The coefficient of (time*duty cycle) is in the order of 10^{-4}, but still contributes significantly as the magnitudes of time and duty cycle are themselves higher compared to current density.

The model was used to predict the area roughness on the intermediate values as given in Table 7 and compared with the experimental data recorded. The predicted values are about ± 30% from the measured values (Figure 49). The entire data are given in Appendix D.

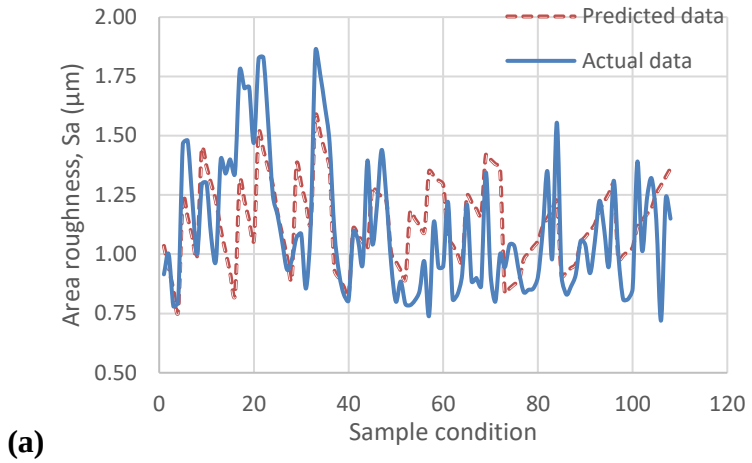

(a)

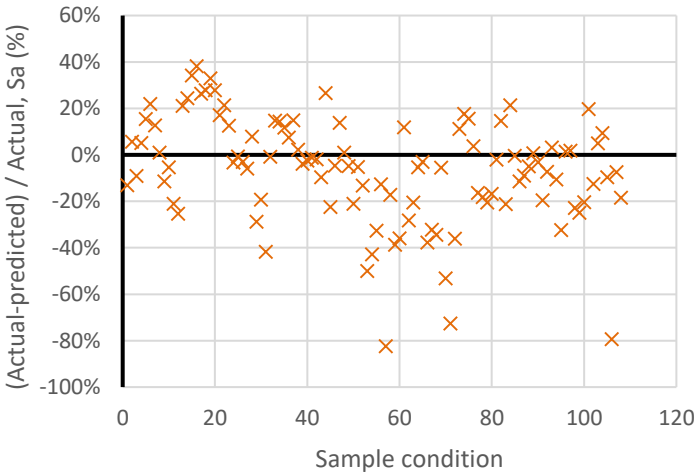

(b)

Figure 49: Actual and predicted data based on regression model for SLM samples, x-axis represents 27 samples measured at 4 locations, giving 108 conditions overall

The residual plots (Figure 50) indicate the goodness of the fit of the model. The histogram plot represents a near bell-curve, indicating that residuals are almost normally distributed. There is no notable pattern in the residual vs fitted values and observation plots. This indicates that for the given factorial levels, the regression model captures majority of explanatory information.

Regression model for R_a of SLM samples is provided in Appendix D.

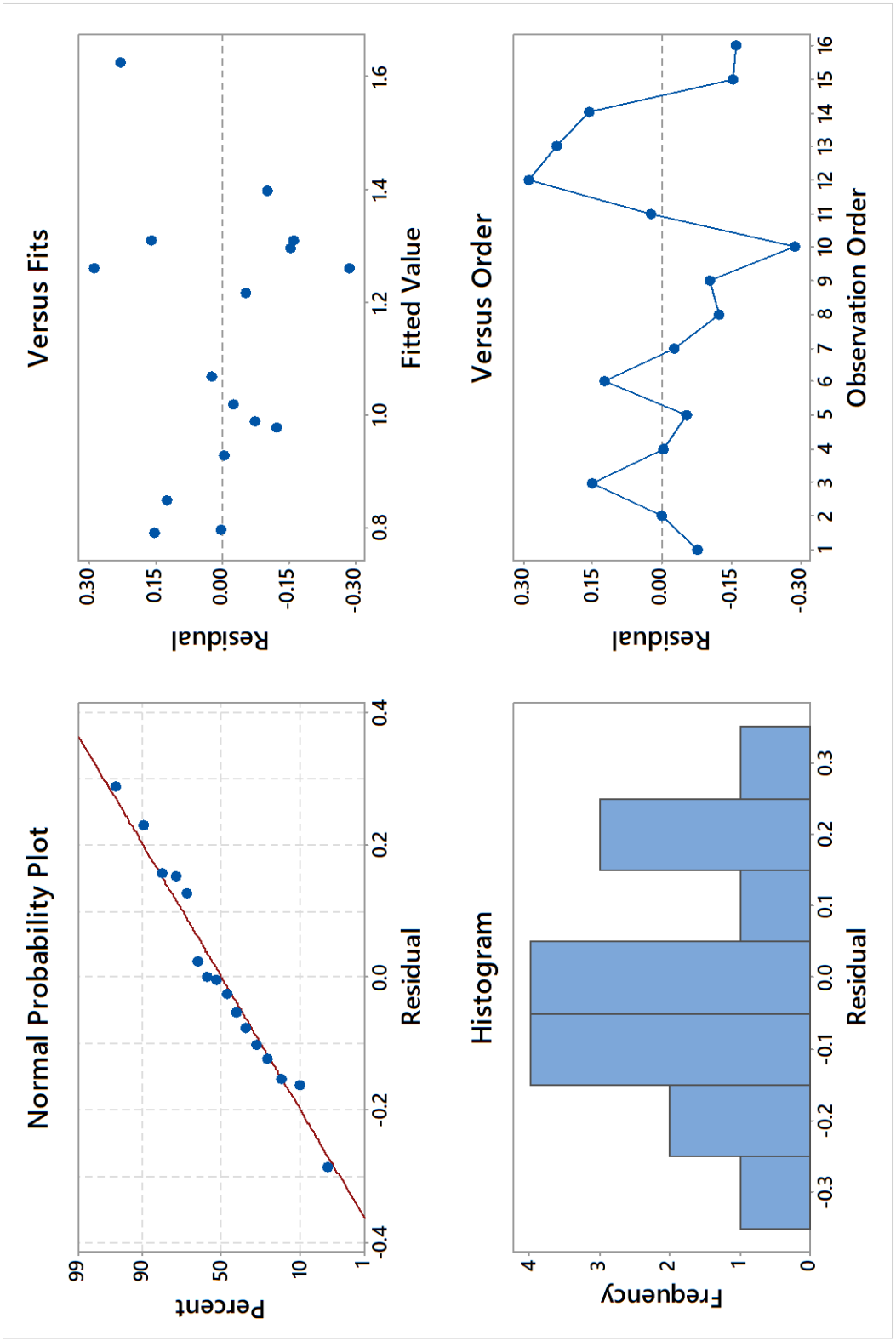

Figure 50: Residual plots for regression model of area roughness (S_a) of SLM samples

5.3.2 Extruded Parts

Regression analysis for extruded polished parts was performed in a similar manner as SLM, to model area roughness (S_a).

$$Sa = 0.975 - 0.373\,J + 0.00093\,t + 0.00577\,dc - 0.0092\,d + 0.0044\,(J * dc) + 0.1063\,(J * d) - 0.000056\,(t * dc) \quad (4)$$

Where,

Table 14: Regression model parameters for extruded samples

J	Current density (A/mm^2)	0.2, 1.2
t	Time (sec)	90, 270
dc	Duty cycle (%)	25, 75
d	Distance (mm)	0, 3

The R^2 value for this model is 80.36%. As the regression equation involves interaction terms, it suggests that the effect of one factor depends on another factor. The coefficient of current density is negative, indicating that higher values of current density leads to reduction in roughness values for extruded parts. The coefficient of time is positive, but the magnitude is very low indicating that there is a slight increase in roughness with high time values. Also, the coefficient of time*duty cycle is in the order of 10^{-4}, but still contributes significantly as the magnitudes of time and duty cycle are themselves higher compared to current density.

The model was used to predict the area roughness on the intermediate values as given in Table 7 and compared with the experimental data recorded. The predicted values are about ± 30% from the measured values (Figure 51). The entire data can be found in Appendix D.

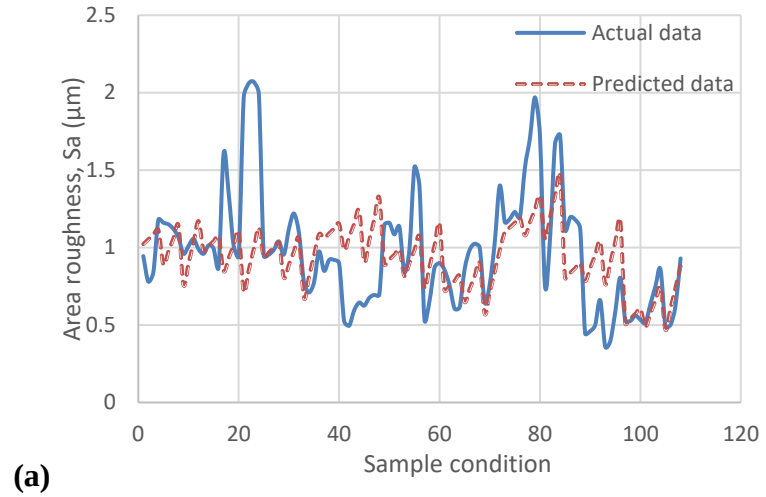

(a)

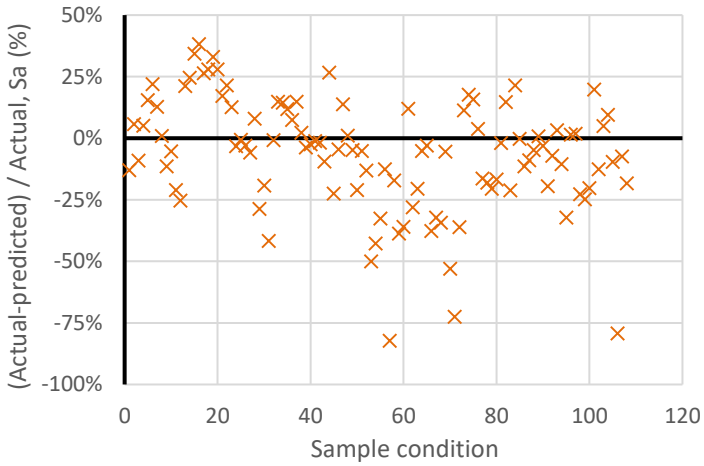

(b)

Figure 51: Actual and predicted data based on regression model for extruded samples, x-axis represents 27 samples measured at 4 locations, giving 108 conditions overall

The residual plots (Figure 52) indicate the goodness of the fit of the model. The histogram plot represents a bell-curve, indicating that residuals are almost normally distributed. There is no notable pattern in the residual vs fitted values and observation plots. This indicates that for the given factorial levels, the regression model captures majority of explanatory information.

Regression model for R_a of extruded samples is provided in Appendix D.

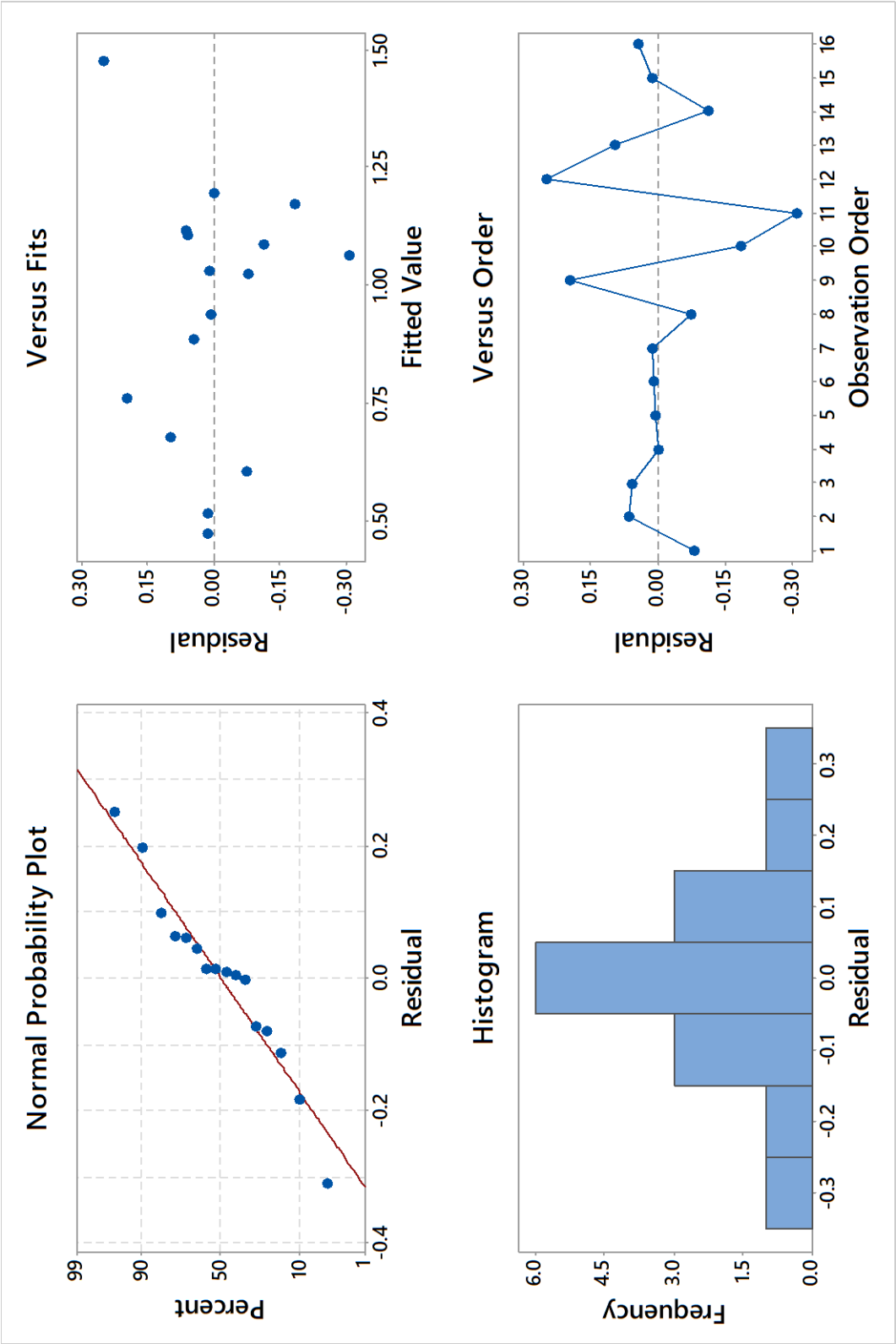

Figure 52: Residual plots for regression model of area roughness (Sa) of extruded samples

6. CONCLUSION AND RECOMMENDATION

This research applied pulsed electrochemical polishing to improve surface finish of selective laser melted (SLM) Inconel 718, and compared against surface finish of the extruded alloy. Local polishing using a titanium rounded end electrode was performed at three levels of current density, duty cycle, and polishing time. This study showed:

1. Submicron surface finish was achieved within the ranges of chosen process variables for (i) line surface finish Ra, and (ii) area surface finish Sa. The average standard deviation of about 0.1 µm was achieved for both SLM'ed and extruded parts.
2. Successful polishing was achieved with duty cycle higher than 50%.
3. For the SLM'ed parts, the best line surface finish (R_a) of 0.28 µm was achieved at 0.7 A/mm^2 current density, 90 s of polishing time and 75% duty cycle. The surface roughness worsened with increase in polishing time.
4. For the extruded parts, the reversed trend was observed. The surface finish of extruded parts improved with higher polishing duration. The best surface finish (R_a) of 0.21 µm was achieved at 0.7 A/mm^2 current density, 270 s of polishing time and 75% duty cycle.
5. The volume defects in SLM'ed parts (pores, cracks, slag, precipitates etc.) deteriorated surface roughness after ECP. The nonconductive slags and precipitates remained while the surrounding matrix was polished away. Such pore, crack, and slag were not seen in extruded part.
6. Regression models for area surface finish (Sa) were generated for both SLM and extruded. The R^2 values of both models were 85.80% and 80.36% respectively.

The following avenues should be considered for future work:

- Investigate the effect of ultrasonic vibrations in electrochemical polishing of SLM'ed and extruded Inconel alloys.
- Increase the experimental level (five or higher) and increase the number of measurement at a location (ten or higher) to improve the regression models.
- Calculate accurately the current density of a spherical end electrode in ECP.

REFERENCES

Aghajani, Ali, Tewes, Jürgen, Parsa, Alireza Basir, Hoffmann, Thorsten, Kostka, Alexander, and Kloewer, Jutta. (2016). Identification of mo-rich m23c6 carbides in alloy 718. *Metallurgical and Materials Transactions A, 47*(9), 4382-4392.

Baicheng, Zhang, Xiaohua, Lee, Jiaming, Bai, Junfeng, Guo, Pan, Wang, Chen-nan, Sun, Muiling, Nai, Guojun, Qi, and Jun, Wei. (2017). Study of selective laser melting (slm) inconel 718 part surface improvement by electrochemical polishing. *Materials & Design, 116*, 531-537.

Bhattacharyya, B, Malapati, M, Munda, J, and Sarkar, A. (2007). Influence of tool vibration on machining performance in electrochemical micro-machining of copper. *International Journal of Machine Tools and Manufacture, 47*(2), 335-342.

Choi, Joon-Phil, Shin, Gi-Hun, Yang, Sangsun, Yang, Dong-Yeol, Lee, Jai-Sung, Brochu, Mathieu, and Yu, Ji-Hun. (2017). Densification and microstructural investigation of inconel 718 parts fabricated by selective laser melting. *Powder Technology, 310*, 60-66.

Co.Ltd., Heanjia Super Metal. (2015). Inconel 718 for aerospace engine applications. Retrieved from https://super-metals.com/news/inconel-718-for-aerospace-engine-applications/

Controllers-VXM, Velmex Motor. (2016). Retrieved from https://www.velmex.com/Products/Controls/VXM_Controller.html

Corporation, Olympus. (2000). Optical microscopes. Retrieved from https://www.olympus-ims.com/en/microscope/terms/feature10/

Corporation, Special Metals. (2007). *Inconel alloy 718*. Retrieved from http://www.specialmetals.com/assets/smc/documents/inconel_alloy_718.pdf

Feng, Zhujian. (2018). *Investigation of horizontal vibration-assisted pulsed electrochemical machining.* (Dissertation), Texas A&M University.

Group, Farinia. (2018). Why choosing inconel 718 for aerospace additive manufacturing? Retrieved from https://www.farinia.com/additive-manufacturing/3d-materials/inconel-718-aerospace-additive-manufacturing

Huang, Ching An, and Chen, Yu Chen. (2009). The effect of water content on the electropolishing behavior of inconel 718 alloy in perchloric–acetic acid mixtures. *Corrosion Science, 51*(9), 1901-1906.

Infinitefocus, Alicona That's metrology:. (2016). Retrieved from http://www.alicona.com/products/infinitefocus/

Jia, Qingbo, and Gu, Dongdong. (2014). Selective laser melting additive manufacturing of inconel 718 superalloy parts: Densification, microstructure and properties. *Journal of Alloys and Compounds*, *585*, 713-721.

Kim, Bo Hyun, Ryu, Shi Hyoung, Choi, Deok Ki, and Chu, Chong Nam. (2004). Micro electrochemical milling. *Journal of Micromechanics and Microengineering, 15*(1), 124.

Lee, E-S. (2000). Machining characteristics of the electropolishing of stainless steel (sts316l). *The International Journal of Advanced Manufacturing Technology, 16*(8), 591-599.

Lee, Shuo-Jen, and Lai, Jian-Jang. (2003). The effects of electropolishing (ep) process parameters on corrosion resistance of 316l stainless steel. *Journal of Materials Processing Technology*, *140*(1-3), 206-210.

Mancisidor, AM, Garciandia, F, San Sebastian, M, Álvarez, P, Díaz, J, and Unanue, I. (2016). Reduction of the residual porosity in parts manufactured by selective laser melting using skywriting and high focus offset strategies. *Physics Procedia, 83*, 864-873.

Metals, High Temp. (2015). Inconel 718 technical data. Retrieved from http://www.hightempmetals.com/techdata/hitempInconel718data.php

Miao, Zhu-jun, SHAN, Ai-dang, WU, Yuan-biao, Jun, LU, Ying, HU, LIU, Jun-liang, and SONG, Hong-wei. (2012). Effects of p and b addition on as-cast microstructure and homogenization parameter of inconel 718 alloy. *Transactions of Nonferrous Metals Society of China, 22*(2), 318-323.

Niu, HJ, and Chang, ITH. (1999). Instability of scan tracks of selective laser sintering of high speed steel powder. *Scripta Materialia, 41*(11), 1229-1234.

Qi, H, Azer, M, and Ritter, A. (2009). Studies of standard heat treatment effects on microstructure and mechanical properties of laser net shape manufactured inconel 718. *Metallurgical and Materials Transactions A, 40*(10), 2410-2422.

Rajurkar, KP, Zhu, Di, McGeough, JA, Kozak, J, and De Silva, A. (1999). New developments in electro-chemical machining. *CIRP annals, 48*(2), 567-579.

Rao, G Appa, Srinivas, M, and Sarma, DS. (2004). Effect of thermomechanical working on the microstructure and mechanical properties of hot isostatically pressed superalloy inconel 718. *Materials Science and Engineering: A, 383*(2), 201-212.

Schafrik, Robert E, Ward, Douglas D, and Groh, Jon R. (2001). Application of alloy 718 in ge aircraft engines: Past, present and next five years. *Superalloys, 718*(625), 1-11.

Shi, Qimin, Gu, Dongdong, Xia, Mujian, Cao, Sainan, and Rong, Ting. (2016). Effects of laser processing parameters on thermal behavior and melting/solidification mechanism during selective laser melting of tic/inconel 718 composites. *Optics & Laser Technology, 84*, 9-22.

system, Velmex bislide positioning. (2016). Retrieved from https://www.velmex.com/Products/BiSlide/BiSlide_Motorized.html

Technologies, Holland Applied. (2014). What is electropolishing and why is it so important in the pharmaceutical industry? Retrieved from https://hollandaptblog.com/2014/03/20/what-is-electropolishing-and-why-is-it-so-important-in-the-pharmaceutical-industry/

Townsend, Andrew, Senin, N, Blunt, Liam, Leach, RK, and Taylor, JS. (2016). Surface texture metrology for metal additive manufacturing: A review. *Precision Engineering, 46*, 34-47.

Trosch, Tanja, Strößner, Johannes, Völkl, Rainer, and Glatzel, Uwe. (2016). Microstructure and mechanical properties of selective laser melted inconel 718 compared to forging and casting. *Materials letters, 164*, 428-431.

Tucho, Wakshum M, Cuvillier, Priscille, Sjolyst-Kverneland, Atle, and Hansen, Vidar. (2017). Microstructure and hardness studies of inconel 718 manufactured by selective laser melting before and after solution heat treatment. *Materials Science and Engineering: A, 689*, 220-232.

Wang, Dengyong, Zhu, Zengwei, Wang, Ningfeng, Zhu, Di, and Wang, Hongrui. (2015). Investigation of the electrochemical dissolution behavior of inconel 718 and 304 stainless steel at low current density in nano3 solution. *Electrochimica Acta, 156*, 301-307.

Wang, Xiaoqing, Gong, Xibing, and Chou, Kevin. (2017). Review on powder-bed laser additive manufacturing of inconel 718 parts. *Proceedings of the Institution of Mechanical Engineers, Part B: Journal of Engineering Manufacture, 231*(11), 1890-1903.

Wang, Zixing, Zhou, Dianhua, Deng, Qun, Chen, Guosheng, and Xie, Wei. (2010). The microstructure and mechanical properties of inconel 718 fine grain ring forging. *Superalloy 718 and Derivatives*, 343-349.

Yadroitsev, I, and Smurov, I. (2011). Surface morphology in selective laser melting of metal powders. *Physics Procedia, 12*, 264-270.

Yang, Li, O'Neil, Chris, and Wu, Yan. The use of electropolishing surface treatment on in718 parts fabricated by laser powder bed fusion process.

Zhang, Bi, Li, Yongtao, and Bai, Qian. (2017). Defect formation mechanisms in selective laser melting: A review. *Chinese Journal of Mechanical Engineering, 30*(3), 515-527. doi:10.1007/s10033-017-0121-5

Zhang, Yinan, Cao, Xinjin, Wanjara, Priti, and Medraj, Mamoun. (2013). Fiber laser deposition of inconel 718 using powders.

APPENDIX A

COSMOS PROGRAM

This program moves the tool 0.5 mm from the workpiece to set the operating IEG.

F C S1M1000, I1M-200, R

Command	**Meaning**
F	Start
C	Cancel any previous commands
S1M1000	Speed command is set to move the motor 1 at the speed of 1000 steps*/sec. Motor 1 moves in direction of x-axis.
I1M-200	Incrementing motion command is set to move the motor 1, 200 steps in the backward direction.
R	End

*Each step equals 2.5 µm

APPENDIX B

DESCRIPTION OF COMPONENTS

i) Velmex bi-slide positioning system and VXM controller

The Velmex Bi-Slide system is a positioning system of high accuracy. The lead screw resolution is 0.00025” and its repeatability is 0.00015” ("Velmex Motorized BiSlide Systems," 2016). The load carrying capacity of Velmex Bi-slide is up to 300 lbs. It uses PTFE bearings which give smoother movement and less friction. It operates without lubrication and it uses strong I-beam cross section made of hard aluminum.

The stepper motors that control the X and Z axis motion of the Bi-Slide can be programmed to move a specific distance at a specific speed in those axes. This is accomplished by COSMOS software. Manual operation of motors is done using a controller provided for the same.

In case of emergency during running a programmed motion of the motors, the motion can be stopped to avoid any damage or losses. The tool and the ultrasonic probe was mounted on the Bi-Slide by designing and fabricating appropriate holder. This enabled the servo-motors to move the tool and the ultrasonic probe at the desired feed rate and drill holes of desired depth. The servomotor motion is programmed in order to have a constant feed-rate into the workpiece.

Figure 53: (a) Velmex Bi-slide positioning system (system, 2016) (b) VXM controller system (Controllers-VXM, 2016)

ii) Alicona IF 3D profiler and Olympus optical microscope

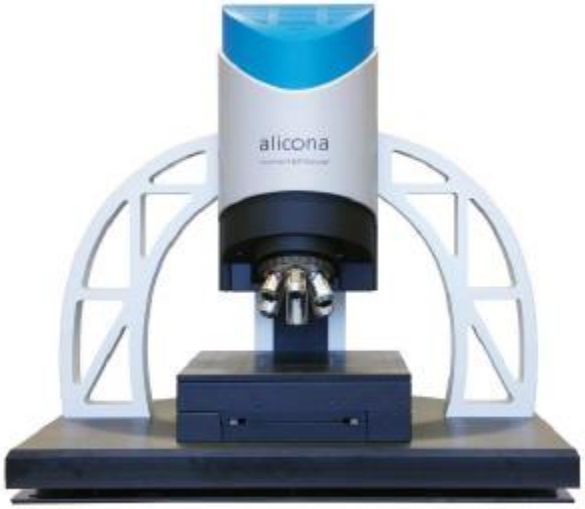

Figure 54: Alicona IF profiler (Infinitefocus, 2016)

The Alicona IF measurement system is a non-contact type of 3D profiler and works on the principle of focus variation. Variety of magnification are available for measurement of form and roughness. This profiler was used to measure area and line roughness of the IN718 samples.

The Olympus microscope with different magnifications was used to analyze the samples after electropolishing them.

Figure 55: Olympus optical microscope (Corporation, 2000)

iii) Drawing of the tool mounting fixture

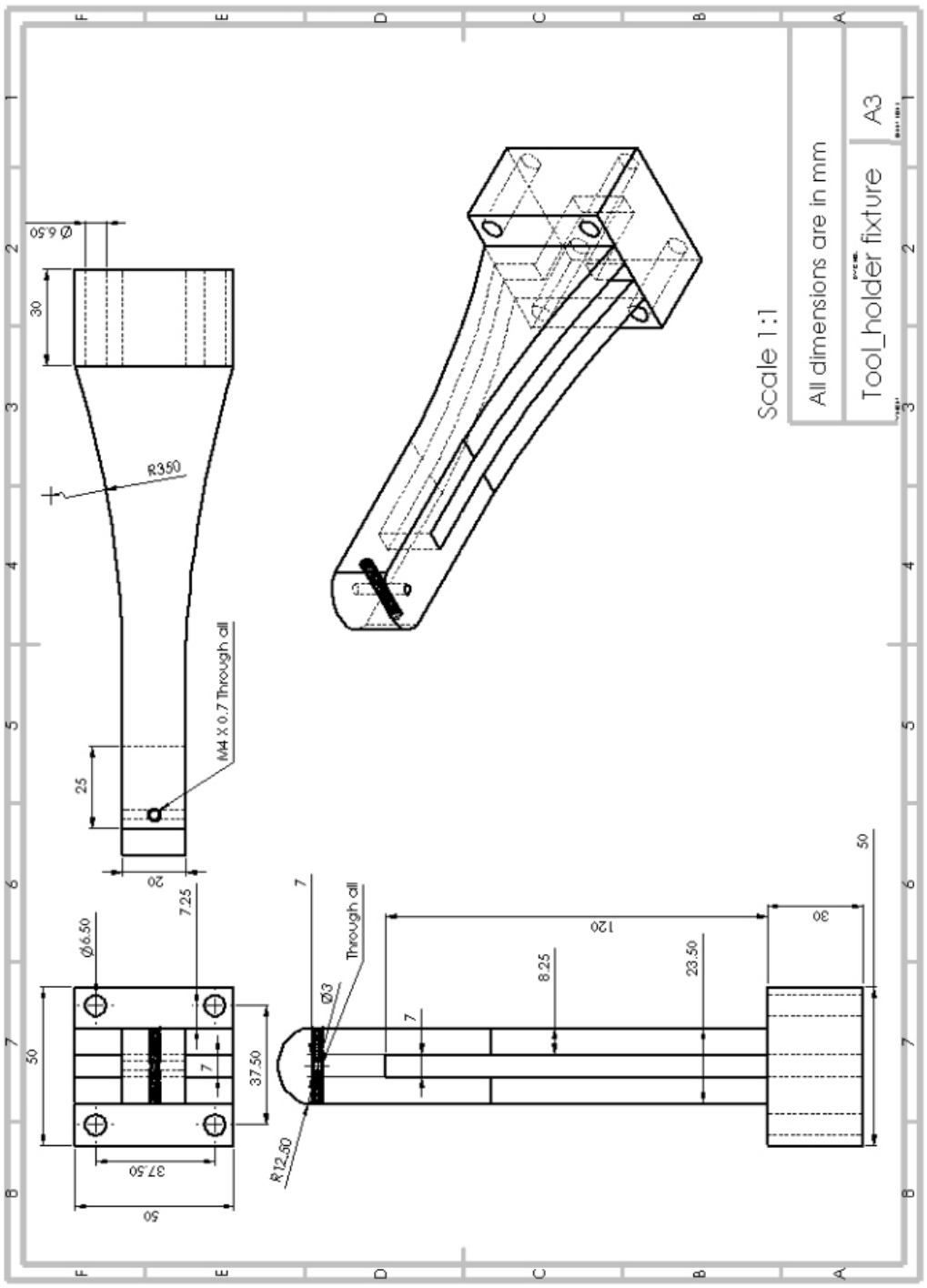

Figure 56: Drawing of the tool mounting fixture

APPENDIX C

SURFACE FINISH DATA

i) For SLM samples (Ra)

Current density (A/mm^2)	Time (sec)	Duty cycle (%)	Distance (mm)	Parallel		Perpendicular	
				Ra1 (µm)	Ra2 (µm)	Ra3 (µm)	Ra4 (µm)
0.20	90	25	0	0.425	0.64	0.57	0.53
0.20	90	25	1	0.4	0.32	0.65	0.64
0.20	90	25	2	0.37	0.34	0.74	0.63
0.20	90	25	3	0.53	0.54	0.54	0.5
0.70	90	25	0	0.75	0.6	0.63	0.57
0.70	90	25	1	0.65	0.66	1.2	0.91
0.70	90	25	2	0.58	0.54	0.78	0.99
0.70	90	25	3	0.85	0.78	0.93	0.79
1.20	90	25	0	0.61	0.58	0.62	0.58
1.20	90	25	1	0.55	0.4	0.93	1.04
1.20	90	25	2	0.34	0.33	0.61	0.63
1.20	90	25	3	0.52	0.41	0.88	0.77
0.20	180	25	0	0.6	0.65	0.73	0.67
0.20	180	25	1	0.55	0.44	0.78	0.72
0.20	180	25	2	0.47	0.71	0.65	0.61
0.20	180	25	3	0.51	0.55	0.6	0.61
0.70	180	25	0	0.79	0.77	0.81	0.79
0.70	180	25	1	0.56	0.51	1.19	1.41
0.70	180	25	2	0.64	0.47	1.3	1.14
0.70	180	25	3	0.58	0.56	0.69	0.75
1.20	180	25	0	0.79	0.73	0.82	0.78
1.20	180	25	1	0.67	0.61	0.92	0.78
1.20	180	25	2	0.81	0.59	1.07	0.97
1.20	180	25	3	0.78	0.58	0.88	0.87
0.20	270	25	0	0.57	0.65	0.67	0.63
0.20	270	25	1	0.49	0.49	0.81	0.8
0.20	270	25	2	0.38	0.46	0.72	1.01
0.20	270	25	3	0.53	0.37	0.57	0.47
0.70	270	25	0	0.8	0.86	0.87	0.83
0.70	270	25	1	0.74	0.65	0.62	0.87
0.70	270	25	2	0.67	0.51	0.99	0.82
0.70	270	25	3	0.51	0.52	0.89	0.93

1.20	270	25	0	1.18	0.66	0.97	0.93
1.20	270	25	1	0.82	0.92	1.57	1.52
1.20	270	25	2	0.8	0.52	1.17	0.93
1.20	270	25	3	0.64	0.61	1.21	1.01
0.20	90	50	0	0.53	0.49	0.86	0.82
0.20	90	50	1	0.49	0.63	0.64	0.82
0.20	90	50	2	0.36	0.28	0.88	0.83
0.20	90	50	3	0.4	0.37	0.45	0.5
0.70	90	50	0	0.51	0.53	0.64	0.58
0.70	90	50	1	0.52	0.41	0.63	0.66
0.70	90	50	2	0.58	0.48	0.75	0.83
0.70	90	50	3	0.89	0.75	0.807	0.82
1.20	90	50	0	0.58	0.64	0.66	0.68
1.20	90	50	1	0.74	0.64	0.59	0.64
1.20	90	50	2	0.92	1.16	0.61	0.78
1.20	90	50	3	0.89	0.71	0.94	0.82
0.20	180	50	0	0.73	0.67	0.76	0.7
0.20	180	50	1	0.38	0.42	0.62	0.68
0.20	180	50	2	0.54	0.42	0.52	0.57
0.20	180	50	3	0.41	0.45	0.55	0.52
0.70	180	50	0	0.51	0.59	0.53	0.61
0.70	180	50	1	0.28	0.29	0.55	0.5
0.70	180	50	2	0.45	0.47	0.57	0.62
0.70	180	50	3	0.47	0.52	0.76	0.75
1.20	180	50	0	0.66	0.63	0.6	0.67
1.20	180	50	1	0.47	0.53	0.29	0.34
1.20	180	50	2	0.54	0.53	0.69	0.76
1.20	180	50	3	0.65	0.64	0.68	0.74
0.20	270	50	0	0.78	0.84	0.59	0.46
0.20	270	50	1	0.53	0.57	0.54	0.58
0.20	270	50	2	0.38	0.38	0.69	0.73
0.20	270	50	3	0.43	0.37	0.61	0.47
0.70	270	50	0	0.56	0.64	0.59	0.47
0.70	270	50	1	0.94	0.66	0.43	0.51
0.70	270	50	2	0.58	0.49	0.46	0.58
0.70	270	50	3	0.62	0.6	0.64	0.52
1.20	270	50	0	0.7	0.65	0.74	0.52
1.20	270	50	1	0.37	0.45	0.35	0.48
1.20	270	50	2	0.51	0.46	0.53	0.57

1.20	270	50	3	0.53	0.58	0.74	0.9
0.20	90	75	0	0.73	0.67	0.74	0.7
0.20	90	75	1	0.58	0.42	0.61	0.71
0.20	90	75	2	0.45	0.58	0.66	0.56
0.20	90	75	3	0.43	0.45	0.55	0.62
0.70	90	75	0	0.29	0.27	0.32	0.3
0.70	90	75	1	0.48	0.32	0.54	0.81
0.70	90	75	2	0.47	0.39	0.68	0.7
0.70	90	75	3	0.54	0.48	0.78	0.87
1.20	90	75	0	0.59	0.53	0.65	0.59
1.20	90	75	1	0.67	0.76	0.57	0.54
1.20	90	75	2	0.73	0.77	1.2	0.96
1.20	90	75	3	0.71	0.75	0.82	0.75
0.20	180	75	0	0.69	0.65	0.53	0.67
0.20	180	75	1	0.4	0.38	0.91	0.72
0.20	180	75	2	0.35	0.34	0.62	0.76
0.20	180	75	3	0.47	0.45	0.68	0.71
0.70	180	75	0	0.35	0.39	0.36	0.4
0.70	180	75	1	0.45	0.57	0.45	0.51
0.70	180	75	2	0.58	0.49	0.91	0.8
0.70	180	75	3	0.61	0.57	0.52	0.72
1.20	180	75	0	0.8	0.76	0.79	0.81
1.20	180	75	1	0.72	0.44	0.9	0.78
1.20	180	75	2	0.81	0.74	0.69	1.04
1.20	180	75	3	1	1.25	1.7	1.01
0.20	270	75	0	0.77	0.5	0.69	0.65
0.20	270	75	1	0.52	0.38	0.63	0.65
0.20	270	75	2	0.32	0.45	0.58	0.54
0.20	270	75	3	0.42	0.65	0.54	0.53
0.70	270	75	0	0.51	0.47	0.56	0.43
0.70	270	75	1	0.7	0.53	0.52	0.49
0.70	270	75	2	0.89	0.65	0.83	1.1
0.70	270	75	3	1.33	0.95	0.95	1.06
1.20	270	75	0	0.94	0.84	0.93	0.89
1.20	270	75	1	0.4	0.34	0.3	0.4
1.20	270	75	2	0.93	0.79	0.56	0.64
1.20	270	75	3	0.94	0.87	0.8	0.75

ii) For SLM samples (Sa)

Current density (A/mm^2)	Time (sec)	Duty cycle (%)	Distance (mm)	Parallel		Perpendicular	
				Sa1 (µm)	Sa2 (µm)	Sa3 (µm)	Sa4 (µm)
0.20	90	25	0	0.95	0.88	1.14	1.11
0.20	90	25	1	0.91	1.09	0.85	0.88
0.20	90	25	2	0.75	0.81	0.82	0.83
0.20	90	25	3	0.79	0.81	0.72	0.73
0.70	90	25	0	1.56	1.37	1.51	1.48
0.70	90	25	1	1.54	1.42	1.15	1.05
0.70	90	25	2	1.16	1.3	1.27	1.21
0.70	90	25	3	1.03	0.97	1.2	1.1
1.20	90	25	0	1.31	1.28	1.42	1.39
1.20	90	25	1	1.33	1.27	1.37	1.39
1.20	90	25	2	1.05	1.09	0.87	0.9
1.20	90	25	3	0.99	0.96	0.85	0.87
0.20	180	25	0	1.41	1.39	1.25	1.18
0.20	180	25	1	1.35	1.33	1.12	1.12
0.20	180	25	2	1.37	1.43	0.91	0.93
0.20	180	25	3	1.38	1.3	0.84	0.89
0.70	180	25	0	1.73	1.82	1.38	1.69
0.70	180	25	1	1.79	1.61	1.59	1.72
0.70	180	25	2	1.78	1.63	1.55	1.54
0.70	180	25	3	1.51	1.43	1.38	1.37
1.20	180	25	0	1.8	1.85	1.94	1.87
1.20	180	25	1	1.9	1.76	1.47	1.25
1.20	180	25	2	1.78	1.34	1.17	1.23
1.20	180	25	3	1.32	1.18	1.16	1.14
0.20	270	25	0	1.23	1.1	1.25	1.07
0.20	270	25	1	1.12	0.98	1.1	0.97
0.20	270	25	2	0.98	0.89	1.03	0.87
0.20	270	25	3	0.95	1	0.82	0.8
0.70	270	25	0	1.11	1.03	1	1.03
0.70	270	25	1	1.05	1.12	1.15	1.18
0.70	270	25	2	0.94	0.77	1.1	1.33
0.70	270	25	3	1.15	1.09	1.18	1.25
1.20	270	25	0	1.86	1.85	1.8	1.91
1.20	270	25	1	1.77	1.75	2.09	1.8

1.20	270	25	2	1.82	1.43	1.73	1.5
1.20	270	25	3	1.25	1.69	1.14	1.05
0.20	90	50	0	1.06	1.14	1.18	1.02
0.20	90	50	1	1.05	0.79	0.85	0.8
0.20	90	50	2	0.87	0.79	0.77	0.71
0.20	90	50	3	0.75	0.86	0.7	0.76
0.70	90	50	0	1.16	1.03	1.04	1.1
0.70	90	50	1	1.08	1.04	1.28	1.02
0.70	90	50	2	0.94	0.98	1.06	0.95
0.70	90	50	3	1.55	1.24	1.04	1.07
1.20	90	50	0	1.02	1.07	1.04	1.14
1.20	90	50	1	1.2	1.21	0.97	1.11
1.20	90	50	2	1.41	1.47	1.04	1.1
1.20	90	50	3	1.31	1.16	1.11	1.04
0.20	180	50	0	0.97	0.95	1.07	1.04
0.20	180	50	1	0.83	0.77	0.96	0.78
0.20	180	50	2	0.94	0.83	0.73	0.74
0.20	180	50	3	0.83	0.75	0.76	0.77
0.70	180	50	0	0.81	0.76	0.78	0.8
0.70	180	50	1	0.67	0.7	0.79	0.85
0.70	180	50	2	0.75	0.94	0.89	0.85
0.70	180	50	3	0.9	1.04	0.87	0.81
1.20	180	50	0	0.75	0.73	0.77	0.52
1.20	180	50	1	1.22	1.05	0.73	0.83
1.20	180	50	2	0.89	1	0.85	0.88
1.20	180	50	3	0.98	0.92	1	0.98
0.20	270	50	0	1.14	1.3	0.77	0.78
0.20	270	50	1	0.84	0.78	0.83	0.85
0.20	270	50	2	0.73	0.93	1.04	0.92
0.20	270	50	3	0.99	0.84	1.1	0.98
0.70	270	50	0	1.05	1.37	0.77	0.89
0.70	270	50	1	1.02	0.75	0.77	0.8
0.70	270	50	2	0.88	0.92	0.84	0.95
0.70	270	50	3	0.95	0.78	1.05	0.95
1.20	270	50	0	1.27	1.42	1.71	1.02
1.20	270	50	1	1.05	0.778	0.83	0.93
1.20	270	50	2	0.78	0.82	0.84	0.97
1.20	270	50	3	0.98	1.02	0.89	0.98
0.20	90	75	0	1.07	0.82	1.11	0.87

0.20	90	75	1	0.92	1.16	0.85	0.82
0.20	90	75	2	1.11	0.96	0.76	0.73
0.20	90	75	3	0.92	0.93	0.75	0.78
0.70	90	75	0	0.84	0.84	0.82	0.92
0.70	90	75	1	0.89	0.81	0.7	0.94
0.70	90	75	2	0.88	0.83	1.03	0.96
0.70	90	75	3	0.91	0.9	0.89	0.85
1.20	90	75	0	1.08	1.11	1.15	1.24
1.20	90	75	1	1.47	1.23	1.13	1.02
1.20	90	75	2	1.08	0.88	1.23	1.17
1.20	90	75	3	1.49	1.62	1.06	1.09
0.20	180	75	0	0.98	0.83	1.06	1.33
0.20	180	75	1	0.88	0.78	1.19	0.97
0.20	180	75	2	0.87	0.86	1.21	1.25
0.20	180	75	3	0.92	0.91	1.19	1.08
0.70	180	75	0	0.95	1.16	1.25	0.94
0.70	180	75	1	1.01	1.07	0.9	0.91
0.70	180	75	2	1	0.84	1.02	0.93
0.70	180	75	3	1.06	1.04	0.86	0.84
1.20	180	75	0	1.04	1.41	1.09	1.44
1.20	180	75	1	1.32	0.89	0.81	0.78
1.20	180	75	2	0.87	1.03	1.06	1.12
1.20	180	75	3	1.18	1.44	1.07	1.45
0.20	270	75	0	1.16	0.83	1.1	1.05
0.20	270	75	1	0.81	0.81	1	0.96
0.20	270	75	2	0.85	0.77	0.88	0.93
0.20	270	75	3	0.84	0.87	0.93	0.85
0.70	270	75	0	1.3	1.48	1.15	1.16
0.70	270	75	1	0.98	1.05	0.92	0.99
0.70	270	75	2	1.25	1.21	1.07	1.2
0.70	270	75	3	1.35	1.29	1.16	1.15
1.20	270	75	0	1.16	1.13	0.99	1.2
1.20	270	75	1	0.73	0.71	0.69	0.72
1.20	270	75	2	1.27	1.2	1.5	0.75
1.20	270	75	3	1.01	1.29	1.13	1.08

iii) For extruded samples (Ra)

Current density (A/mm^2)	Time (sec)	Duty cycle (%)	Distance (mm)	Parallel		Perpendicular	
				Ra1 (µm)	Ra2 (µm)	Ra3 (µm)	Ra4 (µm)
0.20	90	25	0	0.84	0.98	0.91	0.78
0.20	90	25	1	0.36	0.28	0.45	0.31
0.20	90	25	2	0.45	0.48	0.53	0.41
0.20	90	25	3	0.51	0.56	0.45	0.49
0.20	90	50	0	0.78	0.81	0.87	0.84
0.20	90	50	1	0.56	0.53	0.57	0.51
0.20	90	50	2	0.585	0.49	0.65	0.53
0.20	90	50	3	0.65	0.67	0.68	0.61
0.20	90	75	0	0.7	0.73	0.76	0.66
0.20	90	75	1	0.605	0.63	0.65	0.59
0.20	90	75	2	0.585	0.59	0.6	0.53
0.20	90	75	3	0.645	0.65	0.68	0.61
0.20	180	25	0	0.77	0.89	0.72	0.91
0.20	180	25	1	0.555	0.54	0.51	0.48
0.20	180	25	2	0.555	0.47	0.49	0.58
0.20	180	25	3	0.495	0.51	0.53	0.59
0.20	180	50	0	0.74	0.63	0.71	0.58
0.20	180	50	1	0.79	0.81	0.85	0.76
0.20	180	50	2	0.65	0.68	0.63	0.59
0.20	180	50	3	0.8	0.76	0.78	0.83
0.20	180	75	0	0.58	0.45	0.55	0.65
0.20	180	75	1	1.295	1.03	1.1	0.98
0.20	180	75	2	1.655	1.87	1.34	1.21
0.20	180	75	3	1.35	1.25	1.15	1.04
0.20	270	25	0	0.73	0.78	0.75	0.69
0.20	270	25	1	0.49	0.53	0.57	0.45
0.20	270	25	2	0.48	0.51	0.54	0.55
0.20	270	25	3	0.525	0.56	0.51	0.59
0.20	270	50	0	0.72	0.61	0.64	0.81
0.20	270	50	1	0.705	0.67	0.69	0.63
0.20	270	50	2	0.79	0.76	0.79	0.74
0.20	270	50	3	0.78	0.79	0.71	0.69
0.20	270	75	0	0.55	0.58	0.51	0.48
0.20	270	75	1	0.51	0.58	0.47	0.45

0.20	270	75	2	0.62	0.61	0.63	0.58
0.20	270	75	3	0.67	0.63	0.61	0.56
0.70	90	25	0	0.67	0.55	0.71	0.59
0.70	90	25	1	0.53	0.55	0.58	0.61
0.70	90	25	2	0.575	0.57	0.54	0.61
0.70	90	25	3	0.51	0.54	0.6	0.49
0.70	90	50	0	0.64	0.61	0.68	0.59
0.70	90	50	1	0.33	0.35	0.31	0.37
0.70	90	50	2	0.345	0.35	0.31	0.39
0.70	90	50	3	0.42	0.45	0.49	0.38
0.70	90	75	0	0.54	0.57	0.51	0.58
0.70	90	75	1	0.35	0.36	0.31	0.29
0.70	90	75	2	0.445	0.48	0.36	0.39
0.70	90	75	3	0.455	0.46	0.51	0.61
0.70	180	25	0	0.63	0.61	0.69	0.67
0.70	180	25	1	0.6	0.61	0.63	0.69
0.70	180	25	2	0.58	0.71	0.66	0.55
0.70	180	25	3	0.565	0.57	0.59	0.51
0.70	180	50	0	0.54	0.49	0.45	0.62
0.70	180	50	1	0.66	0.63	0.62	0.59
0.70	180	50	2	0.865	0.81	0.84	0.89
0.70	180	50	3	0.795	0.81	0.76	0.65
0.70	180	75	0	0.45	0.47	0.41	0.52
0.70	180	75	1	0.32	0.31	0.37	0.29
0.70	180	75	2	0.47	0.41	0.49	0.51
0.70	180	75	3	0.555	0.51	0.53	0.59
0.70	270	25	0	0.58	0.55	0.41	0.61
0.70	270	25	1	0.49	0.46	0.43	0.49
0.70	270	25	2	0.37	0.31	0.35	0.38
0.70	270	25	3	0.375	0.39	0.4	0.36
0.70	270	50	0	0.34	0.36	0.31	0.35
0.70	270	50	1	0.655	0.76	0.65	0.71
0.70	270	50	2	0.605	0.61	0.67	0.59
0.70	270	50	3	0.73	0.72	0.78	0.69
0.70	270	75	0	0.21	0.17	0.35	0.41
0.70	270	75	1	0.525	0.58	0.52	0.61
0.70	270	75	2	0.575	0.54	0.5	0.48
0.70	270	75	3	1.09	1.15	1.32	0.98
1.20	90	25	0	0.67	0.51	0.64	0.61

1.20	90	25	1	0.66	0.61	0.59	0.55
1.20	90	25	2	0.615	0.63	0.69	0.51
1.20	90	25	3	0.62	0.64	0.58	0.51
1.20	90	50	0	0.34	0.49	0.39	0.31
1.20	90	50	1	0.695	0.67	0.71	0.86
1.20	90	50	2	0.945	0.91	0.89	0.895
1.20	90	50	3	0.885	0.86	0.86	0.76
1.20	90	75	0	0.43	0.51	0.65	0.41
1.20	90	75	1	0.655	0.69	0.61	0.65
1.20	90	75	2	1.015	1.02	1.34	1.21
1.20	90	75	3	0.895	0.876	0.89	0.85
1.20	180	25	0	0.5	0.51	0.61	0.47
1.20	180	25	1	0.745	0.75	0.78	0.71
1.20	180	25	2	0.765	0.71	0.81	0.82
1.20	180	25	3	0.54	0.56	0.57	0.61
1.20	180	50	0	0.43	0.38	0.48	0.54
1.20	180	50	1	0.295	0.31	0.32	0.38
1.20	180	50	2	0.325	0.34	0.37	0.31
1.20	180	50	3	0.395	0.41	0.43	0.48
1.20	180	75	0	0.45	0.49	0.33	0.51
1.20	180	75	1	0.345	0.35	0.39	0.29
1.20	180	75	2	0.42	0.41	0.407	0.41
1.20	180	75	3	0.46	0.47	0.48	0.31
1.20	270	25	0	0.6	0.71	0.59	0.51
1.20	270	25	1	0.375	0.38	0.39	0.41
1.20	270	25	2	0.355	0.39	0.31	0.34
1.20	270	25	3	0.35	0.38	0.31	0.32
1.20	270	50	0	0.28	0.31	0.29	0.21
1.20	270	50	1	0.31	0.33	0.34	0.32
1.20	270	50	2	0.415	0.42	0.45	0.41
1.20	270	50	3	0.565	0.58	0.51	0.55
1.20	270	75	0	0.35	0.37	0.49	0.32
1.20	270	75	1	0.32	0.31	0.29	0.27
1.20	270	75	2	0.505	0.51	0.48	0.47
1.20	270	75	3	0.62	0.61	0.65	0.67

iv) For extruded samples (Sa)

Current density (A/mm^2)	Time (sec)	Duty Cycle (%)	Distance (mm)	Parallel		Perpendicular	
				Sa1 (µm)	Sa2 (µm)	Sa3 (µm)	Sa4 (µm)
0.20	90	25	0	0.945	1.025	0.99	1.06
0.20	90	25	1	0.78	1.015	1	1.03
0.20	90	25	2	0.84	0.92	0.93	0.91
0.20	90	25	3	1.18	0.97	1.01	0.93
0.20	90	50	0	0.85	1.145	0.91	0.94
0.20	90	50	1	0.92	1.08	0.87	0.84
0.20	90	50	2	0.92	1.025	0.77	0.78
0.20	90	50	3	0.9	0.97	0.84	0.82
0.20	90	75	0	1.165	0.915	1.19	1.2
0.20	90	75	1	1.185	1.08	1.23	1.2
0.20	90	75	2	1.23	1.035	1.21	1.17
0.20	90	75	3	1.195	0.965	1.1	0.99
0.20	180	25	0	0.96	0.945	0.95	0.97
0.20	180	25	1	1.015	1.025	1.01	1.02
0.20	180	25	2	0.995	1.02	0.98	1.01
0.20	180	25	3	0.875	0.9	0.89	0.86
0.20	180	50	0	1.145	1.27	1.27	1.24
0.20	180	50	1	1.16	2.06	1.05	1.04
0.20	180	50	2	1.085	2.29	0.98	0.99
0.20	180	50	3	1.135	1.5	0.94	0.93
0.20	180	75	0	1.115	1.09	1.19	1.22
0.20	180	75	1	1.195	1.165	1.23	1.24
0.20	180	75	2	1.18	1.06	1.17	1.14
0.20	180	75	3	1.125	0.935	0.99	0.91
0.20	270	25	0	0.945	0.95	0.93	0.96
0.20	270	25	1	0.955	1.02	1.02	0.89
0.20	270	25	2	0.985	0.95	1.04	0.93
0.20	270	25	3	1.04	0.765	1.1	0.98
0.20	270	50	0	0.855	1.17	0.95	0.92
0.20	270	50	1	0.755	1.145	0.724	0.69
0.20	270	50	2	0.605	0.98	0.61	0.59
0.20	270	50	3	0.615	0.725	0.88	0.89
0.20	270	75	0	0.53	0.785	0.51	0.57
0.20	270	75	1	0.526	0.805	0.55	0.55

0.20	270	75	2	0.56	0.895	0.52	0.51
0.20	270	75	3	0.535	1.035	0.51	0.51
0.70	90	25	0	1.16	0.925	1.13	1.16
0.70	90	25	1	1.15	0.855	1.11	1.05
0.70	90	25	2	1.12	0.775	1.03	1.02
0.70	90	25	3	1.065	0.83	0.97	0.97
0.70	90	50	0	0.525	0.51	0.49	0.53
0.70	90	50	1	0.495	0.535	0.53	0.54
0.70	90	50	2	0.595	1.105	1.21	1
0.70	90	50	3	0.645	1.35	1.38	1.32
0.70	90	75	0	1.515	0.705	1.84	1.82
0.70	90	75	1	1.705	0.7	1.59	1.69
0.70	90	75	2	1.97	0.88	1.61	1.64
0.70	90	75	3	1.725	0.936	1.7	1.71
0.70	180	25	0	1.61	1.255	1.57	1.65
0.70	180	25	1	1.35	1.045	1.4	1.3
0.70	180	25	2	1.01	0.985	0.98	1.04
0.70	180	25	3	0.945	0.935	0.91	0.98
0.70	180	50	0	0.84	0.845	0.82	0.87
0.70	180	50	1	0.985	0.87	0.86	0.88
0.70	180	50	2	1.52	1.125	1.21	1.04
0.70	180	50	3	1.395	1.055	1.05	1.06
0.70	180	75	0	0.445	0.555	0.44	0.45
0.70	180	75	1	0.46	0.55	0.45	0.47
0.70	180	75	2	0.5	0.66	0.49	0.51
0.70	180	75	3	0.66	0.945	0.61	0.71
0.70	270	25	0	0.955	0.935	1.17	1.17
0.70	270	25	1	1.12	0.707	1.12	1.17
0.70	270	25	2	1.22	0.6	1.01	0.95
0.70	270	25	3	1.095	0.885	0.78	0.67
0.70	270	50	0	0.86	0.865	0.85	0.87
0.70	270	50	1	0.985	0.84	0.96	1.01
0.70	270	50	2	1.025	0.965	1.03	1.02
0.70	270	50	3	1	1.105	1	1
0.70	270	75	0	0.515	0.605	0.5	0.53
0.70	270	75	1	0.635	0.79	0.58	0.69
0.70	270	75	2	0.75	1.315	0.73	0.77
0.70	270	75	3	0.86	1.48	0.84	0.88
1.20	90	25	0	0.96	1.195	0.93	0.99

1.20	90	25	1	1.01	1.215	1.01	1.01
1.20	90	25	2	1.055	1.19	1.05	1.06
1.20	90	25	3	0.99	1.045	0.99	0.99
1.20	90	50	0	0.625	1.83	0.65	0.6
1.20	90	50	1	0.675	1.64	0.7	0.65
1.20	90	50	2	0.695	1.625	0.71	0.68
1.20	90	50	3	0.695	1.705	0.69	0.7
1.20	90	75	0	0.755	0.815	0.77	0.74
1.20	90	75	1	1.055	1.075	1	1.11
1.20	90	75	2	1.67	1.6	1.69	1.65
1.20	90	75	3	1.725	1.41	1.7	1.75
1.20	180	25	0	1.97	1.205	1.98	1.96
1.20	180	25	1	2.06	1.235	1.92	2.2
1.20	180	25	2	2.07	1.155	2.12	2.02
1.20	180	25	3	1.995	0.95	1.99	2
1.20	180	50	0	0.535	0.465	0.53	0.58
1.20	180	50	1	0.655	0.475	0.56	0.54
1.20	180	50	2	0.87	0.82	0.65	0.67
1.20	180	50	3	0.9	1.095	0.98	0.91
1.20	180	75	0	0.36	0.715	0.74	0.69
1.20	180	75	1	0.395	0.785	0.76	0.81
1.20	180	75	2	0.585	0.86	0.83	0.89
1.20	180	75	3	0.805	0.955	0.96	0.95
1.20	270	25	0	0.775	0.54	0.78	0.79
1.20	270	25	1	0.71	0.55	0.8	0.81
1.20	270	25	2	0.775	0.515	0.9	0.89
1.20	270	25	3	0.975	0.51	1.02	1.05
1.20	270	50	0	0.645	0.525	0.63	0.66
1.20	270	50	1	0.765	0.575	0.78	0.75
1.20	270	50	2	1.035	0.875	1.09	0.98
1.20	270	50	3	1.4	0.98	1.39	1.41
1.20	270	75	0	0.49	0.48	0.5	0.48
1.20	270	75	1	0.5	0.475	0.53	0.47
1.20	270	75	2	0.625	0.515	0.69	0.56
1.20	270	75	3	0.93	0.64	0.97	0.89

v) for SLM samples (Rq)

Current density (A/mm^2)	Time (sec)	Duty cycle (%)	distance	Parallel		Perpendicular	
				Rq1	Rq2	Rq3	Rq4
0.20	90	25	0	0.59	0.85	1.14	1.24
0.20	90	25	1	0.5	0.42	0.8	0.85
0.20	90	25	2	0.45	0.45	0.97	0.78
0.20	90	25	3	0.68	0.66	0.67	0.63
0.70	90	25	0	1.04	0.76	1.14	1.21
0.70	90	25	1	0.87	0.79	1.51	1.2
0.70	90	25	2	0.75	0.72	0.95	1.22
0.70	90	25	3	1.09	1.07	1.27	1.03
1.20	90	25	0	0.8	0.75	1.46	1.35
1.20	90	25	1	0.79	0.49	1.21	1.35
1.20	90	25	2	0.45	0.43	0.82	0.81
1.20	90	25	3	0.66	0.54	1.17	0.97
0.20	180	25	0	0.79	0.82	1.05	1.04
0.20	180	25	1	0.76	0.54	1.01	0.93
0.20	180	25	2	0.58	0.93	0.82	0.76
0.20	180	25	3	0.67	0.73	0.78	0.77
0.70	180	25	0	1.05	1.077	1.33	2.38
0.70	180	25	1	0.72	0.64	1.64	1.79
0.70	180	25	2	0.83	0.59	1.65	1.46
0.70	180	25	3	0.74	0.76	1.27	1.41
1.20	180	25	0	1.05	0.92	2.52	2.69
1.20	180	25	1	0.88	0.82	1.15	1.04
1.20	180	25	2	1.01	0.74	1.52	1.24
1.20	180	25	3	0.99	0.77	1.13	1.12
0.20	270	25	0	0.69	0.79	0.94	1.26
0.20	270	25	1	0.68	0.6	1	0.99
0.20	270	25	2	0.49	0.56	0.89	1.33
0.20	270	25	3	0.72	0.45	0.74	0.63
0.70	270	25	0	0.74	0.5	0.85	1.14
0.70	270	25	1	0.99	0.93	0.94	1.28
0.70	270	25	2	0.94	0.67	1.38	1.08
0.70	270	25	3	0.61	0.77	1.08	1.36
1.20	270	25	0	1.58	0.86	2.15	1.79
1.20	270	25	1	1.09	1.14	2.01	2.01

1.20	270	25	2	1.06	0.68	1.53	1.16
1.20	270	25	3	0.81	0.78	1.67	1.98
0.20	90	50	0	0.68	0.61	1.15	1.01
0.20	90	50	1	0.63	0.82	0.83	1.01
0.20	90	50	2	0.45	0.35	1.16	1.06
0.20	90	50	3	0.5	0.6	0.59	0.65
0.70	90	50	0	0.88	0.65	0.71	0.62
0.70	90	50	1	0.66	0.58	0.92	1.04
0.70	90	50	2	0.73	0.59	0.98	1.11
0.70	90	50	3	1.18	1	1.01	1.02
1.20	90	50	0	0.83	0.71	0.8	0.91
1.20	90	50	1	1.11	0.87	0.85	0.86
1.20	90	50	2	1.4	2.14	0.77	1.05
1.20	90	50	3	1.12	0.93	1.25	1.17
0.20	180	50	0	0.66	0.69	0.94	0.95
0.20	180	50	1	0.48	0.51	0.78	0.91
0.20	180	50	2	0.71	0.53	0.65	0.73
0.20	180	50	3	0.5	0.59	0.71	0.66
0.70	180	50	0	0.74	0.74	1.18	0.8
0.70	180	50	1	0.37	0.38	0.76	0.64
0.70	180	50	2	0.65	0.79	0.71	0.87
0.70	180	50	3	0.61	0.84	1.08	0.98
1.20	180	50	0	0.35	0.29	0.6	0.93
1.20	180	50	1	0.59	0.68	0.37	0.45
1.20	180	50	2	0.7	0.89	0.93	0.92
1.20	180	50	3	0.82	0.79	0.87	0.89
0.20	270	50	0	0.6	0.47	0.79	0.6
0.20	270	50	1	0.69	0.74	0.66	0.75
0.20	270	50	2	0.47	0.48	0.87	0.95
0.20	270	50	3	0.54	0.47	0.76	0.63
0.70	270	50	0	0.81	0.88	0.78	0.65
0.70	270	50	1	1.72	1.06	0.57	0.69
0.70	270	50	2	0.72	0.67	0.58	0.77
0.70	270	50	3	0.82	0.79	0.87	0.64
1.20	270	50	0	1.04	0.75	1.26	0.74
1.20	270	50	1	0.47	0.69	0.43	0.63
1.20	270	50	2	0.74	0.65	0.71	0.73
1.20	270	50	3	0.78	0.81	0.94	1.09
0.20	90	75	0	0.64	0.55	1.01	1.01

0.20	90	75	1	0.71	0.53	0.75	0.87
0.20	90	75	2	0.57	0.73	0.85	0.7
0.20	90	75	3	0.55	0.61	0.74	0.78
0.70	90	75	0	0.38	0.42	0.56	0.8
0.70	90	75	1	0.67	0.42	0.83	1.42
0.70	90	75	2	0.64	0.55	0.96	1.06
0.70	90	75	3	0.72	0.65	1.06	1.18
1.20	90	75	0	0.48	0.59	0.85	0.85
1.20	90	75	1	0.95	1.31	0.79	0.67
1.20	90	75	2	0.97	1.01	2.46	1.96
1.20	90	75	3	1.01	0.88	1.11	1.03
0.20	180	75	0	0.63	0.57	0.67	0.87
0.20	180	75	1	0.52	0.49	1.21	0.85
0.20	180	75	2	0.44	0.43	0.75	0.99
0.20	180	75	3	0.68	0.54	0.85	0.92
0.70	180	75	0	0.78	0.44	0.89	1.28
0.70	180	75	1	0.62	0.76	0.59	0.72
0.70	180	75	2	0.8	0.65	1.19	1.05
0.70	180	75	3	0.75	0.75	0.65	0.97
1.20	180	75	0	0.97	0.73	0.53	1.07
1.20	180	75	1	1.35	0.68	1.61	1.92
1.20	180	75	2	1.18	1.05	0.92	1.42
1.20	180	75	3	2.44	1.79	2.44	1.65
0.20	270	75	0	0.98	0.62	0.97	0.91
0.20	270	75	1	0.64	0.56	1.03	0.81
0.20	270	75	2	0.42	0.62	0.77	0.68
0.20	270	75	3	0.54	0.9	0.68	0.68
0.70	270	75	0	0.76	0.85	0.76	0.53
0.70	270	75	1	1.21	0.98	0.64	0.67
0.70	270	75	2	1.17	0.84	1.03	1.37
0.70	270	75	3	2.08	1.41	1.23	1.35
1.20	270	75	0	1.76	1.42	0.59	0.88
1.20	270	75	1	0.7	0.5	0.39	0.59
1.20	270	75	2	1.47	1.02	0.79	0.88
1.20	270	75	3	1.15	1.18	1.01	1.01

vi) For SLM samples (Sq)

Current density (A/mm^2)	Time (sec)	Duty cycle (%)	Distance (mm)	Parallel		Perpendicular	
				Sq1	Sq2	Sq3	Sq4
0.20	90	25	0	1.12	1.15	1.48	1.43
0.20	90	25	1	1.15	1.41	1.09	1.14
0.20	90	25	2	0.96	1.04	1.05	1.06
0.20	90	25	3	1.02	1.02	0.9	0.94
0.70	90	25	0	1.98	1.77	1.92	1.9
0.70	90	25	1	1.98	1.8	1.48	1.33
0.70	90	25	2	1.46	1.65	1.6	1.53
0.70	90	25	3	1.3	1.23	1.52	1.4
1.20	90	25	0	1.7	1.65	1.87	1.82
1.20	90	25	1	1.73	1.65	1.75	1.79
1.20	90	25	2	1.36	1.43	1.14	1.17
1.20	90	25	3	1.3	1.32	1.08	1.12
0.20	180	25	0	1.79	1.8	1.61	1.51
0.20	180	25	1	1.74	1.71	1.42	1.45
0.20	180	25	2	1.77	1.86	1.14	1.18
0.20	180	25	3	1.94	1.82	1.07	1.14
0.70	180	25	0	2.29	2.48	1.85	2.33
0.70	180	25	1	2.32	2.1	2.08	2.26
0.70	180	25	2	2.29	2.09	1.99	2.01
0.70	180	25	3	1.91	1.87	1.77	1.75
1.20	180	25	0	2.32	2.47	2.66	2.5
1.20	180	25	1	2.58	2.41	1.91	1.64
1.20	180	25	2	2.38	1.75	1.59	1.55
1.20	180	25	3	1.72	1.52	1.47	1.45
0.20	270	25	0	1.62	1.44	1.64	1.42
0.20	270	25	1	1.48	1.29	1.29	1.27
0.20	270	25	2	1.29	1.16	1.42	1.12
0.20	270	25	3	1.21	1.29	1.06	1.03
0.70	270	25	0	1.81	1.45	1.45	1.55
0.70	270	25	1	1.5	1.66	1.74	1.68
0.70	270	25	2	1.27	1.04	1.43	1.73
0.70	270	25	3	1.52	1.43	1.51	1.98
1.20	270	25	0	2.45	2.47	2.45	2.57
1.20	270	25	1	2.29	2.25	2.76	2.4

1.20	270	25	2	2.36	1.85	2.22	1.95
1.20	270	25	3	1.59	2.22	1.45	1.33
0.20	90	50	0	1.35	1.56	1.6	1.3
0.20	90	50	1	1.76	1	1.21	1.01
0.20	90	50	2	1.14	1.08	0.99	0.91
0.20	90	50	3	0.97	1.1	0.91	0.98
0.70	90	50	0	1.76	1.38	1.41	1.5
0.70	90	50	1	1.47	1.36	1.72	1.37
0.70	90	50	2	1.21	1.28	1.39	1.23
0.70	90	50	3	2.62	1.62	1.37	1.38
1.20	90	50	0	1.53	1.47	1.46	1.55
1.20	90	50	1	1.66	1.59	1.31	1.43
1.20	90	50	2	1.99	2.2	1.51	1.52
1.20	90	50	3	1.72	1.51	1.42	1.35
0.20	180	50	0	1.23	1.21	1.42	1.33
0.20	180	50	1	1.05	0.99	1.24	0.98
0.20	180	50	2	1.2	1.06	0.93	0.95
0.20	180	50	3	1.07	1.03	1.02	0.99
0.70	180	50	0	1.26	1.33	1.21	1.41
0.70	180	50	1	0.98	1.28	1.39	1.16
0.70	180	50	2	1.19	1.22	1.2	1.15
0.70	180	50	3	1.22	1.69	1.14	1.05
1.20	180	50	0	1.76	1.73	1.83	0.87
1.20	180	50	1	2.23	1.54	1.08	1.05
1.20	180	50	2	1.25	1.69	1.05	1.11
1.20	180	50	3	1.27	1.15	1.27	1.27
0.20	270	50	0	2.14	2.34	0.98	1.01
0.20	270	50	1	1.22	1.01	1.06	1.11
0.20	270	50	2	0.98	1.25	1.5	1.27
0.20	270	50	3	1.35	1.47	1.94	1.5
0.70	270	50	0	1.01	1.55	1.04	1.49
0.70	270	50	1	1.82	0.98	1.02	1
0.70	270	50	2	1.6	1.45	1.09	1.27
0.70	270	50	3	1.3	1.1	1.49	1.4
1.20	270	50	0	2.19	2.43	2.76	2.04
1.20	270	50	1	1.76	1.16	1.28	1.58
1.20	270	50	2	1.19	1.2	1.12	1.32
1.20	270	50	3	1.54	1.78	1.19	1.26
0.20	90	75	0	1.39	1.05	1.43	1.11

0.20	90	75	1	1.18	1.47	1.08	1.05
0.20	90	75	2	1.41	1.23	0.98	0.93
0.20	90	75	3	1.17	1.19	0.97	0.99
0.70	90	75	0	1.57	1.68	1.55	1.75
0.70	90	75	1	1.49	1.32	1.07	1.37
0.70	90	75	2	1.28	1.19	1.48	1.33
0.70	90	75	3	1.29	1.33	1.21	1.14
1.20	90	75	0	1.97	2.03	1.92	2.3
1.20	90	75	1	2.37	1.9	1.98	1.91
1.20	90	75	2	1.96	1.41	2.39	1.61
1.20	90	75	3	2.12	2.19	1.54	1.57
0.20	180	75	0	1.28	1.1	1.88	2.27
0.20	180	75	1	1.15	1.01	1.85	1.27
0.20	180	75	2	1.13	1.14	1.53	1.68
0.20	180	75	3	1.18	1.19	1.78	1.56
0.70	180	75	0	1.66	1.97	2.11	1.36
0.70	180	75	1	1.56	1.93	1.38	1.45
0.70	180	75	2	1.53	1.16	1.5	1.33
0.70	180	75	3	1.43	1.44	1.12	1.1
1.20	180	75	0	2.03	2.9	2.2	2.92
1.20	180	75	1	3	1.7	1.89	1.21
1.20	180	75	2	1.69	1.93	1.47	1.54
1.20	180	75	3	1.77	2.22	1.56	2.38
0.20	270	75	0	1.53	1.11	1.48	1.45
0.20	270	75	1	1.1	1.12	1.42	1.29
0.20	270	75	2	1.15	1.04	1.17	1.26
0.20	270	75	3	1.11	1.15	1.24	1.1
0.70	270	75	0	2.74	2.97	2.26	2.13
0.70	270	75	1	1.5	1.4	1.23	1.54
0.70	270	75	2	1.67	1.63	1.37	1.55
0.70	270	75	3	1.96	1.84	1.75	1.69
1.20	270	75	0	2.29	2.42	2.1	2.48
1.20	270	75	1	1.56	1.48	1.32	1.5
1.20	270	75	2	1.88	1.62	3.57	1.14
1.20	270	75	3	1.46	1.82	1.61	1.48

vii) For extruded samples (Rq)

Current density ($A/mm^{2)}$	Time (sec)	Duty cycle (%)	Distance	Rq1	Rq2	Rq3	Rq4
0.20	90	25	0	1.33	1.72	1.79	1.75
0.20	90	25	1	0.85	1.02	1.33	1.28
0.20	90	25	2	0.94	1.22	1.41	1.38
0.20	90	25	3	1	1.3	1.33	1.46
0.20	90	50	0	1.27	1.55	1.75	1.81
0.20	90	50	1	1.05	1.27	1.45	1.48
0.20	90	50	2	1.075	1.23	1.53	1.5
0.20	90	50	3	1.14	1.41	1.56	1.58
0.20	90	75	0	1.19	1.47	1.64	1.63
0.20	90	75	1	1.095	1.37	1.53	1.56
0.20	90	75	2	1.075	1.33	1.48	1.5
0.20	90	75	3	1.135	1.39	1.56	1.58
0.20	180	25	0	1.26	1.63	1.6	1.88
0.20	180	25	1	1.045	1.28	1.39	1.45
0.20	180	25	2	1.045	1.21	1.37	1.55
0.20	180	25	3	0.985	1.25	1.41	1.56
0.20	180	50	0	1.23	1.37	1.59	1.55
0.20	180	50	1	1.28	1.55	1.73	1.73
0.20	180	50	2	1.14	1.42	1.51	1.56
0.20	180	50	3	1.29	1.5	1.66	1.8
0.20	180	75	0	1.07	1.19	1.43	1.62
0.20	180	75	1	1.785	1.77	1.98	1.95
0.20	180	75	2	2.145	2.61	2.22	2.18
0.20	180	75	3	1.84	1.99	2.03	2.01
0.20	270	25	0	1.22	1.52	1.63	1.66
0.20	270	25	1	0.98	1.27	1.45	1.42
0.20	270	25	2	0.97	1.25	1.42	1.52
0.20	270	25	3	1.015	1.3	1.39	1.56
0.20	270	50	0	1.21	1.35	1.52	1.78
0.20	270	50	1	1.195	1.41	1.78	1.6
0.20	270	50	2	1.28	1.5	1.88	1.71
0.20	270	50	3	1.27	1.53	1.8	1.66
0.20	270	75	0	1.04	1.32	1.6	1.45
0.20	270	75	1	1	1.32	1.56	1.42
0.20	270	75	2	1.11	1.35	1.72	1.55
0.20	270	75	3	1.16	1.37	1.7	1.53
0.70	90	25	0	1.16	1.29	1.8	1.56

0.70	90	25	1	1.02	1.29	1.67	1.58
0.70	90	25	2	1.065	1.31	1.63	1.58
0.70	90	25	3	1	1.28	1.69	1.46
0.70	90	50	0	1.61	1.35	1.77	1.56
0.70	90	50	1	1.3	0.72	1.4	1.35
0.70	90	50	2	1.315	0.72	1.4	1.37
0.70	90	50	3	1.39	0.82	1.58	1.36
0.70	90	75	0	1.51	0.94	1.6	1.56
0.70	90	75	1	1.32	0.73	1.4	1.27
0.70	90	75	2	1.415	0.85	1.45	1.37
0.70	90	75	3	1.425	0.83	1.6	1.59
0.70	180	25	0	1.6	0.98	1.78	1.65
0.70	180	25	1	1.57	0.98	1.72	1.67
0.70	180	25	2	1.55	1.08	1.75	1.53
0.70	180	25	3	1.535	0.94	1.68	1.49
0.70	180	50	0	1.51	0.86	1.54	1.6
0.70	180	50	1	1.63	1	1.71	1.57
0.70	180	50	2	1.835	1.18	1.93	1.87
0.70	180	50	3	1.765	1.18	1.85	1.63
0.70	180	75	0	1.42	0.84	1.5	1.5
0.70	180	75	1	1.29	0.68	1.46	1.27
0.70	180	75	2	1.44	0.78	1.58	1.49
0.70	180	75	3	1.525	1.19	1.62	1.57
0.70	270	25	0	1.55	1.23	1.5	1.59
0.70	270	25	1	1.46	1.14	1.52	1.47
0.70	270	25	2	1.34	0.99	1.44	1.36
0.70	270	25	3	1.345	1.07	1.49	1.34
0.70	270	50	0	1.31	1.04	1.4	1.33
0.70	270	50	1	1.625	1.44	1.74	1.56
0.70	270	50	2	1.575	1.29	1.76	1.57
0.70	270	50	3	1.12	1.4	1.87	1.67
0.70	270	75	0	0.6	0.85	1.44	1.39
0.70	270	75	1	0.915	1.26	1.61	1.59
0.70	270	75	2	0.965	1.22	1.59	1.46
0.70	270	75	3	1.48	1.83	2.41	1.96
1.20	90	25	0	1.06	1.19	1.73	1.59
1.20	90	25	1	1.05	1.29	1.46	1.53
1.20	90	25	2	1.005	1.31	1.56	1.49
1.20	90	25	3	1.01	1.32	1.45	1.49
1.20	90	50	0	0.73	1.17	1.26	1.29
1.20	90	50	1	1.085	1.35	1.58	1.84

1.20	90	50	2	1.335	1.59	1.76	1.875
1.20	90	50	3	1.275	1.54	1.73	1.74
1.20	90	75	0	0.82	1.19	1.52	1.39
1.20	90	75	1	1.045	1.37	1.48	1.63
1.20	90	75	2	1.405	1.7	2.21	2.19
1.20	90	75	3	1.285	1.556	1.76	1.83
1.20	180	25	0	0.89	1.19	1.48	1.45
1.20	180	25	1	1.135	1.43	1.65	1.69
1.20	180	25	2	1.155	1.39	1.68	1.8
1.20	180	25	3	0.93	1.19	1.44	1.59
1.20	180	50	0	0.82	1.01	1.35	1.66
1.20	180	50	1	0.685	0.94	1.19	1.5
1.20	180	50	2	1.145	0.97	1.24	1.43
1.20	180	50	3	1.215	1.04	1.3	1.6
1.20	180	75	0	1.27	1.12	1.2	1.63
1.20	180	75	1	1.165	0.98	1.26	1.41
1.20	180	75	2	1.24	1.04	1.277	1.53
1.20	180	75	3	1.28	1.1	1.35	1.43
1.20	270	25	0	1.42	1.34	1.46	1.63
1.20	270	25	1	1.195	1.01	1.26	1.53
1.20	270	25	2	1.175	1.02	1.18	1.46
1.20	270	25	3	1.17	1.01	1.18	1.44
1.20	270	50	0	1.1	0.94	1.16	1.75
1.20	270	50	1	1.13	0.96	1.21	1.86
1.20	270	50	2	1.235	1.05	1.32	1.27
1.20	270	50	3	1.385	1.21	1.38	1.41
1.20	270	75	0	1.17	1	1.36	1.18
1.20	270	75	1	1.14	0.94	1.16	1.13
1.20	270	75	2	1.325	1.14	1.35	1.33
1.20	270	75	3	1.44	1.24	1.52	1.53

viii) For extruded samples (Sq)

Current density (A/mm^2)	Time (sec)	Duty cycle (%)	Distance (mm)	Sq1	Sq2	Sq3	Sq4
0.20	90	25	0	1.17	1.22	1.28	1.37
0.20	90	25	1	1.03	0.97	1.28	1.32
0.20	90	25	2	1.01	1.2	1.41	1.17
0.20	90	25	3	1.55	1.51	1.35	1.19
0.20	90	50	0	1.6	1.4	1.46	1.5
0.20	90	50	1	1.43	1.52	1.44	1.37
0.20	90	50	2	1.9	1.4	1.33	1.33
0.20	90	50	3	1.34	1.42	1.24	1.24
0.20	90	75	0	1.12	1.23	1.21	1.19
0.20	90	75	1	1.29	1.3	1.38	1.37
0.20	90	75	2	1.34	1.35	1.3	1.31
0.20	90	75	3	1.28	1.27	1.21	1.22
0.20	180	25	0	1.19	1.21	1.18	1.18
0.20	180	25	1	1.26	1.28	1.28	1.3
0.20	180	25	2	1.23	1.26	1.27	1.27
0.20	180	25	3	1.12	1.09	1.13	1.13
0.20	180	50	0	2.3	2.18	1.6	1.69
0.20	180	50	1	1.83	1.67	2.7	2.76
0.20	180	50	2	1.25	1.33	2.98	2.98
0.20	180	50	3	1.18	1.28	1.95	1.91
0.20	180	75	0	3.01	3.63	1.39	1.49
0.20	180	75	1	2.97	3.5	1.51	1.53
0.20	180	75	2	3.46	2.92	1.36	1.37
0.20	180	75	3	2.33	2.88	1.21	1.21
0.20	270	25	0	1.19	1.25	1.22	1.24
0.20	270	25	1	1.34	1.16	1.32	1.35
0.20	270	25	2	1.36	1.19	1.22	1.22
0.20	270	25	3	1.45	1.3	0.98	0.99
0.20	270	50	0	1.29	1.35	1.65	1.63
0.20	270	50	1	1.55	1.47	1.53	1.6
0.20	270	50	2	1.56	1.63	1.34	1.27
0.20	270	50	3	1.4	1.34	0.99	0.88
0.20	270	75	0	1.1	1.07	1.14	1.15
0.20	270	75	1	0.97	1.02	1.13	1.13

0.20	270	75	2	1.05	1.01	1.25	1.22
0.20	270	75	3	1.25	1.26	1.33	1.33
0.70	90	25	0	1.14	1.06	1.21	1.22
0.70	90	25	1	1.23	1.19	1.14	1.08
0.70	90	25	2	1.22	1.16	1.01	1.03
0.70	90	25	3	1.16	1.15	1.11	1.08
0.70	90	50	0	0.69	0.69	0.65	0.7
0.70	90	50	1	0.68	0.66	0.71	0.72
0.70	90	50	2	0.74	1.01	1.65	1.48
0.70	90	50	3	0.86	0.87	1.82	1.74
0.70	90	75	0	0.9	0.85	0.93	0.972
0.70	90	75	1	0.97	0.91	0.94	0.97
0.70	90	75	2	0.96	0.93	1.21	1.25
0.70	90	75	3	0.93	0.945	1.3	1.28
0.70	180	25	0	1.46	1.47	1.63	1.6
0.70	180	25	1	1.46	1.54	1.36	1.33
0.70	180	25	2	1.36	1.42	1.26	1.27
0.70	180	25	3	1.48	1.46	1.2	1.19
0.70	180	50	0	1.14	1.18	1.12	1.17
0.70	180	50	1	1.32	1.32	1.15	1.23
0.70	180	50	2	2.12	1.93	1.65	1.38
0.70	180	50	3	1.89	1.73	1.35	1.37
0.70	180	75	0	0.76	0.72	0.82	0.82
0.70	180	75	1	0.96	0.86	0.77	0.73
0.70	180	75	2	1.2	1.18	0.96	0.92
0.70	180	75	3	1.15	1.24	1.3	1.21
0.70	270	25	0	1.13	1.13	1.27	1.19
0.70	270	25	1	0.98	1.01	0.95	0.9
0.70	270	25	2	0.78	0.76	0.79	0.77
0.70	270	25	3	0.81	0.84	1.09	1.14
0.70	270	50	0	1.15	1.23	1.14	1.16
0.70	270	50	1	1.31	1.4	1.22	1.13
0.70	270	50	2	1.49	1.4	1.35	1.39
0.70	270	50	3	1.38	1.36	1.49	1.49
0.70	270	75	0	1.07	1.13	0.98	1.08
0.70	270	75	1	1.35	1.24	1.17	1.18
0.70	270	75	2	1.62	1.48	1.77	1.87
0.70	270	75	3	1.91	1.96	1.97	1.92
1.20	90	25	0	1.51	1.52	1.54	1.56

1.20	90	25	1	1.55	1.5	1.57	1.54
1.20	90	25	2	1.59	1.59	1.55	1.52
1.20	90	25	3	1.52	1.58	1.31	1.29
1.20	90	50	0	2.11	2.1	2.37	2.34
1.20	90	50	1	2.34	2.28	2.17	2.24
1.20	90	50	2	2.58	2.46	2.18	2.24
1.20	90	50	3	2.23	2.12	2.17	2.18
1.20	90	75	0	1.32	1.28	1.42	1.41
1.20	90	75	1	1.46	1.65	1.49	1.78
1.20	90	75	2	2.46	2.33	2.12	2.14
1.20	90	75	3	2.02	2.04	1.91	1.79
1.20	180	25	0	1.4	1.49	1.53	1.56
1.20	180	25	1	1.52	1.55	1.58	1.59
1.20	180	25	2	1.52	1.5	1.49	1.46
1.20	180	25	3	1.5	1.31	1.27	1.15
1.20	180	50	0	0.66	0.68	0.75	0.69
1.20	180	50	1	0.69	0.75	0.77	0.76
1.20	180	50	2	0.79	0.82	1.29	1.26
1.20	180	50	3	0.99	1.08	1.33	1.73
1.20	180	75	0	1.22	1.33	1.35	1.22
1.20	180	75	1	1.29	1.14	1.06	1.11
1.20	180	75	2	0.87	0.95	1.12	1.17
1.20	180	75	3	0.95	0.94	1.25	1.24
1.20	270	25	0	0.7	0.73	0.71	0.76
1.20	270	25	1	0.7	0.71	0.76	0.73
1.20	270	25	2	0.73	0.75	0.68	0.7
1.20	270	25	3	0.74	0.68	0.67	0.68
1.20	270	50	0	0.85	0.86	0.89	0.93
1.20	270	50	1	0.96	1.08	0.88	0.96
1.20	270	50	2	1.06	1.1	1.2	1.2
1.20	270	50	3	1.13	1.18	1.3	1.26
1.20	270	75	0	0.91	0.89	0.88	0.91
1.20	270	75	1	0.88	0.84	0.84	0.8
1.20	270	75	2	1.12	0.91	0.82	0.79
1.20	270	75	3	1.39	1.21	0.96	1.06

APPENDIX D

REGRESSION MODEL

i) SLM parts

$$Ra = 0.602 - 0.191\,J - 0.00021\,t + 0.0007\,dc - 0.0493\,d + 0.0013(J * t) + 0.0014(J * dc) + 0.248\,(J * d) \quad (5)$$

Where,

J	Current density (A/mm^2)	0.2, 1.2
t	Time (sec)	90, 270
dc	Duty cycle (%)	25, 75
d	Distance (mm)	0, 3

The R^2 for this regression model is 78.93%.

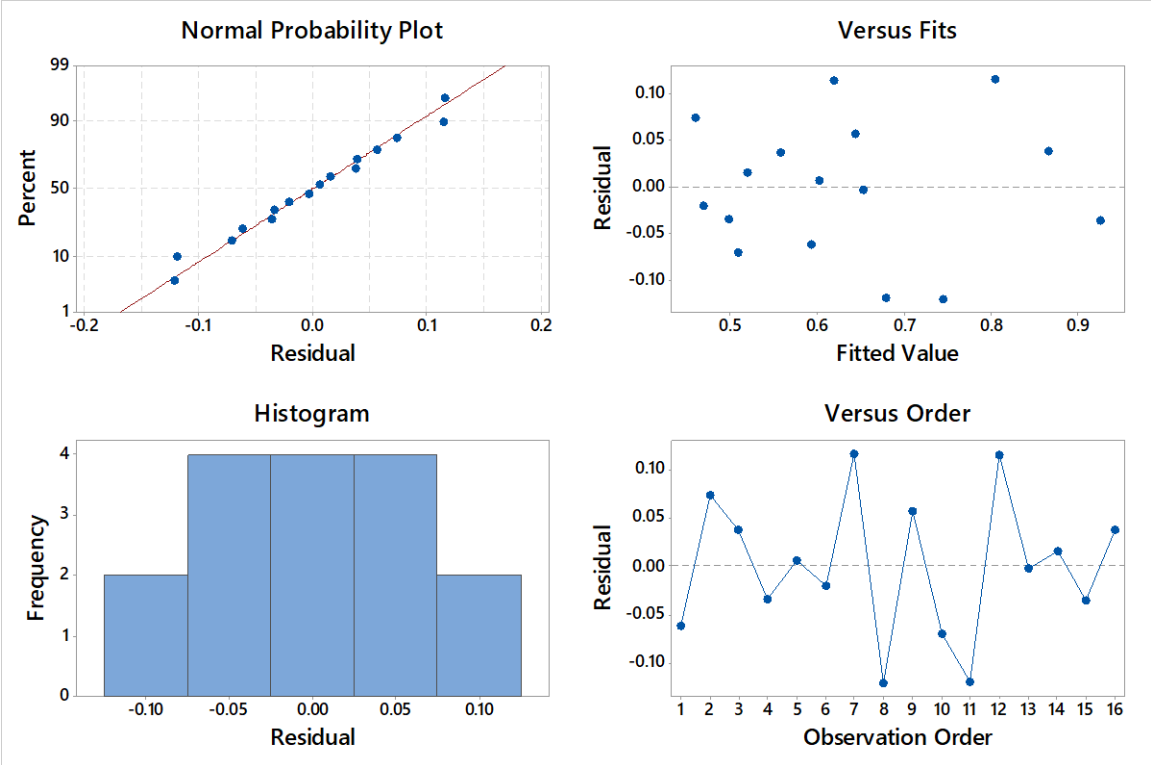

Figure 57: Residual plots of regression model for Ra of SLM samples

ii) Extruded parts

$$Ra = 1.06 - 0.193\,J - 0.000635\,t - 0.0041\,dc - 0.19\,d + 0.075\,(J * d) + 0.00273(dc * d) \quad (6)$$

Where,

J	Current density (A/mm^2)	0.2, 1.2
t	Time (sec)	90, 270
dc	Duty cycle (%)	25, 75
d	Distance (mm)	0, 3

The R^2 for this regression model is 83.68%.

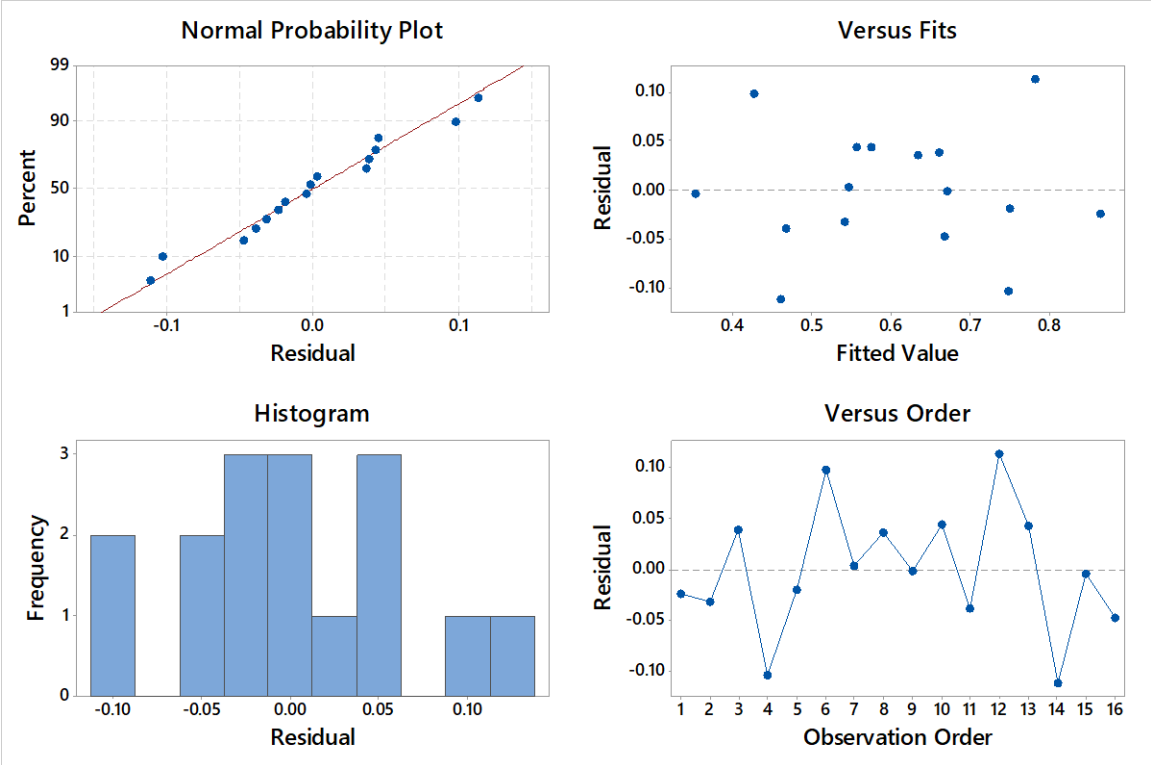

Figure 58: Residual plots of regression model for Ra of extruded samples